Design and Optimization of a Continuous Bioreactor for Enhanced Cell Production

by

Rithvija Avvari

A dissertation submitted to the Graduate Faculty of
Auburn University
in partial fulfillment of the
requirements for the Degree of
Doctor of Philosophy

Auburn, Alabama
May 7, 2022

Key words: continuous bioreactor, mammalian cell culture, CFD modeling, optimization, roller bottle

Approved by

Dr. Thomas R. Hanley, Chair, Professor, Chemical Engineering
Dr. Paul W. Todd, Chief Scientist Emeritus, Techshot, Inc.
Dr. Allan E. David, Associate Professor, Chemical Engineering
Dr. Selen Cremaschi, Professor, Chemical Engineering
Dr. Anthony G. Moss, Associate Professor, Biological Sciences

Abstract

This research investigated a novel continuous bioreactor which can be operated both in batch and chemostat modes. The bioreactor showed significant improvement in cell growth due to addition of a spiroid which increased gas-liquid contact areas. The bioreactor consists of a cylindrical wall and is horizontally rotated on a roller bed. The spiroid is embedded in the cylindrical wall of the bioreactor to increase oxygen transfer to the liquid phase which fills two-thirds of the bioreactor. The bioreactor has two rotary inlets and outlets for batch, continuous or fed-batch operation and real-time sampling. The rotation rate of the reactor can be adjusted to control the flow of gas and liquid in the spiroid. When the partially filled reactor is rotating, the spiroid picks up slugs of gas and liquid near the reactor exit and delivers them to the reactor entrance. The flow though spiroid at different rotation rates, spiroid diameter and spiroid length was studied using computational fluid dynamics (CFD) to determine conditions for optimum operation. As flow through spiroid is a complex phenomenon, the CFD model was simplified to a straight tube and different parameters (shear stress, velocity vectors, wall turbulence, turbulence parameters) for different dimensions were studied to determine the optimum size of the spiroid.

To test the viability of the reactor for cellular production and growth, biological tests using *Saccharomyces cerevisiae* (yeast) were conducted at different rotation rates, operation modes (batch, continuous) and steady state levels. Cell growth monitoring and metabolite concentration (glucose) measurements in the bioreactor with and without the spiroid demonstrated the advantage of the bioreactor in increased cell production (57% increased cells and 27% less operating time). The bioreactor was further used to optimize the cell line production. Higher cell production was seen at 8 RPM for yeast at a flow rate of 0.6 ml/min.

3D printing techniques were used to prototype the reactor to reduce the degradation of the material with continued use of various cell lines and make it biocompatible and autoclavable. Mammalian cell culture using Chinese hamster ovary (CHO) cells showed promising results for producing high cell densities of 2.4 x 10^6 cells/ml for a period of 14 days. Cell viabilities could be maintained up to 90% with the use of spiroid in the reactor. Higher CHO cell densities were obtained at higher rotation rate of 10rpm and high medium flow rate of 4ml/min. These results show the potential of the bioreactor to continuously culture a variety of cell lines including shear sensitive cells for long durations without leakage.

Acknowledgments

First and foremost, I am extremely thankful to my advisor and mentor Dr. Thomas R. Hanley for providing me the opportunity, his invaluable advice and continued support during my PhD research. His immense knowledge and guidance helped me throughout my research and to establish my skillset. I could not have imagined having a better advisor and mentor for my PhD study and I am forever grateful to him.

I would also like to thank Dr. Paul W. Todd for his supervision, insightful comments in evaluating and improving my research approach. Besides, my sincere thanks also go to Dr. Allan E. David, who provided me with the cell line strains, access to BSL2, and the relative analytical instruments for my experiments. Moreover, I would like to acknowledge my committee members Dr. Paul W. Todd, Dr. Allan E. David, Dr. Selen Cremaschi, Dr. Anthony G. Moss for their insightful comments and suggestions. I would like to thank Dr. Bart Prorok for serving as the University Reader for the current dissertation. I would also like to extend my thanks to Marjan Azadi for the cell culture training.

I thank all the graduate students (previous and present) in my group for their guidance and assistance. I would like to extend my gratitude to the chair of Department of Chemical Engineering Dr. Mario Eden and all the staff in the department. I am very thankful to all my course instructors who helped me achieve more knowledge. A special mention to Dr. Abhinav Sannidhi for helping me through this journey. Additionally, I would like to extend my gratitude to Elaine Manning for helping me throughout this process and Brian Schwieker for helping me with my experimental space.

I wholeheartedly thank all my colleagues and my friends Srinath Yamalakonda, Vamshi Reddy, Sindhu Ravali, Vivek, Madhuri Nori, Vinita Shinde, Amod Parkhi, Rohit, Jinesh and Archana Bansode for their support and encouragement that made my life in Auburn delightful. Last but not the least, my sincere thanks go to my parents Mrs. Rama Devi Avvari and Mr. Raghu Avvari and my sister Rudrani Avvari. My immense love to my nephew Vihaan Guda for always keeping me entertained. Without their relentless love, continuous support, and encouragement, I would not be able to complete this journey.

Table of Contents

List of Tables

List of Figures

List of Abbreviations

μ	molecular dynamic viscosity (Pa-s)
μ_t	turbulent or eddy viscosity (Pa-s)
3D	Three Dimensional
ATF	Alternating tangential flow filtration
BHK	Baby Hamster Kidney fibroblasts
CFD	Computational Fluid Dynamics
CHO	Chinese Hamster Ovary
D	Dilution rate (hr^{-1})
d	diameter (m)
DHA	docosahexaenoic acid
DO	Dissolved oxygen
DOE	Design of Experiments
F	Flowrate (ml/min)
FBS	Fetal Bovine serum
G_b	generation term due to the buoyancy, ($J\ s^{-1}\ m^{-3}$ or $kg\ m^{-1}\ s^{-3}$);
G_k	generation term because of the mean velocity gradients ($J\ s^{-1}\ m^{-3}$ or $kg\ m^{-1}\ s^{-3}$)
GM	Glucose monitor
k	turbulence kinetic energy per unit mass ($J\ kg^{-1}$ or $m^2\ s^{-2}$)
ν	kinematic viscosity ($m^2\ s^{-1}$)
k_La	volumetric mass transfer coefficient (s^{-1})
L	length (m)

MRF Multiple Reference Frame

MSC mesenchymal stromal cells

OD_{600} optical density at 600nm

RANS Reynolds-Averaged Navier-stokes

rpm rotations per minute

SLA stereolithography

SLS Selective Laser Sintering

SS Steady state

SUB Single-use Bioreactors

t time (s)

TFF Tangential flow filtration

VOF volume of fluid

Y_M effects from the fluctuating dilatation in the compressible turbulence on the overall dissipation rate (J s^{-1} m^{-3} or kg m^{-1} s^{-3})

YPD yeast peptone dextrose

ε dissipation rate per unit mass (J kg^{-1} s^{-1} or m^2 s^{-3})

$\boldsymbol{\tau}$ mean residence time (hr)

Chapter 1 – Introduction

Researchers in the field of bioprocessing are investigating various biomanufacturing techniques to decrease capital costs, increase productivity and improve product quality. Continuous bioprocessing is emerging in upstream processing and is preferred over traditional batch processing. With standardizations and control strategies in place, safety and efficacy can be achieved. One important area of investigation is the design and operation of bioreactors.

A bioreactor provides a suitable environment (adequate nutrients and oxygen) for cell cultures to proliferate under controlled conditions. These devices are used extensively in stem cell research (model systems, production of monoclonal antibodies and other proteins), cancer therapy, tissue engineering (scaffolds) and pharmaceutical industries (vaccines and antibiotics) on a large scale. Various bioreactors with different design principles have been developed to culture cells at a higher rate. Increasing productivity while reducing shear is one common goal for these reactors.

Cells are typically suspended in liquid, and the liquid flow around these cells generates mechanical forces that may be detrimental to the cells. Hence, the focus is always to develop reactors that provide minimum shear. In most studies, oxygen transfer within the reactor is a major issue as oxygen is sparingly soluble in the aqueous medium. Most bioreactors provide mixing with the use of impellers resulting in high shear that can cause cell death. Aeration is obtained by continuously supplying oxygen with the help of spargers. A reactor environment that best provides low shear and high oxygen transfer along with controlled growth conditions will be suitable for cell cultures at a larger scale.

This dissertation focuses on developing a rotating continuous bioreactor with an internal spiroid embedded on the outer wall that enhances oxygen transfer to the liquid phase. When the

partially-filled reactor is rotating, the spiroid picks up slugs of gas and liquid near the reactor exit and delivers them to the entrance of the reactor. The rotational rate of the reactor can be adjusted to control the flow of gas and liquid in the spiroid (Avvari et al., 2021). The bioreactor is produced using rapid prototyping and can be operated in either batch or continuous mode.

The objectives of this dissertation are:

- to model flow and oxygen transfer (hydrodynamic properties) in the spiroid considering all factors affecting the rate of oxygen transfer.
- to optimize the spiroid for enhanced oxygen transfer using computational fluid dynamics (CFD) and experimentation determining cell growth.
- to conduct cell culture experiments optimizing reactor production for specific cell lines (*Saccharomyces cerevisiae*, Chinese Hamster ovary (CHO)).

References

Avvari, R., Todd, P. W., & Hanley, T. R. (2019, November). Spiroid Design Optimization in a Rotating Continuous Bioreactor for Enhanced Oxygen Mass Transfer. In *2019 AIChE Annual Meeting*. AIChE.

Chapter 2 – Literature Review

2.1 - Cell Culture:

Animal and human cell cultures are widely used as significant tools in various branches of live sciences. Applications of these tools include modeling diseases, cancer research, monoclonal antibody production and therapeutic protein production. The history of cell culture dates to 1665 when the English physicist, Hooke, published his microscopic observations of live organisms. Followed by these studies, Antonie van Leeuwenhoek started working on microscopic observations of various insects, animal cells and human tissues. He was the first person to use histological staining and for his work and became the "Father of Microbiology"(Jedrzejczak-Silicka, 2017).

Cell culture was initially carried out using frog nerve fibers (American et al., 1962). In the early twentieth century, Ross Harrison and Leo Loeb used salt solutions and other buffer medium to keep tissues alive. The hanging drop technique developed by Ross Harrison showed that cells migrated from the tissue to the surrounding environment when it was placed in a drop of medium. The hanging drop method was later adapted by Carrel and his colleague Montrose to study the growth and coverage of cells on glass plates. They also studied that these cells could be transferred into new glass plates several times (Taylor, 2015). This technique of growing cells on glass surfaces is now followed in laboratories for research studies on mammalian cells. Thus, an idea of continuous culture was developed leading to the introduction of the term tissue culture in 1911(Jedrzejczak-Silicka, 2017). The tissue culture method was also employed in studying the primary lesions which occur in cells and cause cancer (Paul, 1962).

John Enders cultured minced tissue on the sides of a "rotating tube" (which is now called the roller bottle). He believed that this technique would help in exchange of nutrients and provided respiration during the time the culture was not in contact with the media. This was the beginning of culturing viruses outside the body and the development of vaccines. In 1951, HeLa cells were isolated and cultured by George Gey and were found to grow so aggressively that they also contaminated other human tumors. This led to the unique marking of HeLa cells (Taylor, 2015). The first hybrid mammalian cells were produced by fusing human and mouse cells in 1965 followed by the production of monoclonal antibodies by Georges Kohler and Cesar Milstein (Hernandez et al., 2014).

2.2 Continuous Bioreactors

Fed-batch and continuous perfusion culture techniques, when combined with sophisticated process strategies, can result in ten to hundred-fold higher productivity (Tapia et al., 2016). Gabardo et al., 2014 investigated the production of ethanol from whey and whey permeate in a continuous fluidized bed bioreactor. K. marxianus strains were cultivated in batch and continuous fluidized bed bioreactors for ethanol productivity comparisons. Continuous cultures generated 6.01 g L^{-1} h^{-1} of ethanol while batch cultivations produced 2.53 g L^{-1} h^{-1}. Based on these findings, two stages of successive continuous operations were carried out to boost ethanol productivity even more. The productivity and concentrations of ethanol were increased to 6.97 g L^{-1} h^{-1} and 70.4 g L^{-1} h^{-1}, respectively.

Monoclonal antibody production from CHO cells in a continuous-flow microbioreactor was three times higher than in a stirred-tank fed-batch reactor. These sequential biopharmaceutical chips can be used for initial screening applications in biopharmaceuticals (Garza-García et al.,

2014). Semi-continuous and continuous flow reactors can sustain cell cultures for longer periods of time. Production of chloroperoxidase in a semi-continuous flow bioreactor led to the harvesting of mycelium free supernatant for 200 days and continuous flows yielded pure enzymes at a rate of 117 mg/day (Hager, 1989).

Mass transfer coefficients were analyzed in the production of hydrogen gas using Rhodospirillum rubrum (Najafpour et al., 2004). Experiments were conducted in batch and continuous bioreactors. A k_La value of 2.7 h^{-1} was observed in batch reactors and a value of 162 h^{-1} was seen in continuous bioreactors. A 59% increase in k_La values was observed in the continuous reactor. A loop of interconnected bioreactors can be used for self-regenerative life support systems in space. Experiments conducted by Gòdia et al., 2002 predicted that these loop bioreactors can be run continuously at the pilot scale.

Citric acid production studies in a continuous airlift bioreactor depicted that the concentration could be maintained stable for 20 days (Rymowicz et al., 1993). Continuous cultures exhibit oscillations that affect the bioreactor stability and productivity. This can be studied and controlled using population balance modelling leading to steady state operations (Zhu et al., 2000). Berson et al., 2008 developed the concept of an automatic feeding roller bottle, instead of a traditional roller bottle, for the continuous culture of cells. A spiroid of tubing placed inside the reservoir delivered fresh media to the cell culture continuously. Hybridoma cell lines were tested, and cell densities were maintained at a steady state for 10 days. Antibody production rate was 3.7 times higher than the traditional roller bottle.

A unique continuous perfusion bioreactor was designed for the large-scale growth of tissue-engineered structures (Gardel et al., 2013). This bidirectional bioreactor facilitates mechanical stimulation of cells by exploiting the shear stress generated by perfusion. To examine

the bioreactor's performance, goat bone marrow stromal cells were cultivated for 14 to 21 days. When comparing continuous cultures to static cultures, alkaline phosphate levels are higher in continuous cultures. Cell movement and distribution were found in SEM measurements, indicating the benefits of culturing the scaffolds in this reactor.

Human carcinoma cells were cultured in a device with continuous perfusion of medium. The unit consists of a circular microfluidic chamber, several narrow perfusion channels, and ports for fluidic access. A 10 x 10 array consists of such individual cells. Cell density of 5×10^7 cells/ml was noticed. This constituted for around 10-fold increase than values reported for cultures in other bioreactors (Hung et al., 2005). Encapsulated hybridoma cells in perfused fluidized-bed reactors produced monoclonal antibodies at a rate of 2.75 $\mu g m L^{-1} h^{-1}$. Continuous operation for 35 days represented a fivefold increase than batch and fed-batch operations (Lecina et al., 2011).

While batch and fed-batch methods are the most used methods in mammalian cell manufacturing, the demand for perfusion systems is growing. The wave-induced bioreactor can generate a cell density of 2.14×10^8 cells/ml and remain in operation for two weeks. The employment of TFF and ATF methods results in cell cultures with a consistency of $20\text{-}35 \times 10^6$ cells/ml, however increasing viscosity creates limits (Clincke et al., 2013). Shear rate increase with the use of cell retention devices such as TFF can be reduced with the use of low shear centrifugal pumps, which in turn maximizes the cell growth, particle concentration and product recovery to comparable levels of ATF (Wang et al., 2017). Coronel et al., 2019 grew suspension cells to a density of 50 x 106 cells/ml in perfusion mode using both ATF and TFF systems in an orbital shaken bioreactor. Cell retention is also affected by the material and pore size used in the ATF device. Changing the hollow fiber material in ATF from polyether sulfone to polysulfone increased the retention rate from 15 ± 8% to 43 ± 18% (Su et al., 2021).

2.3 - Effect of Shear Stress

Many cell types are surrounded by fluids such as the vascular endothelial cells which form the inner layers of blood vessels. The liquid flow around these cells causes mechanical forces also called the shear stress which impacts the cell morphology and behavior in many ways. To avoid these forces, many in vitro experiments are conducted in static conditions. These results do not consider the shear effects on the cell wall. To mimic more in vivo behavior, the experiments must be conducted including flow especially for epithelial cells. The effects of shear stresses depend both on the magnitude and duration of shear forces applied on a cell line. Longer durations with fewer magnitudes also cause detrimental effects. Addition of polymers (like Pluronic) act as barriers around the cell wall and form a protective layer (Hua et al., 1993).

According to Elias et al., 1995, turbulent shear stress effects on KG-1 cells (human erythrocytic leukemia) were decreased with the use of FBS serum. The rate of growth of these cells was high at 2.5 rad/s, and they could not proliferate at higher rotation rates due to the generation of turbulent shear effects. Studies on human brain microvascular endothelial cells showed that under the influence of shear stress of 4-12 dyne/cm^2 (for 40 hours) the proliferation of the cells decreased when compared to static conditions. The cells did not elongate and align when shear stress was applied, which is generally seen in static conditions (DeStefano et al., 2017).

Cell viability and protein secretion levels studied in a packed-bed perfusion bioreactor under a shear stress of 0.21-0.25 N/m^2 readily showed a decrease in cell number. This reduction in the number of cells in the bioreactor is attributed to the continuous shear applied. It was concluded that shear stress must be considered as an important process parameter in the construction of packed bed bioreactors (Duruksu, 2019).

Hepatocytes are very sensitive to shear stresses. A modular bioreactor was tested to culture hepatocytes for over 24 hours. The shear stress in this reactor was first verified to be of the order of 10-5 Pa using preliminary simulations. At flow rates below 500 μL/min, the shear stress could be maintained at 10-5 Pa which maximized cell viability (Mazzei et al., 2010). Aeration and agitation are two important factors for improving oxygen transfer in the bioreactor. Increase in agitation rates, results in high shear forces and causes cell lysis at an early stage of cell culture. To avoid such cases, it is necessary to run the reactors at an optimized agitation rate or rotation rate, which doesn't influence cell viability or proliferation.

The phenomenon of cell lysis at high agitation rates can clearly be seen in suspension bioreactors which study pluripotency of embryonic stem cells (ESCs). To study the pluripotency of ESCs, Gareau et al., 2014 conducted experiments at rotation rates of 100 rpm (6 dyne/cm^2) and 60 rpm (3 dyne/cm^2). These experiments showed that at 60 rpm, pluripotency was maintained by 120% and 141% of static controls for Rex-1 and Sox-2 respectively. While the results for 100 rpm rate show that pluripotency was maintained by 80% and 176% respectively. These studies clearly conclude that cells in suspension bioreactors experience shear and this affects the ability to give rise to cells.

Turbulent zones in a bioreactor are one of the important factors to be considered in the studies of cell culture. These regions tend to generate higher shear forces that damage the cell wall. The effect of these zones was studied in Chinese hamster ovary (CHO) cells by Sieck et al., 2013 using a scale down model. CHO cells are known for growing at a rapid rate under suitable culture conditions. The impact of hydrodynamic stress conditions on CHO cells showed that these cell lines were robust under shear. Although, there was a slight decrease in the monoclonal antibody

production with increasing hydrodynamic stress, cell lysis did not occur, and this decrease was negligible.

Zhang et al., 2013 reported an adaptive response by vascular endothelial cells under step increase of shear stress. These cells were preconditioned to a shear of 15 to 30 dyne/cm^2 for 24 hours and an acute increase shear stress of 30 to 45 dyne/cm^2 was applied. The permeability of endothelial cells nearly doubled for 40 minutes and then decreased gradually. This change was accounted to the adaptive response of the cells under different shear stresses. Out of all the genes, only certain genes responded to the step increase in shear stress transiently.

Aeration of oxygen in the bioreactor for one of the key steps in oxygen transfer is generally done using sparging techniques. Though many methods are available for supplying oxygen to the reactor, sparging of the culture broth with a gas mixture is a practical approach. Chisti, 2000 examined the bubble associated cell damage in sparged bioreactors. Smaller bubbles washed cell lines whereas larger bubbles didn't maintain a stable foam. Consequently, he suggested that the bubble size must be maintained between 10 to 20 mm. The position of impeller and sparger both constitute to cell damage and thus the sparger should be placed such that the rising bubbles do not interact with any impellers. The average energy dissipation must remain below 1.0×10^3 W m^{-3}.

Petersen et al., 1988 discussed the dependence of shear sensitivity on growth pattern, culture age and metabolite concentration. Cell damage was observed when shear stress was increased on hybridoma cells. It was accounted to the fact that accumulation of waste in later stages of cell growth causes cells lysis. The levels of metabolic waste cause physiological changes to the cells which adversely affect shear sensitivity. During the stationary phase, cells appeared to be robust when compared to later stages of growth. The formation of metabolites affects the pH of the medium, resulting in shear sensitivity. The damages cause by agitation and aeration can be

suppressed by using additives such as serums, Pluronic polyols, derivatized cellulose and other protective agents (Papoutsakis, 1991). The addition of surface-chemicals like Pluronic F68 can reduce the hydrophobicity of cell surface and act as protective agents against shear (Wu, 1996).

2.4 - Gas-Liquid Mass Transfer

Aeration is one of the key factors that maximizes the productivity of bioreactors. In aerobic bioprocesses, oxygen is the primary substrate used by microorganisms for growth, maintenance, metabolite production and its scarcity affect the process performance (Garcia-Ochoa et al., 2009). The transfer of gas from gas phase to the microorganism suspended in a bioreactor follows a certain pathway, and it includes eight resistances that exist between the gas bubble and microorganism (Kadic et al., 2014). Most of these resistances are physical and are neglected in bioreactors except the one near the gas-liquid interface. The liquid film resistance controls the overall mass transfer rate.

One of the earliest hypotheses proposed by Lewis and Whitman in 1924 was the two-membrane theory of interphase mass transfer. The idea proposed a thick film in both the gas and liquid phases separated by an interface. This theory proposes that mass transfer occurs through the interface by molecular diffusion through the membrane under steady-state conditions, and small fluxes and mass transfer at low concentrations (Drahansky et al., 2016). A schematic of this theory is shown in Figure 2.1.

The molar flux through each film is described as the product of the driving force by the mass transfer coefficient and is given by the equation

$$J^0 = k_G(p_G - p_i) = k_L(C_i - C_L) \tag{2-1}$$

where J^0 is the molar flux of oxygen (mol/m^2S), k_G is the gas side mass transfer coefficient (mol/ m^2S Pa), k_L is liquid side mass transfer coefficient (m/s), p_G - oxygen partial pressure in gas bubble (Pa), p_i- interface gas phase concentration (Pa), C_i- interface liquid phase concentration (mol/m3), C_L- dissolved oxygen concentration in bulk liquid (mol/m^3)

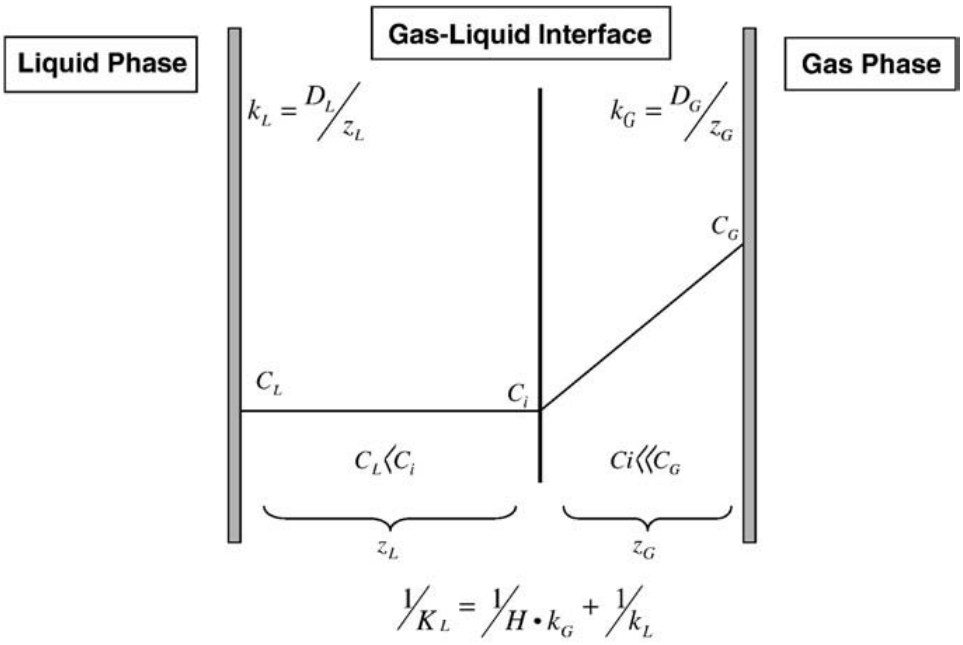

Figure 2.1 - Schematic Representation of Two Film Theory (Garcia-Ochoa, 2009)

As the calculation of interfacial concentrations cannot be done directly, considering the overall mass transfer coefficient yields the following equation:

$$J^0 = K_G(p_G - p^*) = K_L(C^* - C_L) \tag{2-2}$$

where p^* is equilibrium partial pressure with liquid phase (Pa), C^* is saturated oxygen concentration in bulk liquid, K_G (mol/ m^2S Pa) and K_L (m/s) are overall mass transfer coefficients. Combining equations (2-1) and (2-2) with the use of Henry's law ($p^*=HC^*$), the following equation is obtained:

$$\frac{1}{\mathrm{K_L}} = \frac{1}{Hk_G} + \frac{1}{k_L} \tag{2-3}$$

Since oxygen is sparingly soluble in water, H is very large and the greater resistance for mass transfer is on the liquid side of the interface. Thus, neglecting the gas phase resistance reduces the overall mass transfer coefficient to local liquid phase coefficient.

$$K_L = k_L \tag{2-4}$$

The oxygen mass transfer rate per unit reactor volume is obtained by multiplying the gas-liquid interfacial area and the overall flux as follows:

$$N_{O_2} = aJ^0 = k_L a(C^* - C_L) \tag{2-5}$$

k_L and a are difficult to be measured separately and hence the product $k_L a$ which is called the volumetric mass transfer coefficient is measured.

Mass balance for dissolved oxygen in liquid phase can be written as follows:

$$\frac{dC}{dt} = OTR - OUR \tag{2-6}$$

where $\frac{dC}{dt}$ is the oxygen accumulation rate, OTR represents the oxygen transfer rate and OUR represents the oxygen uptake rate.

The volumetric mass transfer coefficient can be measured experimentally by available physical and chemical methods. One of the most widely used chemical methods is sulfite oxidation, which uses sodium sulfite to convert dissolved oxygen to sulfate (Garcia-Ochoa, 2009). Although this method is easy to implement, it has a disadvantage because the hydrodynamics of the solution can change, which in turn can affect the $k_L a$ value. Physical methods are the most used because they utilize the response of oxygen probes to changes in concentration in the medium. The dynamic method can be used to study the influence of operating conditions on volumetric mass transfer coefficients (Sánchez Mirón et al., 2000).

2.5 - Oxygen Transfer

Oxygen is a crucial nutrient for most aerobic organisms. These microorganisms do not directly take up oxygen from a gas phase as they are always in an aqueous environment and rarely in direct contact with a gas. They utilize the dissolved oxygen present in the liquid (medium) surrounding them. The solubility of oxygen in water is low when compared to any other nutrient provided for cell culture. Other nutrients deplete at a slower rate when compared to oxygen and hence it must be supplied continuously into the reactor. Oxygen can be supplied either by continuously providing soluble oxygen in liquid or provide a gas phase to allow oxygen to diffuse from gas into liquid medium (Hu, 2017).

Ju et al. (1991) proposed a possible method of using perfluorocarbon (PFC) emulsions to increase the oxygen carrying capacity in bioreactors. Oxygen enhancement was achieved by adding 15% (v/v) PFC emulsions to the reactor and confirmed using *E. coli* fermentations. At a higher percentage of PFC volume fractions (25%), the enhancement was poor and was due to the increase in viscosity with increase in volume. Addition of oxygen vectors such as n-dodecane to culture broths enhances the oxygen mass transfer without increasing the energy consumption for mixing or aeration (Galaction et al., 2004). A 20% increase in yeast concentration was seen in an airlift bioreactor with the use of n-dodecane as oxygen vector (Jia et al., 1997).

The effect of change in organic phase and aqueous phase concentrations on k_La was also studied by Amaral et al. (2008). Use of olive oil as second liquid phase has a negative impact on the OTR. When perfluorodecalin (0.2 volume fraction) was used in combination of YPD as aqueous phase, a k_La value of 64.6 h^{-1} was observed. Silicone oil when added as an oxygen vector in a three phase airlift bioreactor increased oxygen transfer by 65% and by 84% in a stirred tank

reactor (Quijano et al., 2009). With increase in viscosity of petroleum based liquids, oxygen transfer in airlift bioreactors decreased giving rise to turbulent regions (Mehrnia et al., 2005).

Conventional aqueous systems use spargers to increase the continuous supply of oxygen. Although there is continuously supply of oxygen, oxygen transfer limitations still occur. Rates of oxygen absorption can be increases using oil-in-water systems instead of aqueous medium (Mcmillan et al., 1987). The author deduced from the experiments that with increase in oil volume fraction, the oxygen transfer rate (OTR) increased linearly for a 1.25 L fed-batch E. coli fermentation. The maximum OTR was about 400% on a per liter aqueous phase basis. A 250% OTR enhancement was noticed in reactors using the fermenter headspace pressurization principle. Such reactors were best for cell lines which are very sensitive to the conventional systems (Yang et al., 1992).

To determine the dissolved oxygen concentration, the transfer rate of oxygen from the gas phase to the liquid phase must be known. Gas-liquid mass transfer depends on the characteristics of the physicochemical conditions of the culture, the geometrical parameters of the reactor, the operating conditions, and the number of oxygen-consuming cells (Garcia-Ochoa, 2009). It is mainly influenced by process variables such as impeller speed, air flow rate, temperature, viscosity, and the percentage of loading of biomass supporting particles (Özbek et al., 2001).

The effect of changing the impeller configuration on the novel bioreactor shows that the OTR increases, and the impeller uses less power, both beneficial in cell culture (S. J. Wang et al. 1996). The presence of cells as solid particles decreases oxygen transfer, cell respiration and change in cell concentration in bubble-aerated bioreactors enhances oxygen transfer rate. The decrease in oxygen transfer was accounted to low oxygen permeability near the interface (L. K. Ju et al., 1995). Oosterhuis et al. (1984) proposed a model to study the local dissolved oxygen

concentration in the reactor along with the overall mass transfer coefficients using empirical laws. The model developed could be used to associate the mass transfer coefficients with stirrer speed and gas flow.

Experimental investigation of oxygen transfer coefficient in shaking bioreactors was done using the sulphite oxygen method by Maier et al. (2001). The author postulated that the mass transfer coefficient was affected by operating conditions such as shaking diameter, filling volume, shaking frequency and viscosity of the medium. Based on these observations, the author developed a model for calculating the mass transfer coefficient for various operating conditions in shaking bioreactors. The liquid film on the flask wall had highest impact on the specific mass transfer area. A shaking speed of 120 rpm in cylindrical bioreactors reported a k_La values between10 and 30 h^{-1} and a speed of 75 rpm showed a k_La value of 8 h^{-1} (X. Zhang et al., 2009).

Few of the initial studies for enhancing oxygen transfer phenomenon included the use floating bubble breakers. Rising bubbles from spargers sometimes interfere the position of impellers in reactors decreasing the oxygen mass transfer. Johnson et al., (1990) noticed that the use of foam breakers for mammalian cell cultures along with high aeration rates decreased oxygen mass transfer by 25%. Kang et al., (1991) showed that the use of floating bubble breakers in a three-phase fluidized bed increased volumetric mass transfer coefficient by 25% but decreased with increase in viscosity.

Nikakhtari et al. (2005) depicted the use of a packed bed in an external loop airlift reactor for enhancing oxygen transfer. A mathematical model was developed and studied in comparison with experimental results to analyze the mass transfer of oxygen with respect to time and space. The experimental data perfectly fit into the model showing that there was 3.7 times increase in

OTR in the packed bed loop reactor when compared to the conventional looped reactor indicating the feasibility of the reactor.

Novel bioreactors have been developed to address the issue of aeration and oxygen mass transfer. One such reactor is the shaken helical track bioreactors. Cultivation of mammalian cells on large scale increasing gas-liquid transfer was the main aim of this reactor. With a helical track attached to the wall of the cylinder, there is an increase in gas liquid contact areas which resulted in a 5 to 10-fold increase in mass transfer. CHO cells when cultured in a 55 L helical track reactor showed a significant increase in cell growth compared to the standard reactors. At a shaking speed of 39 rpm, with a working volume of 1000 L, k_La values of 10 h^{-1} were noted. These results were accounted to special velocity field created by orbital shaking in these reactors (X. Zhang et al., 2008).

Single use, technology bioreactors are developing on a larger scale because of their ease of use. The wave bioreactor is a similar kind which cultures cells and has the benefit of disposing once done. Oxygen transfer in standard cell bag systems can be maximized using spargers. Saccharomyces cerevisiae when culture in standard cell bag showed that the mass transfer coefficient was 38 h^{-1}. The wave bioreactor had oxygen transfer coefficients of 60 h^{-1}. This was due to the use of oxygen blended and oxygen sparged cell bags used in this reactor (Mikola et al., 2007).

Berson et al., 2002 studied the growth of four different mammalian cells (CHO, SP2/0, HeLa, and NS/1) in a recirculation loop attached in a roller bottle. With rotation of the reactor, the loop picks up gas liquid plugs and delivers them to the other end of the chamber. To determine the effectiveness of the recirculation loop, experiments were first conducted in batch mode, which makes the reactor like other conventional bioreactors. After achieving a required density, the

experiments were carried out in continuous mode to test the reactor's ability to maintain it for a longer duration. Data was also generated in standard roller bottles at once for these cell lines for comparison. The cells grew at higher densities when compared to standard roller bottle reactors. An average cell density of 5.4×10^6 cells/mL was seen. This increase in cell densities was accounted to addition of the recirculation loop which continuously supplies the medium with oxygen. Berson accounted that axial liquid mixing resulted in increase of gas liquid mass transfer and added to the list of advantages was the ease of scale up.

Rotation rates of the reactors have a positive impact on oxygen transfer in most rotational bioreactors. Baffled roller bioreactors showed an increasing tendency in the mass transfer with increasing rotational rates between 5 and 50 rpm (H. Nikakhtari et al., 2014). Rotator culture methods provide a continuous flow of oxygenating gas to cultures in rotating bottles. These maintain constant oxygen and carbon dioxide levels in culture medium (New et al., 1979). Conducting cell cultures on a large scale maximizes the capital required. Mini bioreactors can be used for this purpose to avoid excess use of costly substrates. The cell strain and media optimization can be studied in these bioreactors and then easy scale up can be done (Kumar et al., 2004).

Oxygen supply under high viscosity and low shear in plant cell suspensions is possible with the use of the rotating principle in rotating drum fermenters (Tanaka et al., 1983). Three-dimensional growth of endothelial cells for 30 days in rotating wall vessel (RWV) bioreactors was studied with respect to the rotation rate. With increase in rotation rate from 8 rpm to 15 rpm, the production was increased by 73% and 262% respectively (Sanford et al., 2002). High oxygen concentrations were seen at high rotations rates in RWV bioreactor (Kwon et al., 2008). Zhang et al., 2012 investigated the characteristics of gas liquid mass transfer in a rotating drum bioreactor

(RDB). The effect of sparger and lifters in the novel RDB on mass transfer performance was investigated. At an aeration rate of 0.256 vvm, the mass transfer coefficient had little impact with increase in number of lifters whereas it has a high impact when a high aeration rate of 0.513 vvm was used. The reason for this was at high aeration rates, the liquid film renewal occurs quickly causing a movement of bubbles. The performance of this RDB was compared to that of bench scale RDM to determine the percentage increase of mass transfer. In the large scale RDB, the mass transfer coefficient was comparatively low because of a smaller aeration area. A greater width of lifters can increase the transfer rate at low aeration rates (Zhang et al., 2012).

Synthecon's rotary cell culture system (RCCS) produces 3D cultures in a low shear stress, microgravity environment. A horizontally rotating cylinder with a coaxial oxygenator is used as the culture system. The vessel is filled with culture medium providing zero head space. The oxygenator also rotates at the same velocity as the outer wall. RCCS can suspend cells without causing mechanical shear (as seen in spinner flasks) along with high mass transport of nutrients and oxygen. The addition of support materials in a bioreactor has a negative impact on gas-liquid mass transfer. Linear decrease in mass transfer was seen with increase in concentration of biomass support materials (Apar, 2010). With the implementation of good manufacturing standards for cell treatments, innovative suspension bioreactors may create a 25-fold growth of human embryonic cells in six days as compared to static culture flasks (Krawetz et al., 2010).

Computational frameworks based on metabolic–hydrodynamic coupling can provide informative insights on cell lifelines and metabolic responses induced by environmental fluctuations in an industrial bioreactor (G. Wang et al., 2020). The integration of modeling and experiments can be used to determine the transfer of mammalian cell culture processes and the physical characterization of bioreactors. The findings of these analyses can be used to validate

scale up and scale down procedures (Villiger et al., 2018). Guo et al. (2018) investigated the manufacturing and scaling up of docosahexaenoic acid (DHA) using computational fluid dynamics (CFD). Various impeller combinations were studied to generate a homogeneous flow field environment in the bioreactor, and the reactor was optimized to productivity of 326.5 mg/ (L h).

Teng et al., (2021) used a similar technique to analyze the behavior of BHK- 21 cells in three different sized scaled-up bioreactors using CFD. The results of itaconic acid optimization studies in a flask level stirred tank bioreactor utilizing the classical one factor approach and statistical experiment designs demonstrated the viability of high production on scale up (Bafana et al., 2019). He et al. (2019) created a mass transfer approach for calculating gassing requirements in the bioreactor cell culture environment. Predictive modeling may also help with carbon dioxide gassing by estimating the range of a gas flow meter. Das et al., (2019) demonstrated the use of microcarrier-based bioreactor systems for continued development and scale-up of flask-based mesenchymal stromal cells (MSC).

Single-use bioreactors (SUB) may benefit shear-sensitive cell lines and may also be useful in continuous perfusion operations. SUBs enable scalable parallel cultivation on a tiny scale without cleaning, and numerous types of plates and small reaction vessels are already available. When employed on a wider scale, continuous culture systems with cell retention are a better option to batch and fed-batch approaches (Junne et al., 2018). The addition of sensors to all bioreactor scales allows for robust and dependable online monitoring of cellular proliferation in all fed-batch cultures. This can result in rapid process development and risk minimization, and hence a more robust production process (Metze et al., 2020).

2.6 - Computational Fluid Dynamics (CFD)

Design, construction, and evaluation of large-scale bioreactors is time consuming and costly. The use of CFD as a tool to determine the fluid characteristics in bioreactors may give few insights on the factors affecting these parameters (Werner et al., 2014). A hybrid multizonal CFD model was used to predict the behavior of shear forces and mass transfer at different rates in a bioreactor producing xanthum gum. The results from this model could accurately depict the flow characteristics in the bioreactor (Bezzo et al., 2003). The prediction of sludge rheology and design factors for a membrane bioreactor was difficult. The effect of these factors on the hydrodynamics of the bioreactor were nearly impossible to calculate from various experiments.

Brannock et al. (2010) used the bioreactor and membrane module in CFD to determine the effect on sludge settling and rheology on bulk mixing. They also used this as an optimization tool to determine the reactor design features. 3D steady simulations could track particle trajectories (microorganism movements) in a photo bioreactor for an effective tracer time of 11 hours using a commercial code CFX5.7 (Luo et al., 2011). Oxygen transfer being one of the limiting factors in cell growth was modeled by Dhanasekharan et al. (2005) using population balance method (PBM). A multi-fluid Eulerian model was used to interpret the gas liquid mass transfer mechanism. Bubble breakage and coalescence were modelled using the PBM method. To reduce the computational time, flow geometry was composed of 23,000 cells and only one half of the symmetric geometry was used. The mass transfer coefficients and gas holdup results from the CFD model were in a good agreement with the experimental data generated.

Zhang's CFD work (2005) on mammalian cell culture in shake flasks showed a difference in the experimental and simulation results of volumetric mass transfer and power input. Volume of fluid method was used to simulate the gas liquid interface and generate the velocity vectors at

different rotation rates of the shake flasks. The difference in simulated and experimental values was accounted for change in other factors like pH, temperature, and nutrient concentration (Zhang et al., 2005). Bioreactors used for cartilage tissue engineering were modeled for mass transfer and shear stresses based on the position of constructs. A species mass transfer model was used to determine the oxygen depletion around the construct surfaces. Results show oxygen concentrations higher than in vivo, which determines that these concentrations do not affect the growth of chondrocytes. (Williams, Saini, and Wick, 2002).

A simple and fast CFD base compartment model was developed by Delafosse et al., 2014 to generate the spatial distributions of concentrations during the mixing process in stirred bioreactors. Unlike the classical compartment model, this model reproduces with good accuracy. Wang et al., (2010) could simulate the coupled hydrodynamics-reaction kinetic model of a sludge bed bioreactor. They simulated the flow of a three phased (gas-liquid-solid) bioreactor for the first time and evaluated that this method cannot be applied for highly unsteady systems. A 50 L single-use bioreactor was modeled for gas-liquid mixing and bubble size distribution. A multiphase fluid model along with population balance module in FLUENT was used to determine the maximum sparger-to-impeller diameter. The optimum ratio was obtained as 0.8 and was validated using experimental values. A correlation between k_La and operating parameters of the reactor was determined. This relation was used to further optimize the reactor's geometry and design. The k_La measured from experiment at a tip speed of 0.6 and aeration rate of 0.1 vvm was 7.3 hr^{-1} whereas the model predicted it to be 18.2 hr^{-1} for a constant bubble size. The PBM model with bin sizes predicted a more accurate value of 8 hr^{-1}. The significance of these parameters was verified with statistical interactions and conducting a full factorial DOE (Amer et al., 2019). Ashfaq et al. (2019) studied the transport of iodine from a scrubbing solution in a venting system using ANSYS

FLUENT. The dependency of the iodine mass transfer on the diameter of the liquid droplets was postulated using a user defined mass transfer model in FLUENT. A two-phase Euler-Euler multiphase modelling approach was used along with species transport model to describe the phenomenon occurring. Increase in mass transfer, increase of iodine in liquid phase and decrease in gas phase was observed with decrease in droplet diameter. This could verify the dependency of mass transfer on droplet diameter and venturi length. Bubble size distribution is an important factor when considering the hydrodynamics of bubble column bioreactors. The population balance model (PBM) in FLUENT is used to determine the effect of bubble size, bubble breakage, coalescence on the reactor dynamics.

Shi et al., 2019 proposed a bubble-induced turbulent model to determine the bubble breakage effects caused due to turbulent eddies. Two different cases of bubble columns with diameters of D = 0.44 m and D = 0.15 m were studied and the results were consistent with experimental data. Thus, the bubble-induced turbulent model is an appropriate one to study the eddy interactions in bubble columns. Along with this, the mass transfer mechanism can be predicted using surface renewal model making few modifications to include the turbulent eddy interactions (Shi, 2019). Miniature geometries are used to study the effect of different geometric parameters on flow characteristics. These devices are considered safe for fast and hazardous chemical reaction. The large surface to volume ratio available in these devices is proved to increase the heat and mass transfer.

Prakash et al. (2019) studied the flow characteristics in a serpentine pipe and compared the obtained mass transfer to that of a straight pipe. The experiments conducted used a high-speed camera to determine the flow type within the capillary. A straight pipe and serpentine pipe (diameter of 2 mm) with toluene and water were considered for this study. Slug flow regime was

observed in the straight pipe and slug flow with droplets was seen in the serpentine pipe. Mass transfer efficiency improved by a factor of 1.2 in the serpentine pipe. This was accounted to the return bends in the pipe. This phenomenon was simulated in ANSYS to find that there were secondary flows within the serpentine pipe which was used to determine the critical velocity for this geometry (Prakash, 2019). Simulation results help us in understanding the flow characteristics affecting hydrodynamics and mass transfer. Shear stresses, turbulent kinetic energy, turbulent dissipation rate, bubble velocity are few of the many factors contributing to higher cell death (Liu, Zhang, and Zhou, 2019).

Gas holdup, superficial gas velocity, complex fluid behavior can also be studied using computational fluid dynamic simulations (Lu, Long, Ding, and Deng, 2019). Volumetric mass transfer coefficient increases with increase in gas-liquid interfacial area and in areas where turbulent energy dissipation rate is higher. A similar kind of behavior was observed by Santos-Moreau et al. (2019) in CFD studies of stirred tank reactor. A Eulerian multiphase model was used to study the impact of impeller speeds on local mass transfer coefficients. The local values ok kLa were higher at regions close to the impeller. This model was able to predict the interphase mass transfer rate with accuracy as the results obtained showed good agreement with experimental observations.

A sensitivity analysis on the exact geometry of a gas sparger in an airlift loop reactor was done using two-dimensional and three-dimensional simulations in the work of Mudde et al. (2001). Two fluid model was used to consider the effects of virtual mass, drifting velocity, turbulence production and dissipation by the bubbles. Two-dimensional simulations were able to correctly predict most characteristics of the flow behavior but underpredicted gas fractions due to the existence of low frictions in 2-D geometries. The circulation rate was 30% overpredicted in two-

dimensional studies than that of three-dimensional ones. The gas-inlet geometry was particularly sensitive to changes in two-dimensional simulations. Oxygen transfers in pump-oxygenators (artificial lungs) were simulated using ANSYS by Fill et al. (2008) before physical fabrication to predict performance, optimize flow parameters, mass transfer.

2.7 Effect of Temperature on Cell Culture

Cell viability and proliferation is majorly affected by the temperature at which it is stored, handled and cultured. Most mammalian cells thrive at around 37°C but to provide stability they must be maintained at an optimal temperature. Yeast cells can grow over a range of 0°C to 47°C but the growth rate is highest at 30°C (Salari and Salari, 2017). Rodríguez-Carmona et al. (2012) studied the effects of temperature in the production of recombinant antibody fragments in *E. coli*. The results showed that decreasing the temperature from 37°C to 33°C to 30°C increased the product yield.

Recombinant CHO cell lines were tested for temperature dependency by Furukawa et al. (1998). A maximum level of cell growth was seen at 36°C and cells were completely arrested at 32°C. The highest productivity and cellular productivity were obtained when cultured at 35°C and 32°C respectively. Kovářová et al. (1996) examined the growth of *E. coli* at temperatures greater than 37°C in a continuous culture. The culture was grown with glucose and at different dilution rates to determine the steady concentration at 40°C. At 37°C, the growth rate was 0.204 h^{-1}, increasing to 0.485 h^{-1} at 40°C.

HEK-293 cells are used to express recombinant proteins and are cultured at 37°C. A higher protein yield and higher expression is desirable. The studies conducted by Lin et al. (2015) showed that reducing the temperature from 37°C to 33°C (after 24 hours transfection time), the total protein

production increased by a factor of 1.5. A similar decrease in temperature in CHO cells increased the overall product yield by a factor of 3.4 compared to standard temperature of 37°C (Kaufmann et al., 1999). This increase in productivity at low temperatures was accounted to the increase in mRNA levels and its stability (Kou et al., 2011).

Experiments conducted by Oguchi et al. (2003) resulted in a two-fold increase of antibody production when the temperature of CHO cell culture was reduced from 37°C to 31°C. Protein glycosylation using mammalian cells showed that a decrease in temperature from 35.5°C to 34°C reduced the terminal sialic acid by 10% whereas the overall glycosylation profile was unchanged (Sajan et al., 2010).

2.8 - Effect of pH on Cell Culture

Change in pH greatly influences the growth of cells. Some grow at higher pH values while some thrive at neutral and low pH values. Cell lysis takes place if they are cultured below or above the minimum and maximum values of pH. Hence, it is necessary to determine the optimal pH for the culture used in the bioreactor. Hawley-Nelson, et al. (1980) saw an optimal growth rate in human epidermal cells at a pH of 7.0-7.2. Long-term survival of cells was influenced with change in pH. At a pH of 7.6, cells could not be sub-cultured while cultures survived four passages at a pH of 6.8. Tupý et al., 1984 observed that tobacco pollen in suspension culture showed an optimal growth at a pH of 5.9 as it depends on the buffering capacity of pollen medium.

Maximum growth of mammalian cells is observed in the pH range of 7.38 to 7.87 (Cosmo G. Mackenzie, Julia B. Mackenzie, 1961). Ten strains of rumen bacteria were grown at a dilution rate of 0.165 h-1 in a continuous culture. A low pH appeared to decrease the cell yields. Large

changes in pH were observed when the cultures were washed off. S. bovis produces more lactate when the pH falls below 5.75. (Russell and Dombrowski, 1980).

The study of pH values in HeLa cells by Barton, 1971 in batch suspension culture revealed a characteristic pattern. The sample was analyzed for 24 hours It operates as a chemostat to provide more nutrients each time fresh medium is added. As the pH increased from 6.8 to 7.5, an increase in glucose consumption and lactate production of HeLa cells increased. This result couldn't be related to cell multiplication as the rate of increase in glucose consumption and lactate production was seen at a pH of 7.8 when cell multiplication was minimal. The authors linked this pattern of increased and decreased depletion to cell aggregation in suspension culture. In cultured mouse neuroblastoma cells, PH alterations can influence their growth, neurite production, and acetylcholinesterase activity (Bear and Schneider, 1977).

CHO cells grow over a broader range of pH than human or mouse cells, centering at approximately pH 7.2-7.4. Optimum pH was independent of serum concentration in the culture of different mammalian cells (Eagle, 1973). Yoon et al., 2005 studied the effect of culture pH on erythropoietin (EPO) produced by CHO cells. Highest specific growth rate and viable concentrations were obtained at pH values of 7.0 and 7.2, respectively. EPO productivity was optimal at a pH of 7.0. Ozturk et al., 1991 observed a two-fold increase in specific antibody production at a pH of 7.2 in hybridoma cell culture. Saccharomyces cerevisiae when cultured at a pH of 4 showed an increase in reproduction and growth. This condition provided the largest size (2 x 3μ) of yeast cells (Salari and Salari, 2017).

2.9 - 3D Printing / Rapid Prototyping

3D printing techniques have gained popularity over the decades for various biomanufacturing applications. Recent trends are seen in the use of vascular implants for tissue engineering. Blume et al., 2022 outlines the potential of these vascular implants for 3D printing advanced therapeutic drug products in biotechnology. Use of electrode impedance spectroscopy (EIS) along with rapid prototyping in bioreactor design allowed the reactor system to maintain a shear rate of 0.001 dyne cm-2 which can be used to cultivate epithelial cells and this technology integrated with organ-on-chip is a powerful tool for online analytics, (Linz et al., 2021). Photopolymerization is a technique frequently used which refers to the curing of photo-reactive polymers by using a laser, light or ultraviolet (UV) and one such technique is stereolithography (SLA). Materials used for this method are usually liquids that will harden when it is exposed to UV light producing high quality surfaces. (Shahrubudin et al., 2019). Another widely used technique is powder fusion processing, which relies on the deposition of molten or bonded layers of powder to make parts. The Selective laser sintering (SLS) enables fusion of one layer over the other with the help of a laser and has an advantage of less material wastage (Arefin et al., 2021).

References

Amer, M., Feng, Y., & Ramsey, J. D. (2019). Using CFD simulations and statistical analysis to correlate oxygen mass transfer coefficient to both geometrical parameters and operating conditions in a stirred-tank bioreactor. *Biotechnology Progress*, *35*(3), 1–14.

American, T., & Harrison, R. G. (1962). *Cell culture technology : it all started with frog nerve fibres*.

Barton, M. E. (1971). Effect of pH on the growth cycle of HeLa cells in batch suspension culture without oxygen control. *Biotechnology and Bioengineering*, *13*(4), 471–492.

Berson, R. E., & Friederichs, G. (2008). A self-feeding roller bottle for continuous cell culture. *Biotechnology Progress*, *24*(1), 154–157.

Bezzo, F., Macchietto, S., & Pantelides, C. C. (2003). General hybrid multizonal/CFD approach for bioreactor modeling. *AIChE Journal*, *49*(8), 2133–2148.

Chisti, Y. (2000). Animal-cell damage in sparged bioreactors. *Trends in Biotechnology*, *18*(10), 420–432.

Clincke, M. F., Mölleryd, C., Zhang, Y., Lindskog, E., Walsh, K., & Chotteau, V. (2013). Very high density of CHO cells in perfusion by ATF or TFF in WAVE bioreactor^{TM}: Part I: Effect of the cell density on the process. *Biotechnology Progress*, *29*(3), 754–767.

Coronel, J., Behrendt, I., Bürgin, T., Anderlei, T., Sandig, V., Reichl, U., & Genzel, Y. (2019). Influenza A virus production in a single-use orbital shaken bioreactor with ATF or TFF perfusion systems. *Vaccine*, *37*(47), 7011–7018.

Cosmo G. Mackenzie, Julia B. Mackenzie, P. B. (1961). The Effect of pH on and Growth , Protein Synthesis , Of Lipid-Rich Particles Cultured Mammalian Equilibration of Medium with C02. *The Journal of Biophysical and Biochemical Cytology*, *9*, 141–156.

Delafosse, A., Collignon, M. L., Calvo, S., Delvigne, F., Crine, M., Thonart, P., & Toye, D. (2014). CFD-based compartment model for description of mixing in bioreactors. *Chemical Engineering Science*, *106*, 76–85.

DeStefano, J. G., Xu, Z. S., Williams, A. J., Yimam, N., & Searson, P. C. (2017). Effect of shear stress on iPSC-derived human brain microvascular endothelial cells (dhBMECs). *Fluids and Barriers of the CNS*, *14*(1), 1–15.

Drahansky, M., Paridah, M. ., Moradbak, A., Mohamed, A. ., Owolabi, F. abdulwahab taiwo,

Asniza, M., & Abdul Khalid, S. H. . (2016). We are IntechOpen , the world ’ s leading publisher of Open Access books Built by scientists , for scientists TOP 1 %. *Intech*, *i*(tourism), 13.

Elias, C. B., Desai, R. B., Patole, M. S., Joshi, J. B., & Mashelkar, R. A. (1995). Turbulent shear stress—Effect on mammalian cell culture and measurement using laser Doppler anemometer. *Chemical Engineering Science*, *50*(15), 2431–2440.

Eric Berson, R., Pieczynski, W. J., Kurt Svihla, C., & Hanley, T. R. (2002). Enhanced mixing and mass transfer in a recirculation loop results in high cell densities in a roller bottle reactor. *Biotechnology Progress*, *18*(1), 72–77.

Furukawa, K., & Ohsuye, K. (1998). Effect of culture temperature on a recombinant CHO cell line producing a C-terminal α-amidating enzyme. *Cytotechnology*, *26*(2), 153–164.

Gabardo, S., Rech, R., Rosa, C. A., & Ayub, M. A. Ô. Z. (2014). Dynamics of ethanol production from whey and whey permeate byimmobilized strains of Kluyveromyces marxianus in batch andcontinuous bioreactors. *Renewable Energy*, *69*, 89–96.

Galaction, A. I., Cascaval, D., Oniscu, C., & Turnea, M. (2004). Enhancement of oxygen mass transfer in stirred bioreactors using oxygen-vectors. 1. Simulated fermentation broths. *Bioprocess and Biosystems Engineering*, *26*(4), 231–238.

Garcia-Ochoa, F., & Gomez, E. (2009). Bioreactor scale-up and oxygen transfer rate in microbial processes: An overview. *Biotechnology Advances*, *27*(2), 153–176.

Gardel, L. S., Correia-Gomes, C., Serra, L. A., Gomes, M. E., & Reis, R. L. (2013). A novel bidirectional continuous perfusion bioreactor for the culture of large-sized bone tissue-engineered constructs. *Journal of Biomedical Materials Research - Part B Applied Biomaterials*, *101*(8), 1377–1386.

Gareau, T., Lara, G. G., Shepherd, R. D., Krawetz, R., Rancourt, D. E., Rinker, K. D., & Kallos, M. S. (2014). *Shear stress in fl uences the pluripotency of murine embryonic stem cells in stirred suspension bioreactors*. (June 2012), 268–278.

Gòdia, F., Albiol, J., Montesinos, J. L., Pérez, J., Creus, N., Cabello, F., … Lasseur, C. (2002). MELISSA: A loop of interconnected bioreactors to develop life support in Space. *Journal of Biotechnology*, *99*(3), 319–330.

Hua, J., Erickson, L. E., Yiin, T. Y., & Glasgow, L. A. (1993). A review of the effects of shear and interfacial phenomena on cell viability. *Critical Reviews in Biotechnology*, *13*(4), 305–328.

Hung, P. J., Lee, P. J., Sabounchi, P., Lin, R., & Lee, L. P. (2005). Continuous perfusion microfluidic cell culture array for high-throughput cell-based assays. *Biotechnology and Bioengineering*, *89*(1), 1–8.

Indexed, I., Reviewed, P., & Journal, S. (2012). *International Journal of Current Research and Review*. *04*(7), 1–154.

Jedrzejczak-Silicka, M. (2017). History of Cell Culture. In *New Insights into Cell Culture Technology*: *Vol. i* (p. 13).

Jia, S., Wang, M., Kahar, P., Park, Y., & Okabe, M. (1997). Enhancement of yeast fermentation by addition of oxygen vectors in air- lift bioreactor. *Journal of Fermentation and Bioengineering*, *84*(2), 176–178.

Johnson, M., André, G., Chavarie, C., & Archambault, J. (1990). Oxygen transfer rates in a mammalian cell culture bioreactor equipped with a cell-lift impeller. *Biotechnology and Bioengineering*, *35*(1), 43–49.

Ju, L. -K, Lee, J. F., & Armiger, W. B. (1991). Enhancing Oxygen Transfer in Bioreactors by Perfluorocarbon Emulsions. *Biotechnology Progress*, *7*(4), 323–329.

Ju, L. K., & Sundararajan, A. (1995). The effects of cells on oxygen transfer in bioreactors. *Bioprocess Engineering*, *13*(5), 271–278.

Kang, Y., Fan, L. T., Min, B. T., & Kim, S. D. (1991). Promotion of oxygen transfer in three-phase fluidized-bed bioreactors by floating bubble breakers. *Biotechnology and Bioengineering*, *37*(6), 580–586.

Kaufmann, H., Mazur, X., Fussenegger, M., & Bailey, J. E. (1999). Influence of low temperature on productivity, proteome and protein phosphorylation of CHO cells. *Biotechnology and Bioengineering*, *63*(5), 573–582.

Kou, T. C., Fan, L., Zhou, Y., Ye, Z. Y., Liu, X. P., Zhao, L., & Tan, W. S. (2011). Detailed understanding of enhanced specific productivity in Chinese hamster ovary cells at low culture temperature. *Journal of Bioscience and Bioengineering*, *111*(3), 365–369.

Kovářová, K., Zehnder, A. J. B., & Egli, T. (1996). Temperature-dependent growth kinetics of Escherichia coli ML 30 in glucose-limited continuous culture. *Journal of Bacteriology*, *178*(15), 4530–4539.

Kwon, O., Devarakonda, S. B., Sankovic, J. M., & Banerjee, R. K. (2008). Oxygen transport and consumption by suspended cells in microgravity: A multiphase analysis. *Biotechnology and*

Bioengineering, *99*(1), 99–107.

Lecina, M., Tintó, A., Gálvez, J., Gòdia, F., & Cairó, J. J. (2011). Continuous perfusion culture of encapsulated hybridoma cells. *Journal of Chemical Technology and Biotechnology*, *86*(12), 1555–1564.

Lin, C. Y., Huang, Z., Wen, W., Wu, A., Wang, C., & Niu, L. (2015). Enhancing protein expression in HEK-293 cells by lowering culture temperature. *PLoS ONE*, *10*(4), 1–19.

Luo, H. P., & Al-Dahhan, M. H. (2011). Verification and validation of CFD simulations for local flow dynamics in a draft tube airlift bioreactor. *Chemical Engineering Science*, *66*(5), 907–923.

Maier, U., & Büchs, J. (2001). Characterisation of the gas-liquid mass transfer in shaking bioreactors. *Biochemical Engineering Journal*, *7*(2), 99–106.

Mcmillan, J. D., & Wang, D. I. C. (n.d.). *PART I X. ASPECTS OF TRANSPORT PROCESSES Enhanced Oxygen Transfer Using Oil-in-Water Dispersions"*.

Mehrnia, M. R., Towfighi, J., Bonakdarpour, B., & Akbarnejad, M. M. (2005). Gas hold-up and oxygen transfer in a draft-tube airlift bioreactor with petroleum-based liquids. *Biochemical Engineering Journal*, *22*(2), 105–110.

Najafpour, G., Syahidah, K., Ismail, K., & Younesi, H. (2004). *PRODUCTION PROCESS FROM SYNTHESIS GAS , MASS Ar ch Ar ch ive*. *17*(2).

Nikakhtari, H., & Hill, G. A. (2005). Volatile organic chemical mass transfer in an external loop airlift bioreactor with a packed bed. *Industrial and Engineering Chemistry Research*, *44*(24), 9299–9306.

Oguchi, S., Saito, H., Tsukahara, M., & Tsumura, H. (2003). Control of Temperature and pH Enhances Human Monoclonal Antibody Production in CHO Cell Culture. *Animal Cell Technology: Basic & Applied Aspects*, 169–172.

Oosterhuis, N. M. G., & Kossen, N. W. F. (1984). Dissolved oxygen concentration profiles in a production-scale bioreactor. *Biotechnology and Bioengineering*, *26*(5), 546–550.

Ozturk, S. S., & Palsson, B. O. (1991). Growth, Metabolic, and Antibody Production Kinetics of Hybridoma Cell Culture: 2. Effects of Serum Concentration, Dissolved Oxygen Concentration, and Medium pH in a Batch Reactor. *Biotechnology Progress*, *7*(6), 481–494.

Paul, J. (1962). The Cancer Cell in Vitro: A Review. *Cancer Research*, *22*(4), 431–440.

Petersen, J. F., McIntire, L. V., & Papoutsakis, E. T. (1988). Shear sensitivity of cultured

hybridoma cells (CRL-8018) depends on mode of growth, culture age and metabolite concentration. *Journal of Biotechnology*, *7*(3), 229–246.

Quijano, G., Revah, S., Gutiérrez-Rojas, M., Flores-Cotera, L. B., & Thalasso, F. (2009). Oxygen transfer in three-phase airlift and stirred tank reactors using silicone oil as transfer vector. *Process Biochemistry*, *44*(6), 619–624.

Rodríguez-Carmona, E., Cano-Garrido, O., Dragosits, M., Maurer, M., Mader, A., Kunert, R., … Vázquez, F. (2012). Recombinant Fab expression and secretion in Escherichia coli continuous culture at medium cell densities: Influence of temperature. *Process Biochemistry*, *47*(3), 446–452.

Rymowicz, W., Kautola, H., Wojtatowicz, M., Linko, Y. Y., & Linko, P. (1993). Studies on citric acid production with immobilized Yarrowia lipolytica in repeated batch and continuous air-lift bioreactors. *Applied Microbiology and Biotechnology*, *39*(1), 1–4.

Sajan, E., Matanguihan, R., Heidemann, R., Abu-absi, S., Asuncion, W., Yamasaki, G., … Zhang, C. (2010). Cells and Culture. *Cells and Culture*, 785–788.

Salari, R., & Salari, R. (2017). Investigation of the Best Saccharomyces cerevisiae Growth Condition. *Electronic Physician*, *9*(1), 3592–3597.

Sánchez Mirón, A., García Camacho, F., Contreras Gómez, A., Grima, E. M., & Chisti, Y. (2000). Bubble-column and airlift photobioreactors for algal culture. *AIChE Journal*, *46*(9), 1872–1887.

Sanford, G. L., Ellerson, D., Melhado-Gardner, C., Sroufe, A. E., & Harris-Hooker, S. (2002). Three-dimensional growth of endothelial cells in the microgravity-based rotating wall vessel bioreactor. *In Vitro Cellular and Developmental Biology - Animal*, *38*(9), 493–504.

Shi, W., Yang, X., Sommerfeld, M., Yang, J., Cai, X., Li, G., & Zong, Y. (2019). Modelling of mass transfer for gas-liquid two-phase flow in bubble column reactor with a bubble breakage model considering bubble-induced turbulence. *Chemical Engineering Journal*, *371*(April), 470–485.

Sieck, J. B., Cordes, T., Budach, W. E., Rhiel, M. H., Suemeghy, Z., Leist, C., … Soos, M. (2013). Development of a Scale-Down Model of hydrodynamic stress to study the performance of an industrial CHO cell line under simulated production scale bioreactor conditions. *Journal of Biotechnology*, *164*(1), 41–49.

Su, Y., Wei, Z., Miao, Y., Sun, L., Shen, Y., Tang, Z., … Tian, J. (2021). Optimized process

operations reduce product retention and column clogging in ATF-based perfusion cell cultures. *Applied Microbiology and Biotechnology*, *105*(24), 9125–9136.

Taylor, M. W. (2015). Viruses and man: A history of interactions. *Viruses and Man: A History of Interactions*, 1–430.

Tupý, J., & Řhová, L. (1984). Changes and Growth Effect of pH in Pollen Tube Culture. *Journal of Plant Physiology*, *115*(1), 1–10.

Wang, S., Godfrey, S., Ravikrishnan, J., Lin, H., Vogel, J., & Coffman, J. (2017). Shear contributions to cell culture performance and product recovery in ATF and TFF perfusion systems. *Journal of Biotechnology*, *246*, 52–60.

Yang, J. -D, & Wang, N. S. (1992). Oxygen Mass Transfer Enhancement via Fermentor Headspace Pressurization. *Biotechnology Progress*, *8*(3), 244–251.

Yoon, S. K., Choi, S. L., Song, J. Y., & Lee, G. M. (2005). Effect of culture pH on erythropoietin production by Chinese hamster ovary cells grown in suspension at 32.5 and 37.0°C. *Biotechnology and Bioengineering*, *89*(3), 345–356.

Zhang, J., & Friedman, M. H. (2013). Adaptive response of vascular endothelial cells to an acute increase in shear stress frequency. *American Journal of Physiology - Heart and Circulatory Physiology*, *305*(6), 983–991.

Zhang, Q., Wang, Z., Wen, S., Liu, G., Wu, X., & Cong, W. (2012). Gas-Liquid Mass Transfer Characteristics in a Rotating-Drum Bioreactor. *Chemical Engineering and Technology*, *35*(10), 1842–1848.

Zhang, X., Bürki, C. A., Stettler, M., De Sanctis, D., Perrone, M., Discacciati, M., … Wurm, F. M. (2009). Efficient oxygen transfer by surface aeration in shaken cylindrical containers for mammalian cell cultivation at volumetric scales up to 1000 L. *Biochemical Engineering Journal*, *45*(1), 41–47.

Zhang, X., Stettler, M., Reif, O., Kocourek, A., DeJesus, M., Hacker, D. L., & Wurm, F. M. (2008). Shaken helical track bioreactors: Providing oxygen to high-density cultures of mammalian cells at volumes up to 1000 L by surface aeration with air. *New Biotechnology*, *25*(1), 68–75.

Zhu, G. Y., Zamamiri, A., Henson, M. A., & Hjortsø, M. A. (2000). Model predictive control of continuous yeast bioreactors using cell population balance models. *Chemical Engineering Science*, *55*(24), 6155–6167.

Chapter 3 – Design And Optimization of the Spiroid

Abstract

This research investigates a continuous bioreactor with an internal spiroid for enhanced gas-liquid mass transfer. The bioreactor consists of a cylindrical wall and is horizontally rotated on a roller bed. The inlet and outlet ports on the reactor provide continuous flow to the reactor. The spiroid is a simple helix attached to the inner wall of the reactor cylinder. The spiroid increases the gas-liquid contact areas within the reactor to increase oxygen mass transfer. To optimize the oxygen mass transfer, the diameter and length of the spiroid and the rotation rate of the reactor are important factors to be considered. The flow though spiroid at different rotation rates, spiroid diameter and spiroid length was studied using computational fluid dynamics (CFD) to determine conditions for optimum operation. Initial experiments were conducted using a dye at different rotation rates to determine the pumping rate of the spiroid. The results from these experiments were utilized to determine the inlet velocity to be used in the simulations. As flow through spiroid is a complex phenomenon, the CFD model was simplified to a straight tube and different parameters (shear stress, velocity vectors, wall turbulence, turbulence parameters) for different dimensions were studied to determine the optimum size of the spiroid. Results indicate that the optimum rotation rate of the spiroid is 8 rpm. Based on these preliminary simulations a model can be developed for oxygen transfer.

Keywords: continuous bioreactor, spiroid, computational fluid dynamics, optimization

3.1 Introduction

Cell culture plays a prominent role in various bioprocess industries and the use of bioreactors for this purpose is a vital part of this process. Bioreactors of different types are used in pharmaceutical industries, tissue engineering (scaffold preparation), stem cell research and gene therapy. Many researchers developed bioreactors of various kinds to address issues which limit cell production. Continuous supply of oxygen to the cells for survival and agitation or mixing are the two important factors which limit cell growth and production for aerobic bioreactor systems. Other factors which limit the growth to an extent are temperature, pH, culture media, and reactor configuration. These limiting factors can be analyzed using experimental methods which involve designing different reactors and assessing production by varying each parameter or multiple parameters at a time and optimizing them for enhanced production.

With the development of computational and statistical tools for fluid domain analysis, it is possible to study the fluid dynamics of bioreactors. Computational fluid dynamics (CFD) is being used by many researchers to study various flow parameters affecting cell culture in bioreactors. This method is relatively inexpensive when compared to conducting experiments for cell growth or antibody production in bioreactors and can also be used to optimize production (Hutmacher et al., 2008). CFD is increasingly used in bioprocessing, especially in simulating flow distribution in bioreactors. It is evident that the knowledge of hydrodynamics can be of immense help to researchers looking to improve the reactor design, performing optimization and scale-up of the process, and/or aiming to understand of interactions between the various significant input parameters (Rathore et al., 2016). Dhanasekharan et al., 2005 investigated the effect of bubble size distribution on oxygen transfer in an air lift bioreactor. The use of population balance method to study bubble dynamics determined the presence of recirculation in the reactor. These results

could be used for any type of stirred tank bioreactor regardless of scale and geometry. Increased impeller rotation in bioreactors provides optimum mixing but, at the same time increases shear stress. With the use of ANSYS CFX 12.0, the velocity profile predictions for various gas flow rates in a stirred airlift bioreactor showed that low rotation rates result in low mass transfer coefficients (Sergio S. de Jesus, Edgar Leonardo Martinez, Aulus R.R. Binelli, Aline Santana, 2013). Based on the studies of Ravindram, 1987, different droplet diameters were selected and their iodine removal effect on non-submerged venturis was investigated. The model was qualitatively validated as overall iodine removal efficiencies were observed within the range reported by Ali et al., 2013. The mass fraction of gas phase iodine decreases, and the iodine content increases Liquid phase iodine is observed along the length of the venturi. The same gas phase velocity behavior for different droplet diameters is noted due to the smaller liquid phase volume fraction (Ashfaq et al., 2019).

Apart from gas-liquid hydrodynamics, with the help of CFD Niño et al., 2018 modeled mass transfer rates in a 10L bioreactor which were later used to make design modifications for the bioreactor with a helical impeller. The oxygen transfer prediction using CFD in a novel rotating disk bioreactor for tissue culture applications showed that oxygen can be enhanced by convection limiting to low shear environments (Liow et al., 2009). Volumetric mass transfers are comparatively less in shake flasks than in stirred tank bioreactors. Velocity vector distribution studies in a shake flask determined that though there is larger interfacial area in shake flasks, the power dissipated in these flasks is less which results in low mass transfer coefficients than conventional stirred bioreactors (H. Zhang et al., 2005). Amer et al., 2019 used a population balance CFD model to evaluate the influence of ring spargers on mass transfer in a single-use bioreactor and found that the optimal sparger-to-impeller ratio is 0.8. Comprehensive

experimental and model-based bioreactor characterization is critical for realistic scale-up and scale-down approaches and technology transfer across geometrically diverse vessels. Understanding the shear stress limitations of a single cell culture process justifies the use of higher specific power inputs in large-scale animal cell culture, thereby reducing inhomogeneity and gas mass transfer issues (Villiger et al., 2018). Hybrid multi-region CFD modeling methods bring new opportunities for equipment design and process operation and control, such as establishing optimal equipment geometry, baffle placement, and impeller design (Bezzo et al., 2003). Teng et al., 2021 investigated the impacts of scaling up on BHK-21 cells and developed a CFD-based approach for the reactor's hydrodynamics at the lab scale. Brannock et al., 2010 established the applicability of their membrane bioreactor CFD model as a design and optimization tool. It allows for the prediction of how full-scale reactor design parameters (e.g., energy input via aeration or mixers, size and position of inlets, baffles, and membranes) affect hydrodynamics and hence performance. In the future, fluid-structure interactions may be of interest. This is especially true in single-use bioreactors made of flexible bags, where the geometry of the culture bag is influenced by liquid movement (Werner et al., 2014).

This research studied the use of a spiroid in a horizontally rotating bioreactor. The rotating bioreactor with spiroid can be operated at various rotation rates in batch or continuous mode. The purpose of spiroid is to increase gas-liquid contact areas and act as a low shear oxygenator for mixing and aeration in the reactor. For the spiroid to work effectively, the length and diameter are two important process parameters to be considered for enhanced oxygen transfer rate. Computational fluid dynamic simulations were used to analyze the effect of change in these parameters (rotation rate, diameter and length) on the shear stress within the reactor and extent of mass trasfer. Dye experiments were conducted for preliminary studies to determine if the spiroid

was pumping the liquid. As the flow through spiroid is complex, the geometry of the spiroid was simplified to a straight tube to study the formation of gas and liquid slugs. Design of experiments (DOE) was developed in minitab for various rotation rates, diameter and lengths. A total of 27 combinations were run as simulations using ANSYS FLUENT. The rotating bioreactor provided less shear and the optimization of spiroid in terms of rotation rate and the process parameters was done. These simulations will be used to study the species transport between gas and liquid in the spiroid and develop a model for determining mass transfer coefficients.

3.2 Materials and Methods

3.2.1 Experimental Apparatus

The continuous bioreactor used for this study is a scaled up bioreactor and consists of an outer cylindrical shell with a spiroid. The spiroid is embedded onto the inner wall of this cylinder to increase gas-liquid contact areas which helps in enhancing oxygen transfer within the reactor. The bioreactor can be rotated horizontally with the help of a roller bed as shown in Figure 3.1. The inlet/outlet ports present on either side of the reactor help in providing medium and oxygen continuously to the reactor. This bioreactor is prototyped using a 3D printer.

The dimensions of the original and scaled-up bioreactor are summarized in Table 3-1

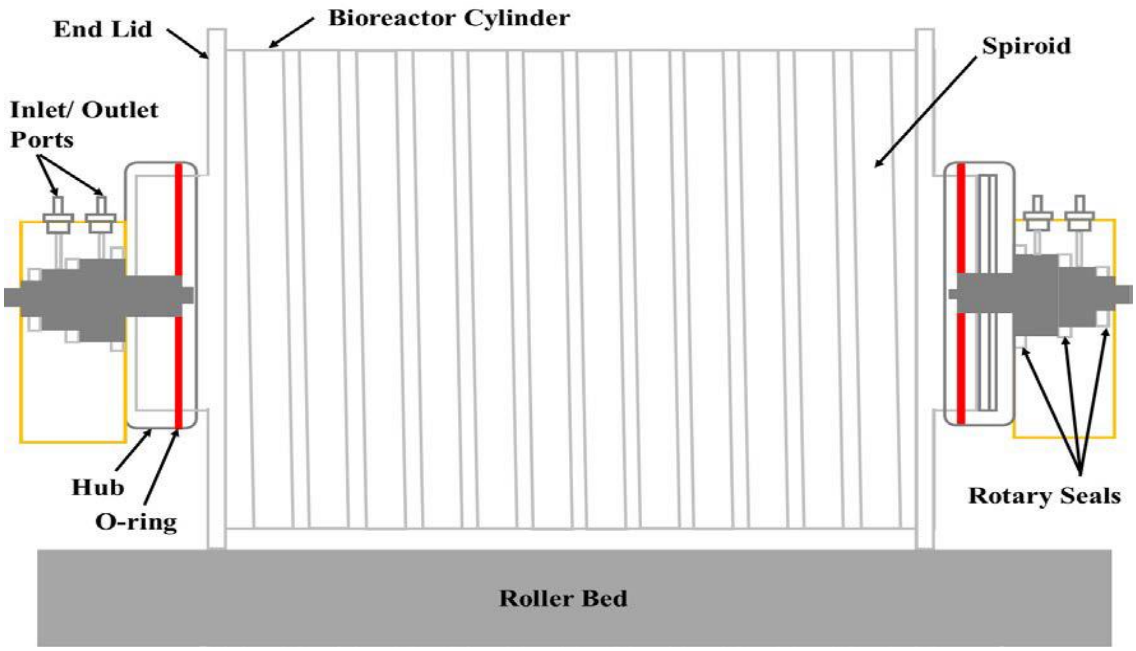

Figure 3.1 Bioreactor Schematic (Fang et al., 2018)

Table 3-1 Bioreactor Dimensions

Parameter	Original Bioreactor	Scaled-up Bioreactor
Chamber Length (m)	0.100	0.193
Chamber Inner Diameter (m)	0.0444	0.0889
Spiroid Length (m)	1.09	3.12
Spiroid Inner Diameter (m)	0.00476	0.00953
Spiroid Turns	8	12
Volume (10^{-4} m^3)	1.11	9.86

3.2.2 Preliminary Dye Experiments

To determine the flow rate through the spiroid and confirm that the spiroid is pumping at an effective rate, dye experiments were conducted at different rotation rates in the scaled-up bioreactor. The reactor was filled up to two-thirds of its volume with water and the roller bed was

activated. At each rotation rate, a food dye was introduced from the inlet of the reactor. Slugs of gas and liquid were clearly seen within the spiroid. The time taken for the dye to flow from the start to the end of the reactor (spiroid length) was noted. This test was repeated at rotation rates of 4, 6, and 8 rpm. Results show that the flow of dye through the spiroid was increased with increase in rotation rates, confirming that the spiroid is pumping effectively. These experiments were auxiliary for conducting simulations as the observed flow in these experiments was used for generating the simulation model.

3.3 Computational Fluid Dynamic Simulations

The optimization of spiroid is a major factor which will enhance the oxygen transfer in the bioreactor. The length and diameter of the spiroid must be capable enough to provide the highest amount of oxygen transfer in the reactor. Making the spiroid too long or short will not serve in enhancing the gas-liquid mass transfer. Hence, optimum range of diameter and length of spiroid is necessary for higher efficiency. ANSYS workbench 19.2 (ANSYS, Inc. Canonsburg, PA, USA) was used in this research to carry out the simulations. CFD simulations were performed as per a full factorial DOE with rotation rates at three levels and diameters and lengths of spiroid at three levels (Table 3-2).

Table 3-2 Range of parameters for simulations

SNO	RPM	DIAMETER	LENGTH
1	4	0.004	0.6
2	4	0.004	0.7
3	4	0.004	1.0
4	4	0.005	0.6
5	4	0.005	0.7
6	4	0.005	1.0
7	4	0.006	0.6
8	4	0.006	0.7

9	4	0.006	1.0
10	6	0.004	0.6
11	6	0.004	0.7
12	6	0.004	1.0
13	6	0.005	0.6
14	6	0.005	0.7
15	6	0.005	1.0
16	6	0.006	0.6
17	6	0.006	0.7
18	6	0.006	1.0
19	8	0.004	0.6
20	8	0.004	0.7
21	8	0.004	1.0
22	8	0.005	0.6
23	8	0.005	0.7
24	8	0.005	1.0
25	8	0.006	0.6
26	8	0.006	0.7
27	8	0.006	1.0

The basic steps for performing any simulation in ANSYS workbench are as follows:

1. Create the geometry (Design Modeler was used in this research)
2. Mesh the geometry using ANSYS meshing tool.
3. Create ‘Named selections’ for the domain of study.
4. Setup the model needed to illustrate the flow phenomenon
5. Run the simulations
6. Analyze and predict the results using CFD-post processing.

Apart from the above-mentioned steps, it is necessary to check for the mesh quality once the mesh is generated to ensure for a better solution convergence. Studying the flow through spiroid geometry is complex and is computationally expensive. As a result, the geometry of spiroid was simplified into a long straight tube and was studied under different operating conditions. To mimic the exact conditions within the spiroid, the assumptions made are steady state, homogenous,

Newtonian fluids, isothermal, pressure-based model. All the simulations were carried out without the influence of gravity. When gravity is included in a straight tube, the slugs forming in the spiroid cannot be represented and all the gas and liquid are pushed towards the end of the tube. For these reasons, gravity was disabled and to hold the slugs together, surface tension between the phases (water and gas) was enabled.

3.3.1 Geometry

The geometry of the bioreactor with the spiroid was created using SolidWorks and imported into ANSYS workbench as shown in Figure 3.2(a). The sectional view of the reactor is shown in Figure 3.2(b). The inlet and outlet ports were represented by small tubes to represent fluid flow through the reactor. The geometry of spiroid alone is shown in Figure 3.2(c). The dimensions of the original bioreactor were used to create this geometry. As it can be seen from Figure 3.2(c), the spiroid geometry is complex and analyzing the flow through one turn (loop) alone is computationally expensive. Hence, the whole spiroid geometry is simplified to a straight tube as shown in Figure 3.2(d). The dimensions of this geometry are varied (as mentioned in DOE) and each case is simulated. To determine two-thirds of the volume of the spiroid with the water and the remaining volume with air, the height of water within the spiroid was numerically calculated. The inlet of spiroid was divided into two segments (air inlet and water inlet) using the calculated height. This way, we could clearly define the amount of water and air entering the spiroid.

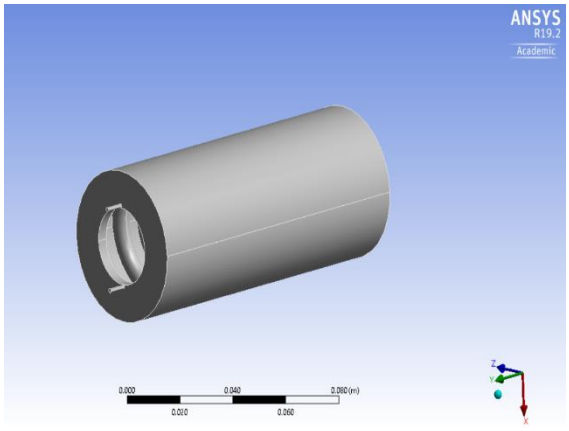

(a) Bioreactor with Spiroid

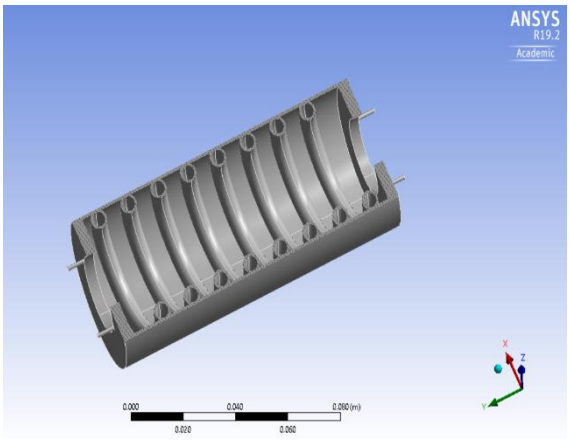

(b) Sectional View

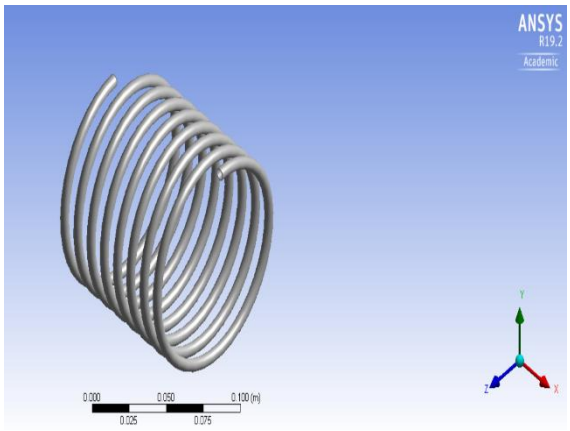

(c) Geometry of Spiroid

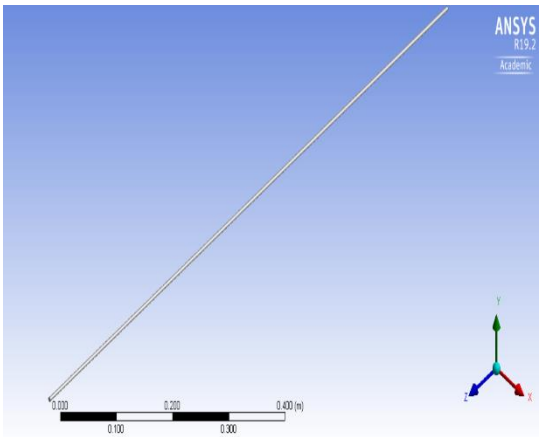

(d) Spiroid as a Straight Tube

Figure 3.2 Geometry of the Novel Bioreactor

3.3.2 Mesh Generation

In ANSYS workbench, the mesh is generated using the mechanical package. As the domain being studied is fluid, a volume mesh is generated throughout the geometry. The physics preference was set as CFD. A finer mesh with large number of elements was not used in this study

as the time of convergence is high. Further, the parts of spiroid (inlet, outlet, pipe wall) were named using the named selection option in meshing toolbar. These named selections were created to determine the boundary conditions at ease in the next step. The ANSYS mesh generated is shown in Figure 3.3. The overall mesh for bioreactor with spiroid is represented by Figure 3.3 (a). Figure 3.3 (c) depicts the mesh for the spiroid alone and Figure 3.3 (d) represents the closer view of the mesh for the straight tube.

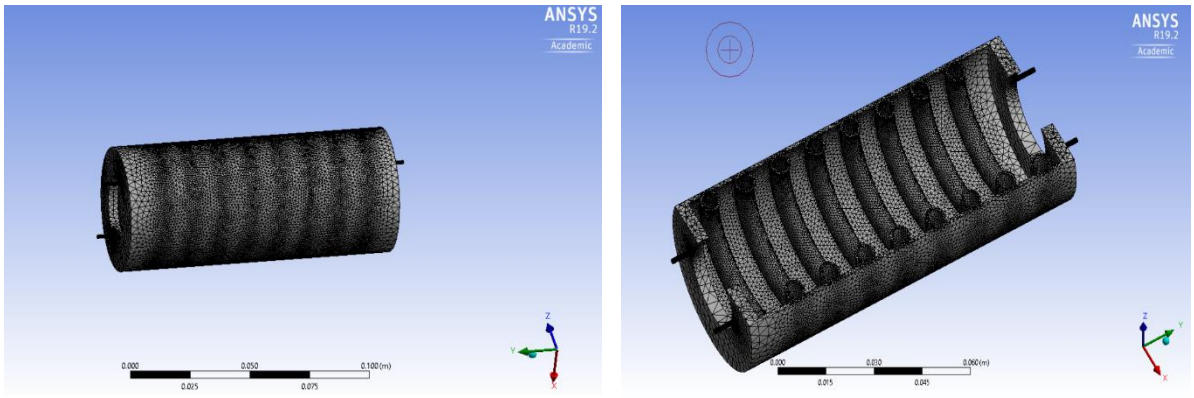

(a) Overall Mesh for Bioreactor with Spiroid (b) Sectional View of the Mesh

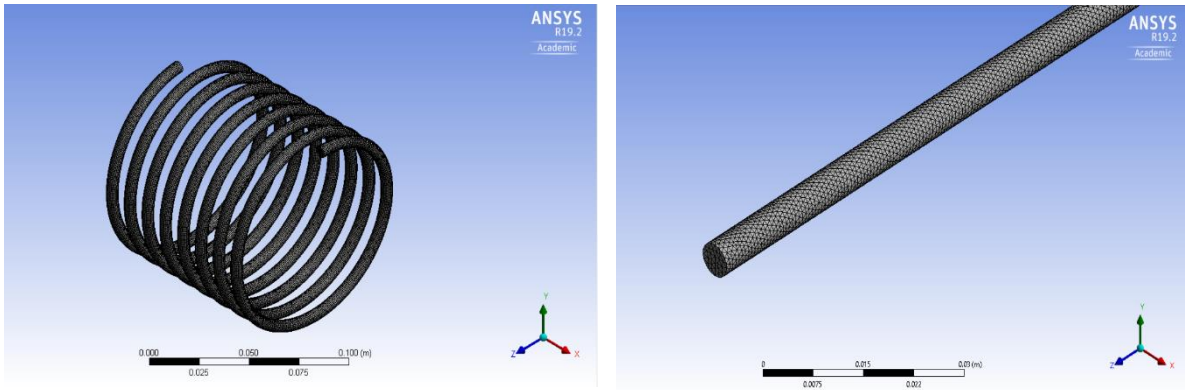

(c) Spiroid Mesh (d) Mesh over Straight tube

Figure 3.3 Meshed Geometry (ANSYS 19.2)

The quality of mesh affects the simulation results, time taken for the solution to converge and the overall performance. This can be determined by the parameter skewness which is obtained from the mesh statistics toolbar. A maximum skewness of 0.95 is permissible for a good quality mesh. The maximum skewness of the straight tube under consideration was 0.84 which is acceptable for the simulations. A mesh sensitivity analysis was also done to ensure the quality.

3.3.3 Theory

At operating conditions of 4, 6 and 8 rpm, the flow through the spiroid is in the low turbulence region (Childs, 2011). Turbulence modeling in ANSYS is possible using the Reynolds-Averaged Navier-stokes (RANS) equations. This provides the most economical way to simulate complex flows. These models include two additional transport equations for calculating the resulting Reynolds stress. k-ε and k-ω are the two turbulence models offered in ANSYS that predict the flow accurately. The k-ε model is known for its robustness, economy, and reasonable accuracy. The k-ω model predicts the flow near the boundary considering a low Reynolds number instead of accounting for mesh quality but takes longer convergence time (ANSYS FLUENT 13 User's Guide, 2013 ;Argyropoulos et al., 2015).

The standard k-ε model is generally used to predict flow characteristics in industries. The turbulence kinetic energy (k) is obtained by using exact equations whereas the dissipation rate (ε) is obtained by physical reasoning. The major assumptions of this model are molecular viscosity is negligible and the flow is fully turbulent. Thus, this model is only applicable to turbulent regions. The RNG k-ε model uses a statistical technique called renormalizing group theory. This model accounts for a large portion of the low Reynolds number zone, making it more applicable to a broader range of flows. The realizable k-ε model includes an exact equation for the turbulent

eddy dissipation rate which makes it the most accurate out of all three models. This can also be used for rotating homogenous flows. The k-ε model with enhanced wall treatment has also been included in this research to ensure the near-wall region is also taken into consideration (ANSYS FLUENT 13 User's Guide, 2013). The transport equations solved by ANSYS setup for k-ε model are as follows (ANSYS FLUENT 13 User's Guide, 2013):

$$\frac{\partial(\rho k)}{\partial t} + \frac{\partial(\rho k v_j)}{\partial x_j} = \frac{\partial}{\partial x_j}\left[\left(\mu + \frac{\mu_t}{\sigma_k}\right)\frac{\partial k}{\partial x_j}\right] + G_k + G_b - \rho\varepsilon - Y_M + S_k \quad (3\text{-}1)$$

$$\frac{\partial(\rho\varepsilon)}{\partial t} + \frac{\partial(\rho\varepsilon v_j)}{\partial x_j} = \frac{\partial}{\partial x_j}\left[\left(\mu + \frac{\mu_t}{\sigma_\varepsilon}\right)\frac{\partial \varepsilon}{\partial x_j}\right] + \rho C_1 S_\varepsilon - \rho C_2 \frac{\varepsilon^2}{k + \sqrt{\nu\varepsilon}} + C_{1\varepsilon}\frac{\varepsilon}{k}C_{3\varepsilon}G_b + S_\varepsilon \quad (3\text{-}2)$$

where $C_1 = max\left[0.43, \frac{\eta}{\eta+5}\right]$; $\eta = S\frac{k}{\varepsilon}$; S is the modulus of the mean strain rate tensor, $S = \sqrt{2S_{ij}S_{ij}}$ (s^{-1}); S_{ij} is the mean strain rate, $S_{ij} = \frac{1}{2}\left(\frac{\partial v_j}{\partial x_i} + \frac{\partial v_i}{\partial x_j}\right)$ (s^{-1}); $C_{1\varepsilon} = 1.44$; $C_2 = 1.9$; $C_{3\varepsilon} = tanh\left|\frac{v_{//}}{v_\perp}\right|$; $v_{//}$ is the component of the flow velocity parallel to the gravitational vector (m s^{-1}); $v_\perp$ is the component of the flow velocity perpendicular to the gravitational vector (m s^{-1}); σ_k is the turbulent Prandtl number for k, $\sigma_k = 1.0$; σ_ε is the turbulent Prandtl number for ε, $\sigma_\varepsilon = 1.2$. k is the turbulence kinetic energy per unit mass (J kg^{-1} or m^2 s^{-2}); μ is the molecular dynamic viscosity (Pa-s); μ_t is the turbulent or eddy viscosity (Pa-s); G_k is the generation term because of the mean velocity gradients (J s^{-1} m^{-3} or kg m^{-1} s^{-3}); G_b is the generation term due to the buoyancy, (J s^{-1} m^{-3} or kg m^{-1} s^{-3}); ε is the dissipation rate per unit mass (J kg^{-1} s^{-1} or m^2 s^{-3}); Y_M is the effects from the fluctuating dilatation in the compressible turbulence on the overall dissipation rate (J s^{-1} m^{-3} or kg m^{-1} s^{-3}); ν is the kinematic viscosity (m^2 s^{-1}); S_k (J s^{-1} m^{-3} or kg m^{-1} s^{-3}) and S_ε (J s^{-2} m^{-3} or kg m^{-1} s^{-4}) are user-defined source terms (ANSYS FLUENT 13 User's Guide, 2013).

3.3.4 Model Setup

The model can be solved using one of two numerical approaches in ANSYS FLUENT. The first is a pressure-based solver, whereas the second is a density-based solver. The velocity field is obtained from the momentum equation in both techniques. The continuity equation is utilized in the density-based method to derive the density field and pressure from the equation of state, but in the pressure-based method, the pressure field is determined by solving pressure correction, which is achieved by manipulating continuity and momentum equations. Pressure-based models are commonly employed for low compressible flows, while density-based models are utilized for high compressible flows. A pressure-based model was employed in this study. The simulations were run at steady-state and gravity was disabled.

Multiphase flow regimes are classified as two phase (gas-liquid, liquid-liquid, gas-solid, solid-liquid) or three phase (gas-solid-liquid). In this study, the gas-liquid multiphase flow was modeled as water and air filling the bioreactor. There are two techniques for numerically computing multiphase flows. The first is the Euler-Lagrange method, whereas the second is the Euler-Euler method. When the volume fraction of the dispersed phase or secondary phase is small (less than 10%) and particle-particle interactions are unimportant, the first approach is considered. The distinct phases are considered as interpenetrated continua in the Euler-Euler method. There are three types of Euler-Euler multiphase models available: the volume of fluid method (VOF) model, the Eulerian Model, and the Mixture Model. When the interface between fluids is of interest, the VOF approach is applied. When the primary and secondary phases have differing velocities, the mixing model is applied. The most complicated multiphase model is the Eulerian model. With computational memory constraints, this technique can describe any number of phases

(ANSYS FLUENT 13 User's Guide, 2013). In this study, the VOF method is employed to simulate flow via a spiroid. The sharp/dispersed option with implicit formulation was used to create the interface between the phases. Water was designated as the primary phase, and air as the secondary phase. At standard conditions, phase interactions such as surface tension were enabled. The boundary conditions for each phase were suitably set, and the pressure in the spiroid's headspace was atmospheric. Rotation rates of 4, 6 and 8 rpm were applied at the moving wall of spiroid. Velocity for each case was calculated and entered at the inlet.

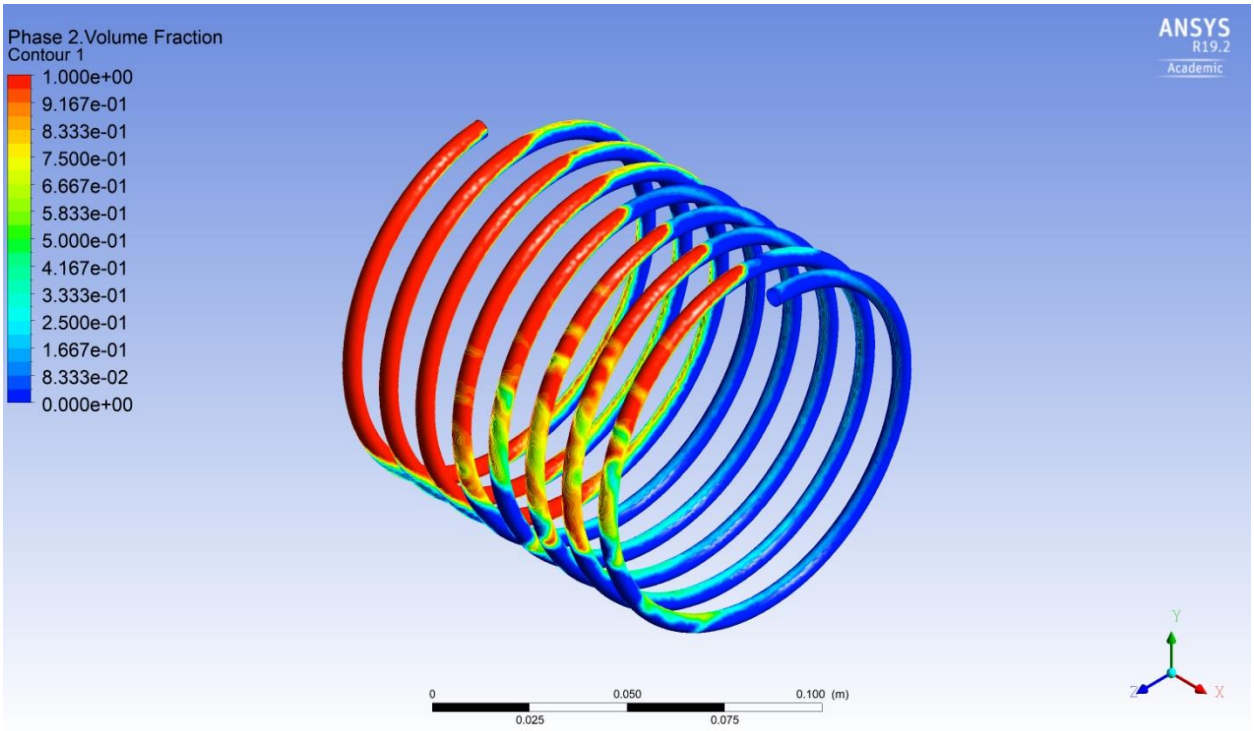

Figure 3.4 Multiphase Contours of Water and Air Using the VOF Method (two-thirds fill)

For the pressure-velocity approach, FLUENT provides four separate algorithms (SIMPLE, SIMPLEC, PISO, COUPLED). SIMPLEC can be used for simple flows, but SIMPLE is a more common technique that was used in this study. With the help of PISO, one could do transient computations. For transient calculations with long time steps, this approach can maintain a stable

calculation. In the case of a steady-state single-phase implementation, the COUPLED algorithm provides a reliable solution. Green-Gauss node-based, cell-based, and least-square cell-based gradients were utilized in this study for efficient convergence criteria, with the green-gauss node-based type being the most efficient (ANSYS FLUENT 13 User's Guide, 2013). The default settings were used for the remaining parameters. The same settings were used for all cases of DOE (except for changing inlet velocity and hydraulic diameter), and the results for each case were analyzed considering the mixing plane between gas and liquid in the spiroid. These simulations are important for analyzing the transport of substances from gas to liquid for further experiments.

3.4 Results and Discussion

The criteria for convergence were checked by using the residual profiles. In case the solution doesn't converge even after long iterations, convergence conclusion can be made if the residuals continue to remain almost the same or decrease at a very small rate. Mass conservation for each was also checked to validate the convergence. Each case in this research took several hours of computation time (Intel(R) Core (TM) i704700MQ CPU @ 2.4 GHz, 8.00 GB RAM and 64-bit operating system). The velocity contours, wall shear and hydrodynamic parameters were generated for each case, with the contours for each case presented below). In each case, with increase in rotation rate, the average wall shear increased (diameter and length constant). Also, at spiroid diameters less than 0.005 m, the FLUENT simulations would not converge. This result was due to low flow rate and less area for flow. For a length of 0.6 m, the mixing in the tube wasn't sufficient since shorter lengths are not efficient for interactions of the gas-liquid slugs. Turbulent eddy dissipation rates determine the breaking of large eddies formed into smaller ones due to shearing action. The turbulent eddy dissipation rate increased with increase in rotation rate.

The higher the eddy dissipation rate, the greater the oxygen transfer as the large size eddies are broken down into smaller sizes leading to larger surface to volume ratios available for mass transfer. The velocity contours for each case remained almost constant. Minor differences were noticed with change in rotation rate. This result was due to the low inlet velocities in each case.

Case 1: d = 0.005 m, L = 0.6 m

The volume fraction of air at different locations along the length of the pipe was changing with rotation. Gas-liquid interface was increased with increase in rotation rate. At 4 rpm, the interaction between the fluids didn't start until half of the length of the tube whereas for 6 and 8 rpm, mixing was seen earlier. The velocity along the plane was almost constant along the length at different rotational rates as shown in Figure 3.5(a), (b) and (c). The minor differences could be accounted to small inlet velocity of the spiroid which doesn't produce major differences in velocity patterns. The rotation rate had little influence on the system velocity.

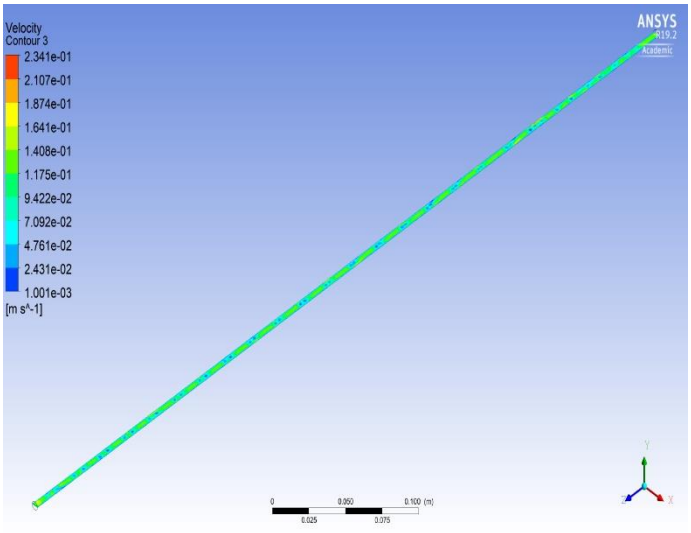

(a) At 4 RPM

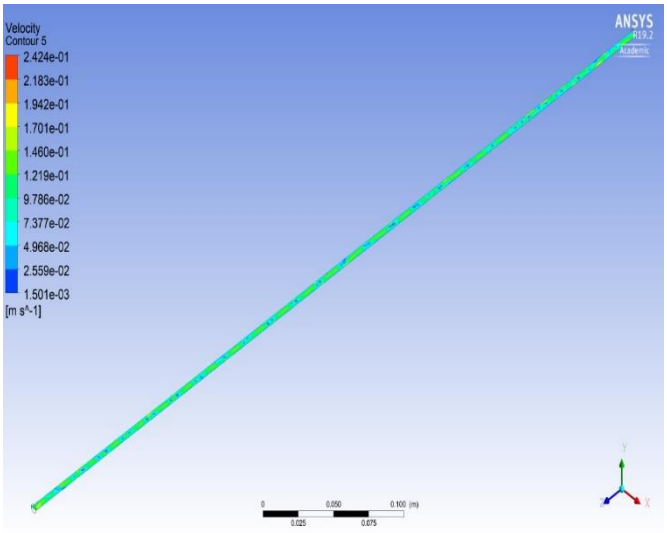

(b) At 6 RPM

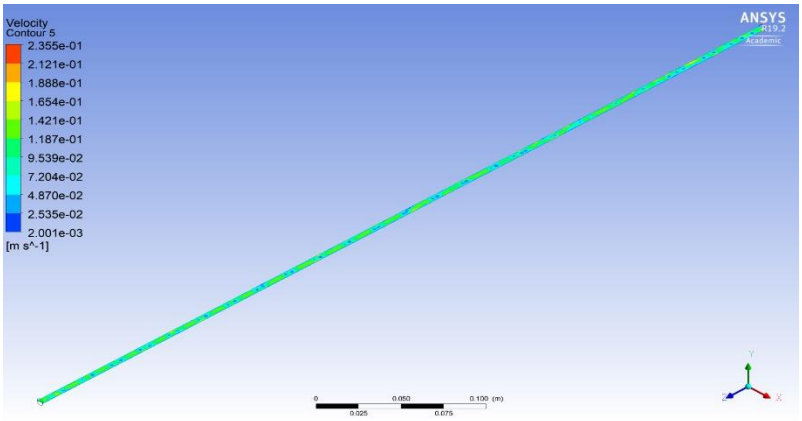

(c) At 8 RPM

Figure 3.5 Velocity Contours at Different Rotation Rates for d = 0.005 m, L = 0.6 m

Shear stress is one of the most important factors to be considered in cell culture. The contours for wall shear stress were generated to obtain the maximum shear stress obtained in the spiroid. With increase in rotation rate from 4 to 6 rpm, an increase in shear stress was noted as observed in Figure 3.6(a) and (b). At 8 rpm, the shear stress was initially near that observed at 6rpm but gradually increased along the length of tube. Higher shear stress values were observed near the interface which could be due to phase interactions. The shear stress in the spiroid at this length were of the order of 10^{-1} Pa, significantly less than values observed in traditional bioreactors. The maximum shear stress observed was 0.96 Pa at 8 rpm.

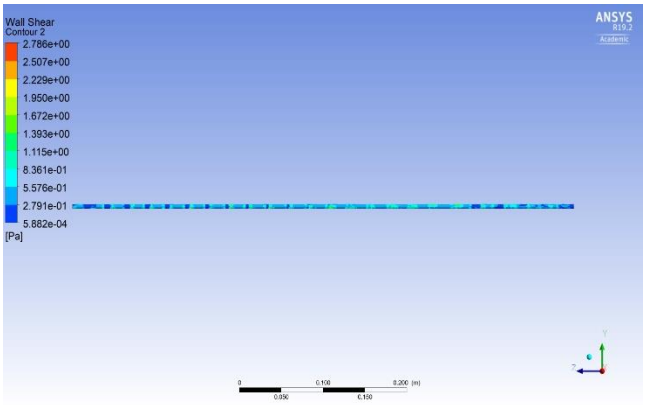

(a) Wall Shear at 4RPM

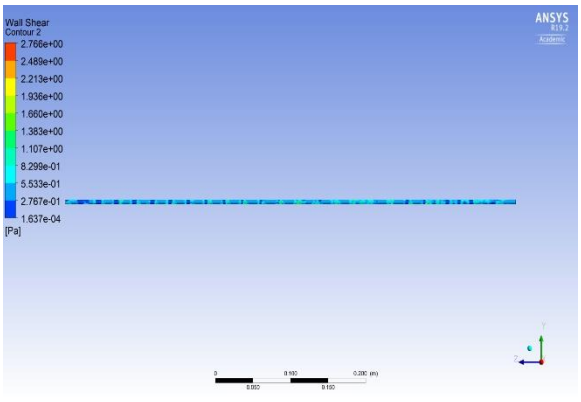

(b) Wall Shear at 6RPM

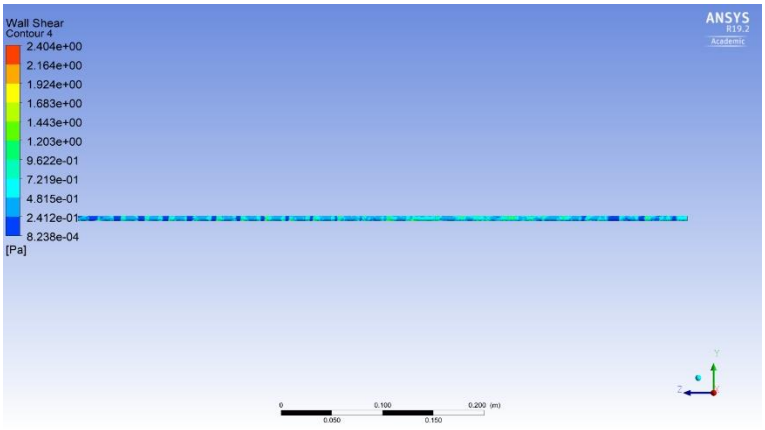

(c) Wall Shear at 8RPM

Figure 3.6 Wall Shear Contours at Different Rotation Rates for d = 0.005 m, L = 0.6 m (YZ plane)

Turbulent eddy dissipation rate greatly impacts the amount of oxygen transfer (volumetric mass transfer coefficients) in the reactor. Figure 3.7 depicts the contours of the maximum turbulent eddy dissipation rate (XY plane) at all three rotation rates. The eddy dissipation rate increased with increase in rotation rate. Increase in eddy dissipation rate implies that large eddies formed in the flow are broken down into smaller sized eddies. The smaller the eddy, the larger the interfacial area available for oxygen transfer. The results from values obtained showed that oxygen transfer can be increased with increase in rotation rate.

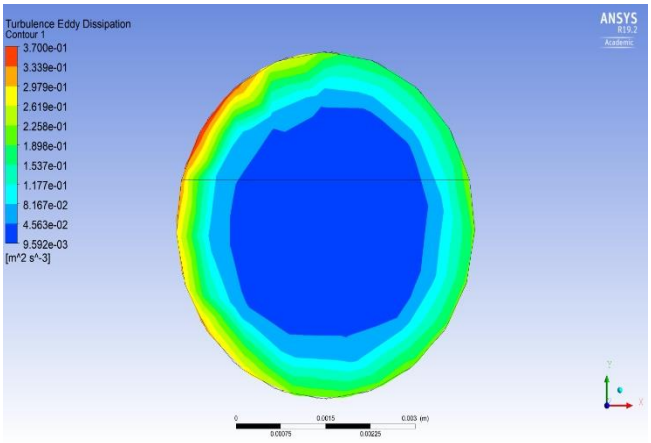

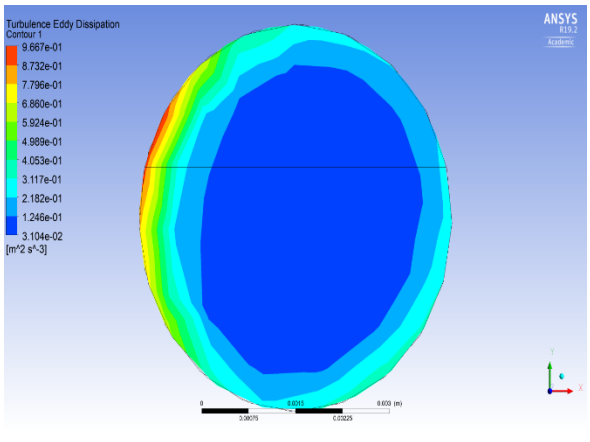

(a) At 4 RPM (b) At 6 RPM

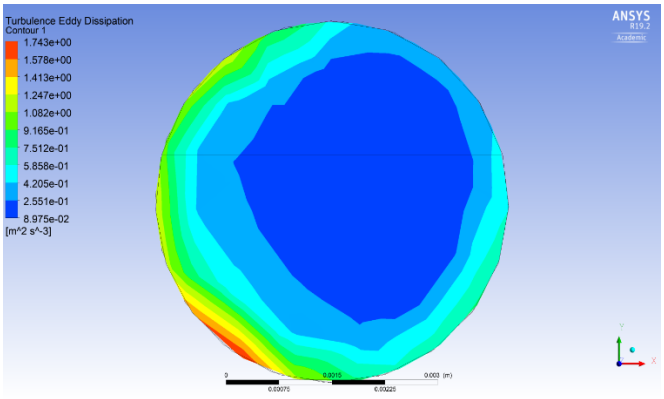

(c) At 8RPM

Figure 3.7 Turbulent Eddy Dissipation Rate at Different Rotation Rates d = 0.005 m, L = 0.6 m (XY plane)

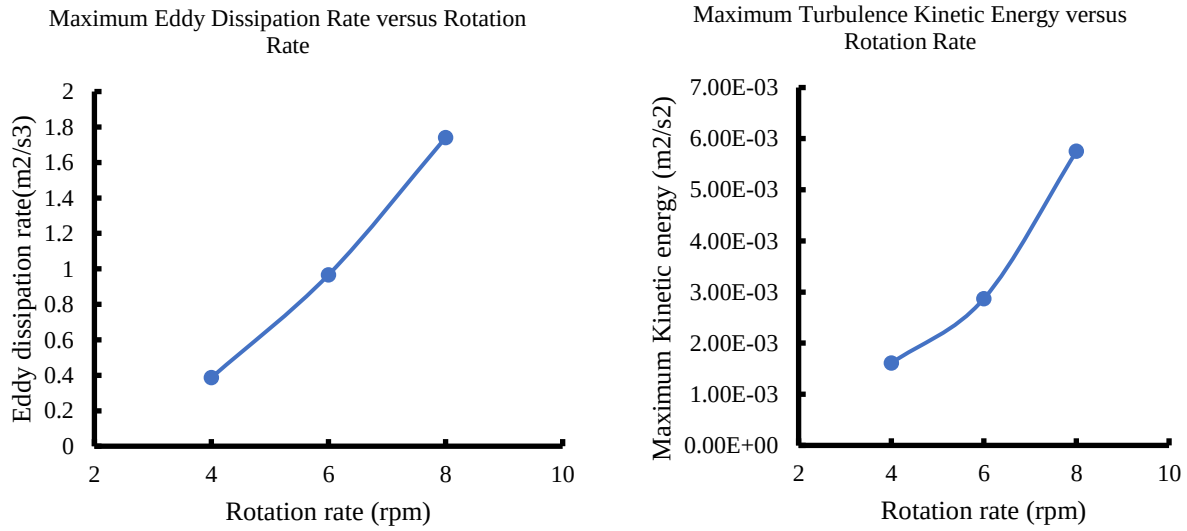

Figure 3.8 Eddy Dissipation Rate and Maximum Kinetic Energy at Different Rotation Rates for d = 0.005 m, L = 0.6 m

Case 2: d = 0.005 m, L = 0.7 m

A pattern similar to that of the 0.6 m length was seen for velocity contours (Figure 3.5). The areas of minimum value of velocity decreased and no major changes for the entire length. Slight changes in velocity contours compared to the previous case could be accounted to the change in length as diameter was kept constant and rotation rates studied were the same.

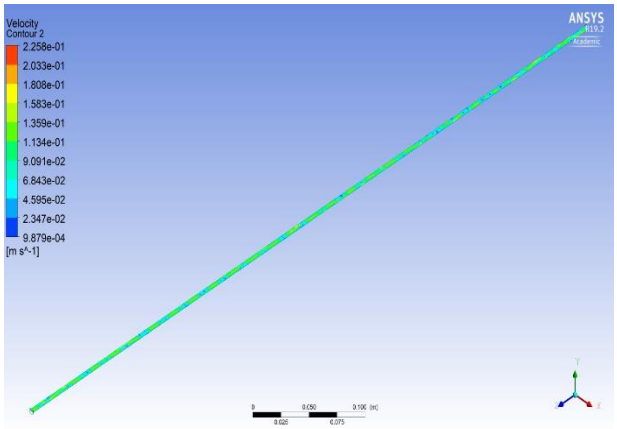

(a) At 4 RPM

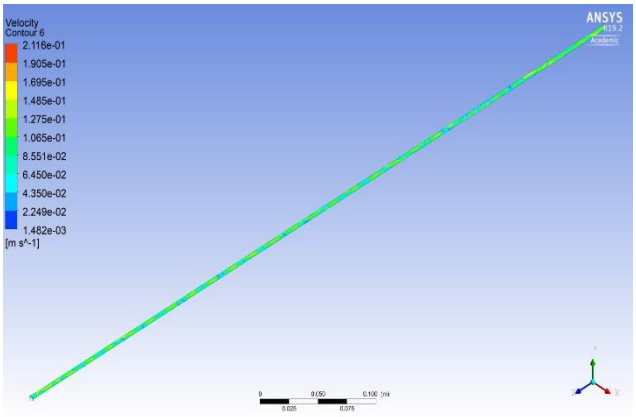

(b) At 6 RPM

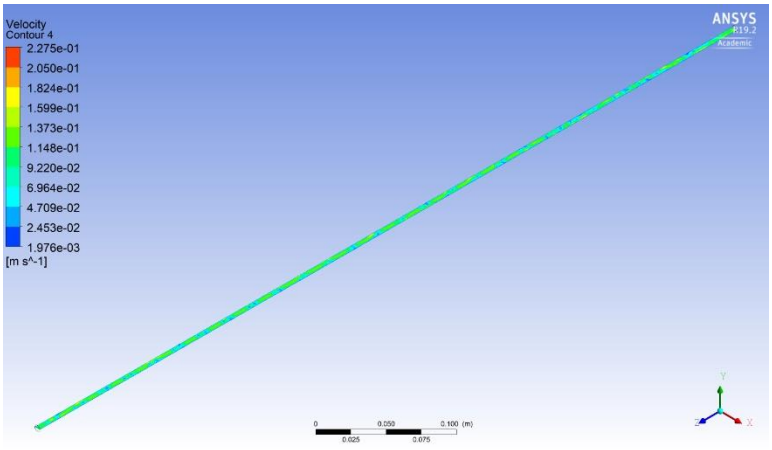

(c) At 8RPM

Figure 3.9 Velocity Contours at Different Rotation Rates for d = 0.005 m, L = 0.7 m

An average wall shear of 0.67 Pa was observed at these dimensions. High shear was seen after half of the length of the pipe, likely due to increasing interactions and mixing between gas and

liquid. The contours of wall shear in Figure 3.10(a), (b) and (c) show that average wall shear increased from 4 rpm to 8 rpm. The distribution of shear stress was changed significantly for a rotation rate of 6 rpm and maximum shear stress occurred in the area where gas-liquid interaction was the highest.

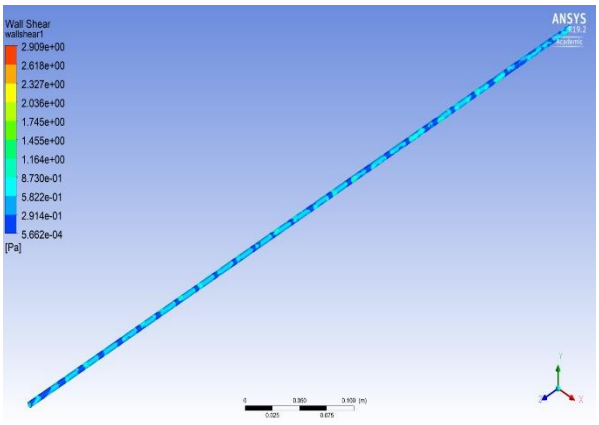

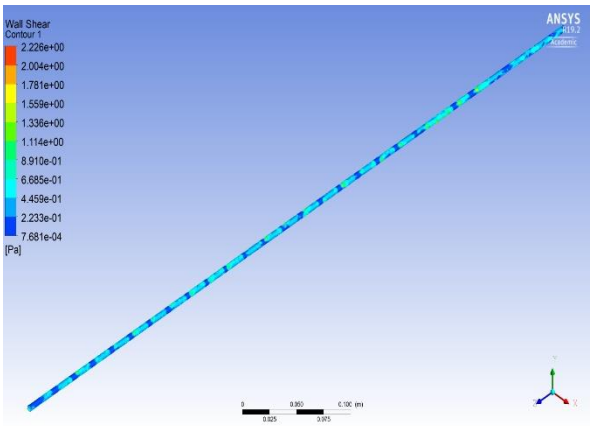

(b) Wall Shear at 6RPM

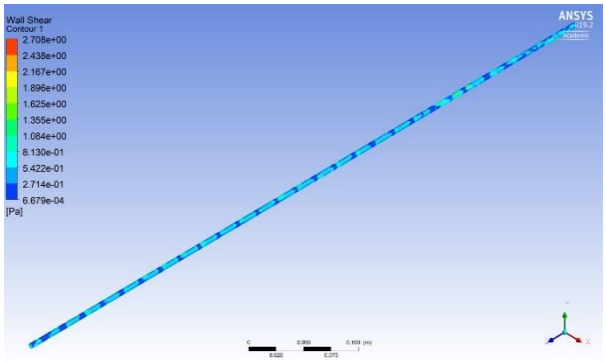

(c) Wall Shear at 8RPM

Figure 3.10 Wall Shear Contours at Different Rotation Rates for d = 0.005 m, L = 0.7 m (YZ plane)

Turbulent eddy dissipation was observed near the rotating wall. Compared to results at a length of 0.6 m, the maximum eddy dissipation rate increased three-fold at 8 rpm. The plots for eddy dissipation rate and kinetic energy with varying rotation rate is shown in Figure 3.12. With change in rotation rate, the eddy dissipation rate also increased.

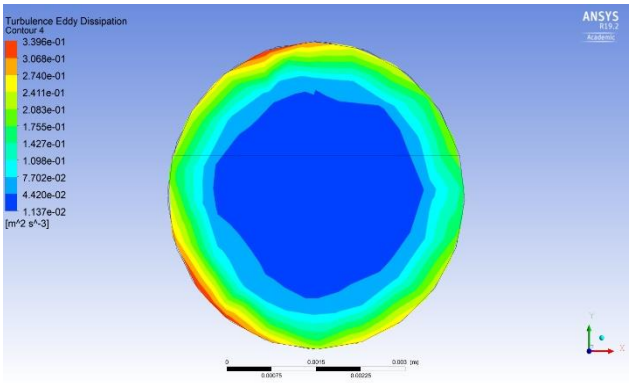

(a) At 4 RPM

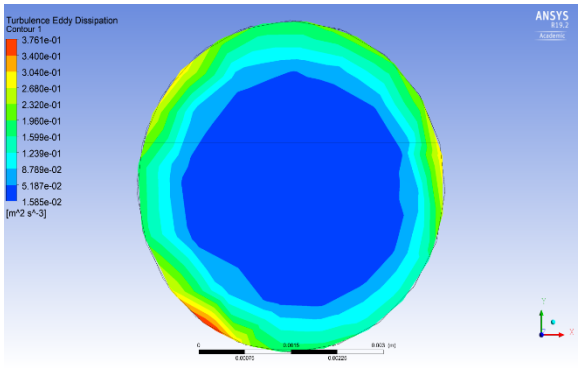

(b) At 6 RPM

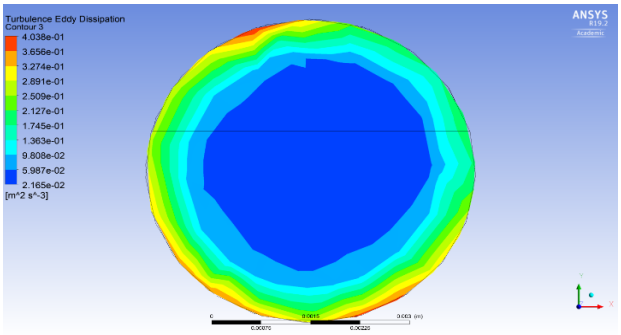

(c) At 8 RPM

Figure 3.11 Turbulent Eddy Dissipation Rate at Different Rotation Rates for d = 0.005 m, L = 0.7 m (XY plane)

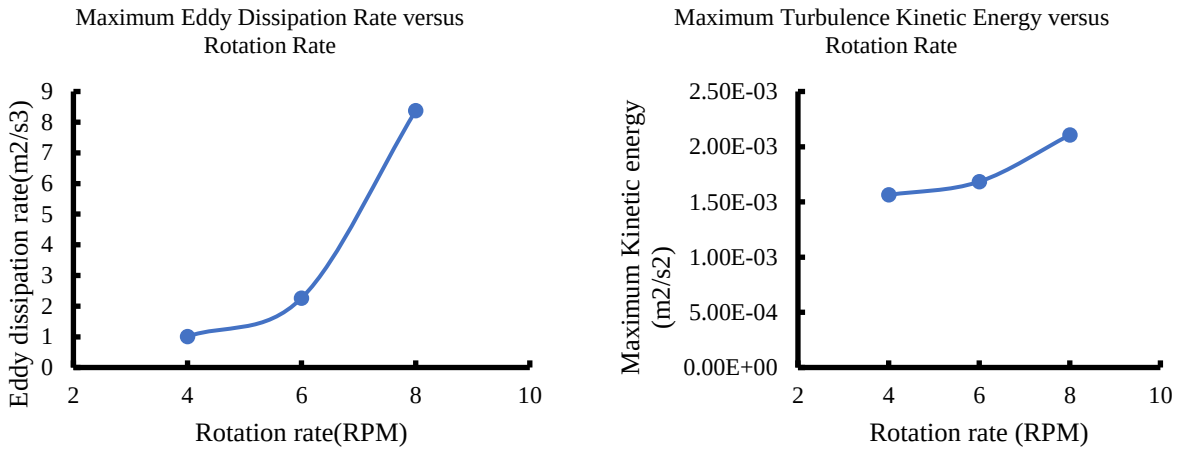

Figure 3.12 - Eddy Dissipation Rate and Maximum Kinetic Energy at Different Rotation Rates for d = 0.005 m, L = 0.7

Case 3: d = 0.005 m, L = 1.0 m

Figure 3.13 shows that the velocity contours were uniform throughout the length. The regions of low velocity (blue) occurred at negligible regions of the pipe. A region of high velocity (red) was seen at a rotation rate of 6rpm towards the bottom of the pipe during rotation. Slight increase in velocity was observed with increase in rotational rate.

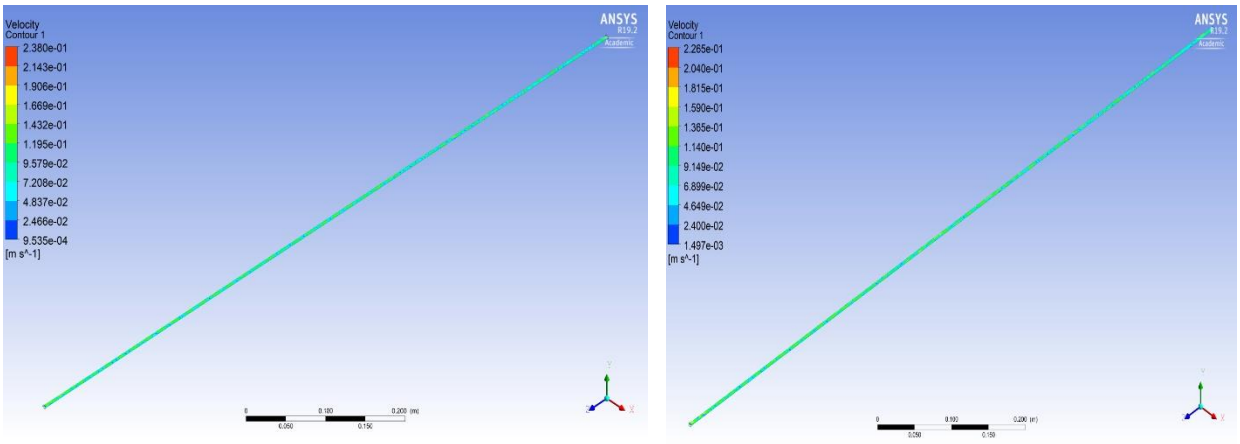

(a) At 4 RPM

(b) At 6 RPM

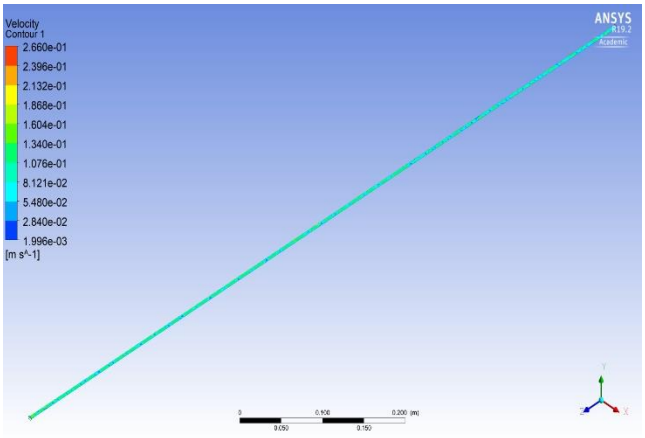

Figure 3.13 - Velocity Contours at Different Rotation Rates for d = 0.005 m, L = 1.0 m

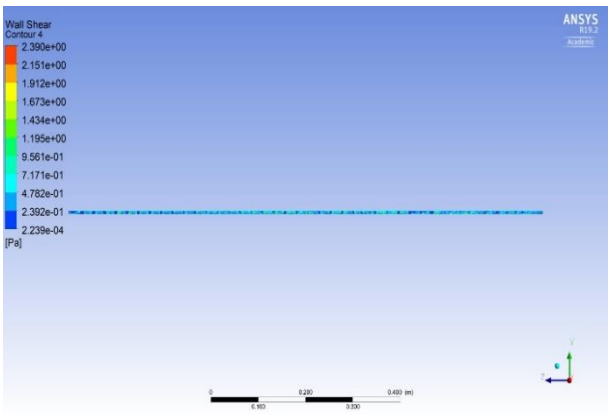

(a) At 4 RPM

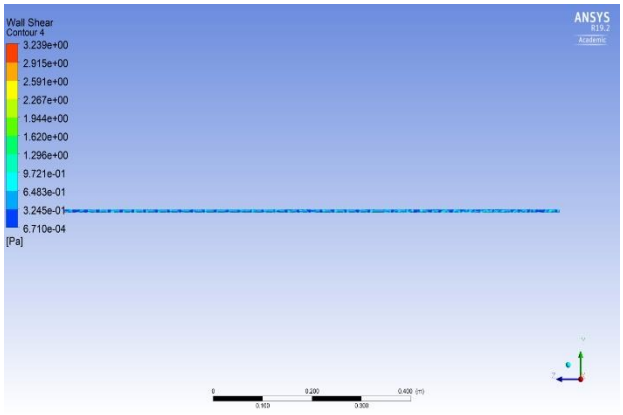

(b) At 6 RPM

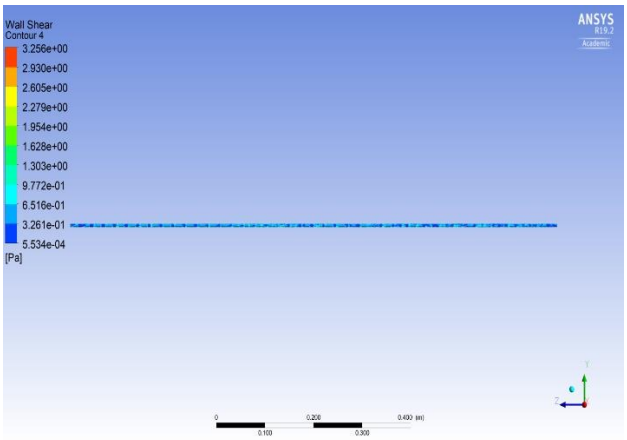

(c) At 8 RPM

Figure 3.14 - Wall Shear Contours at Different Rotation Rates for d = 0.005 m, L = 1.0 m (YZ plane)

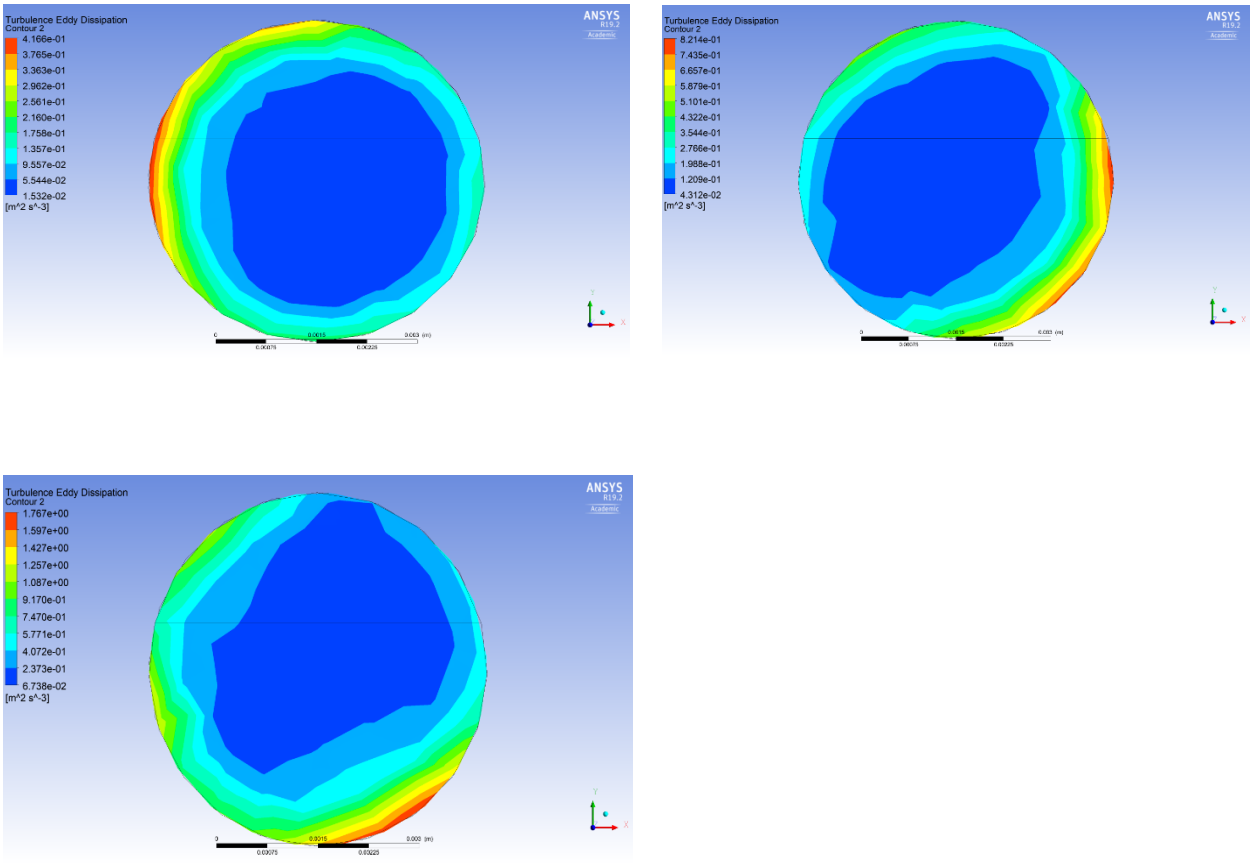

Figure 3.15 Turbulent Eddy Dissipation rate at Different Rotation Rates for d = 0.005 m, L = 1.0 m (XY plane)

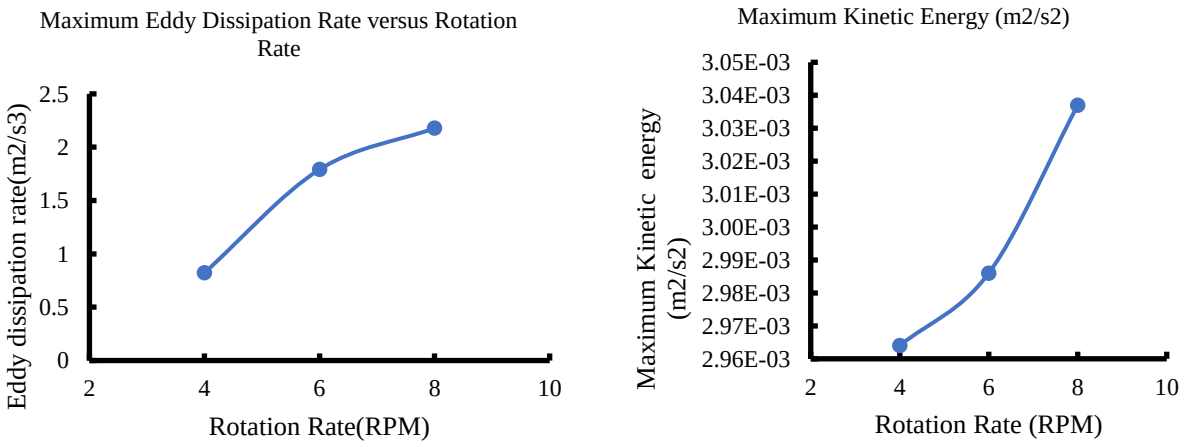

Figure 3.16 - Eddy Dissipation rate and Maximum Kinetic Energy at Different Rotation Rates for d = 0.005 m, L = 1.0 m

Case 4: d = 0.006m, L = 0.6 m

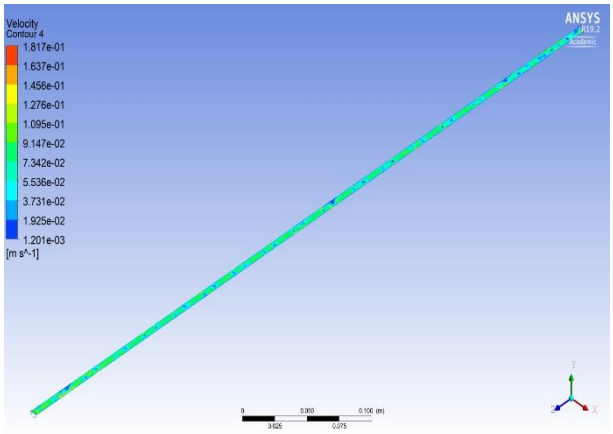

(a) At 4 RPM

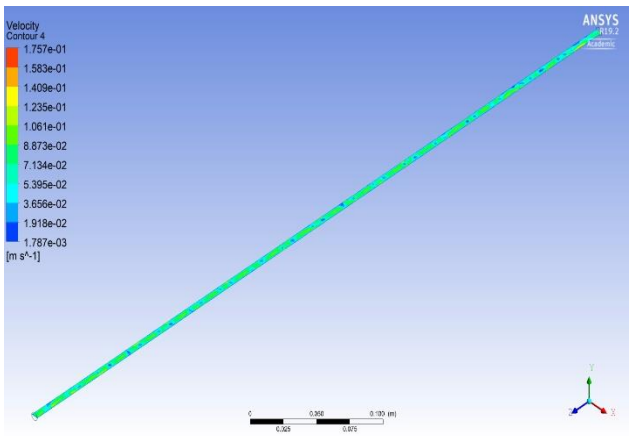

(b) At 6 RPM

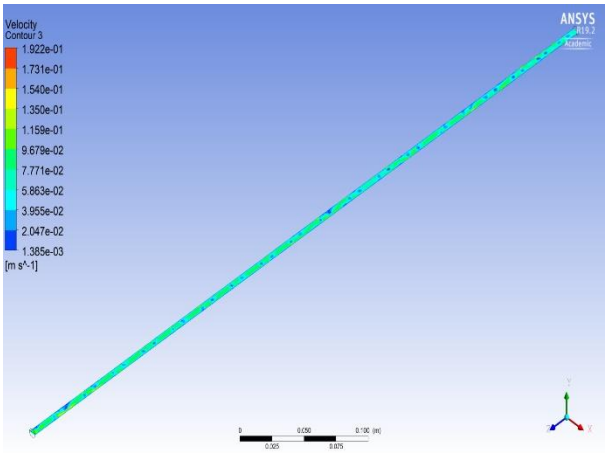

(c) At 8RPM

Figure 3.17 - Velocity Contours at Different Rotation Rates for d = 0.006m, L = 0.6 m (YZ plane)

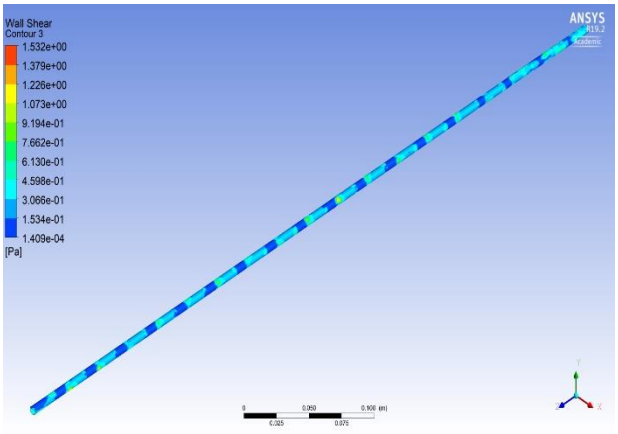

(b) Wall Shear at 4RPM

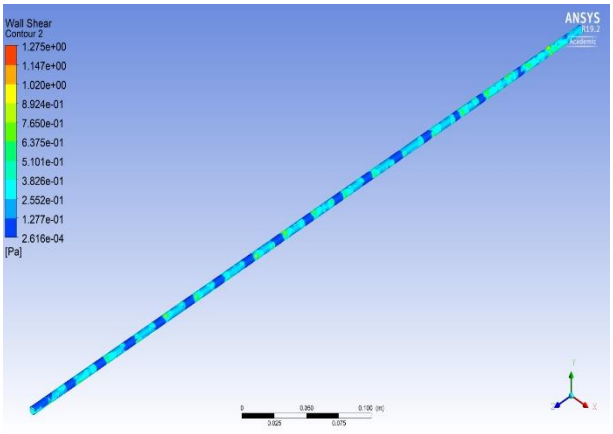

(b) Wall Shear at 6RPM

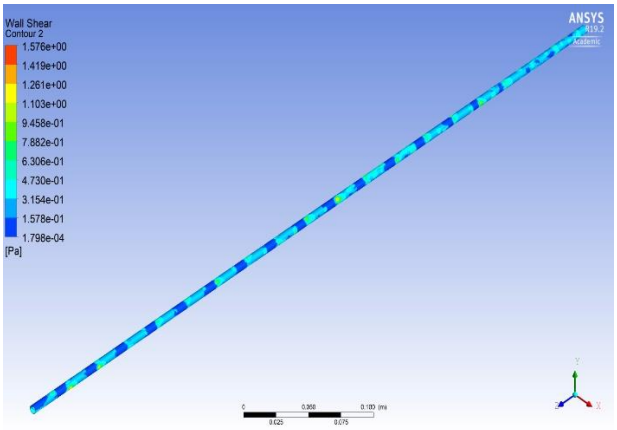

(c) Wall shear at 8RPM

Figure 3.18 - Wall Shear Contours at Different Rotation Rates for d = 0.006m, L = 0.6 m (YZ plane)

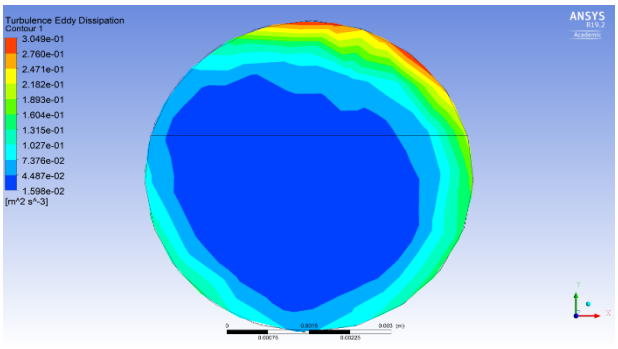

(a) At 4 RPM

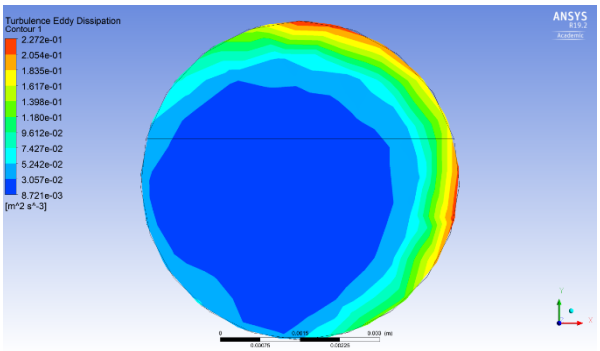

(b) At 6 RPM

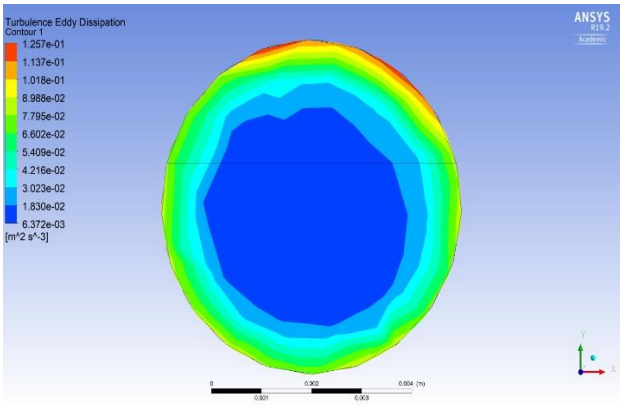

(c) At 8RPM

Figure 3.19 Turbulent Eddy Dissipation Rate at Different Rotation Rates for d = 0.006m, L = 0.6 m (XY plane)

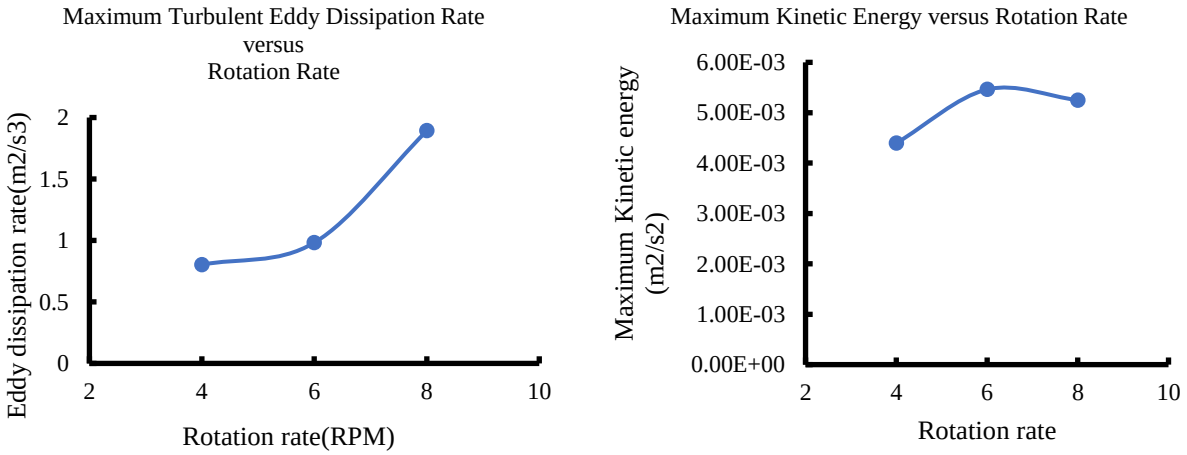

Figure 3.20 - Eddy Dissipation Rate and Maximum Kinetic Energy at Different Rotation Rates for d = 0.006m, L = 0.6 m

Case 5: d = 0.006 m, L = 0.7 m

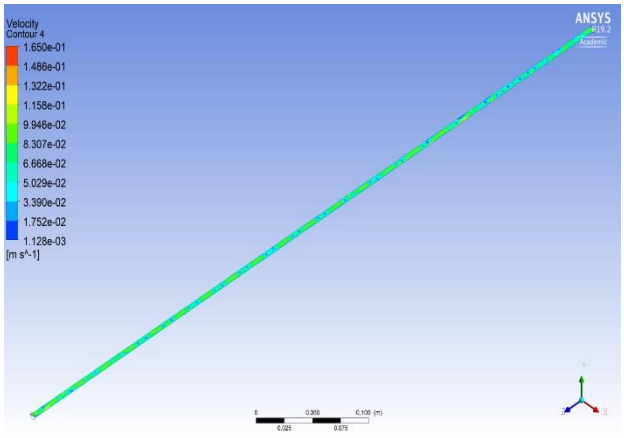

(a) At 4 RPM

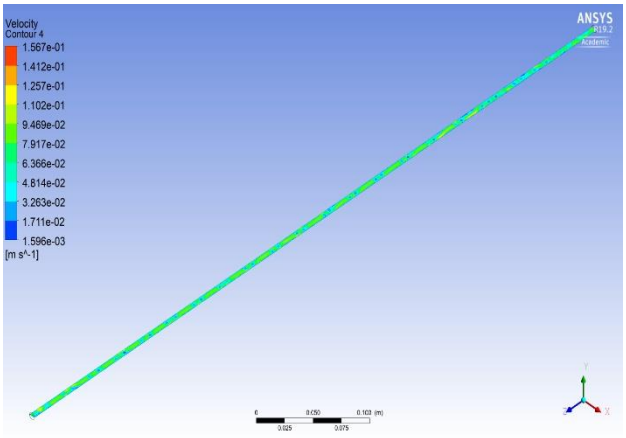

(b) At 6 RPM

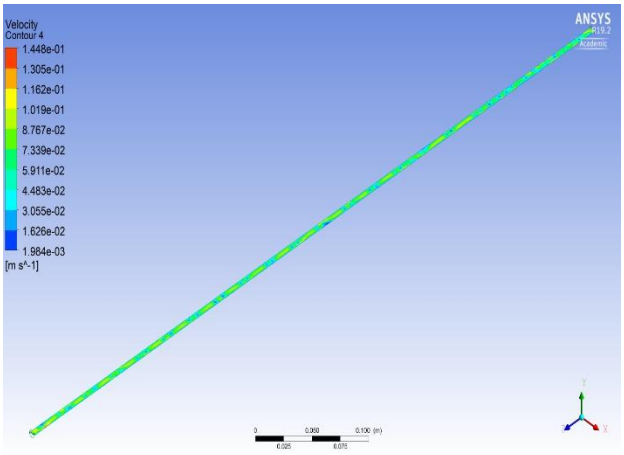

(c) At 8RPM

Figure 3.21 Velocity Contours at Different Rotation Rates for d = 0.006 m, L = 0.7 m (YZ plane)

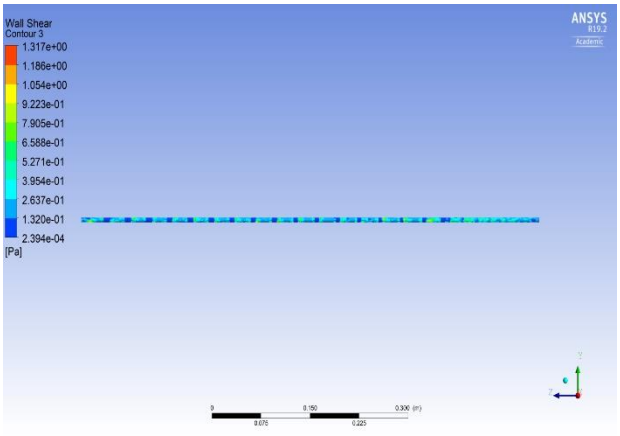

(c) Wall Shear at 4RPM

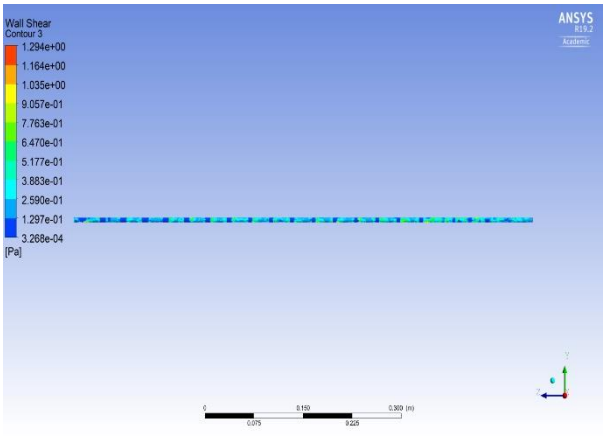

(b) Wall shear at 6RPM

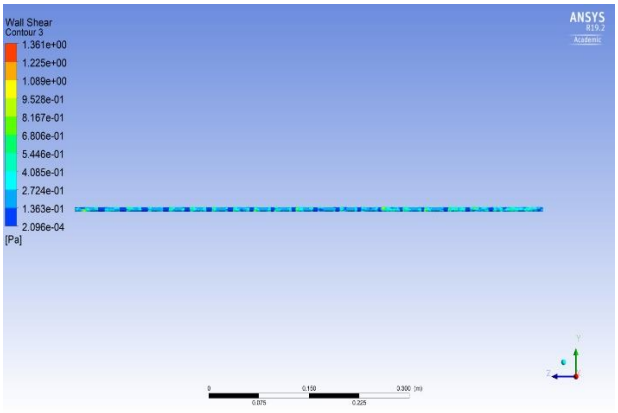

(c) Wall shear at 8RPM

Figure 3.22 - Wall Shear Contours at different Rotation Rates for d = 0.006 m, L = 0.7 m (YZ plane)

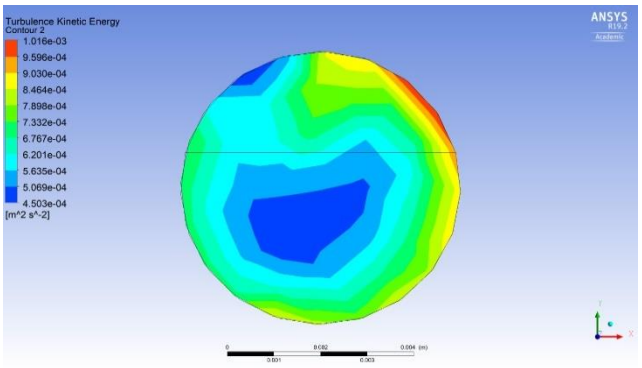

(b) At 4 RPM

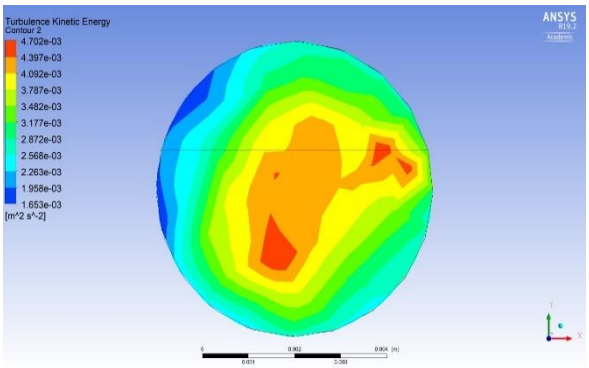

(b) At 6 RPM

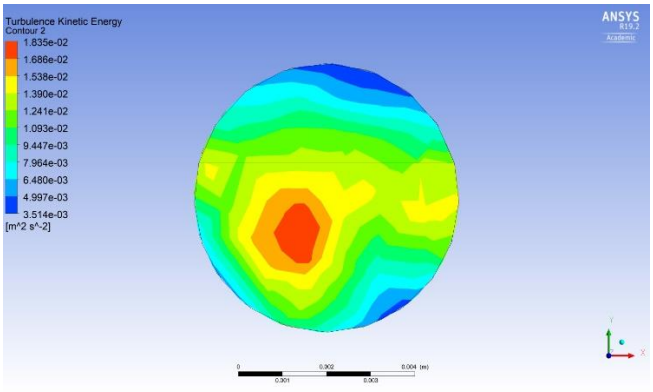

(c) At 8RPM

Figure 3.23 - Turbulent Eddy dissipation Rate at Different Rotation Rates for d = 0.006 m, L = 0.7 m (XY plane)

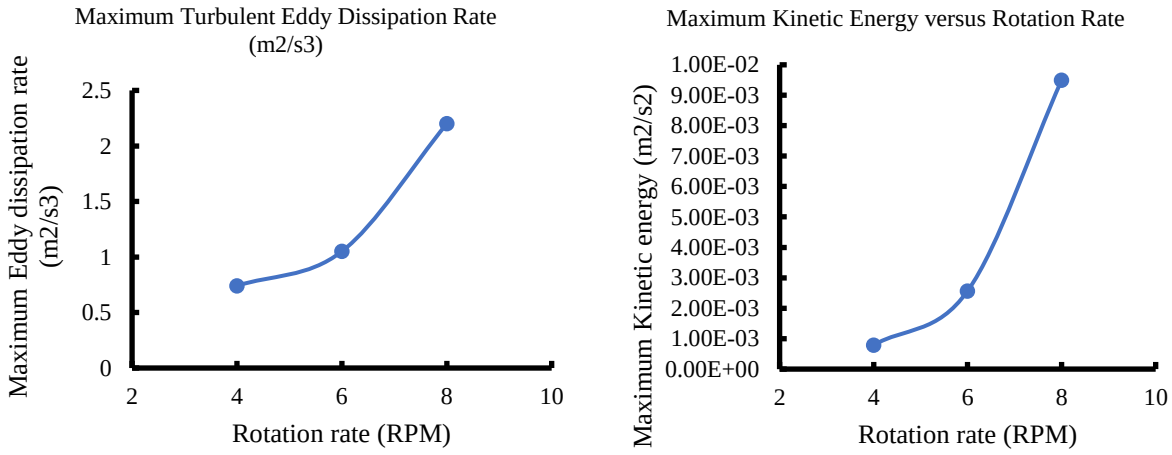

Figure 3.24 - Eddy Dissipation Rate and Maximum Kinetic Energy at Different Rotation Rates for d = 0.006 m, L = 0.7 m

Case 6: d = 0.006 m, L = 1.0 m

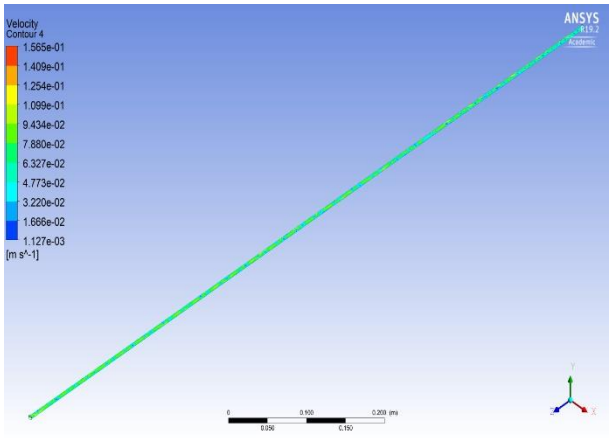

(a) At 4 RPM

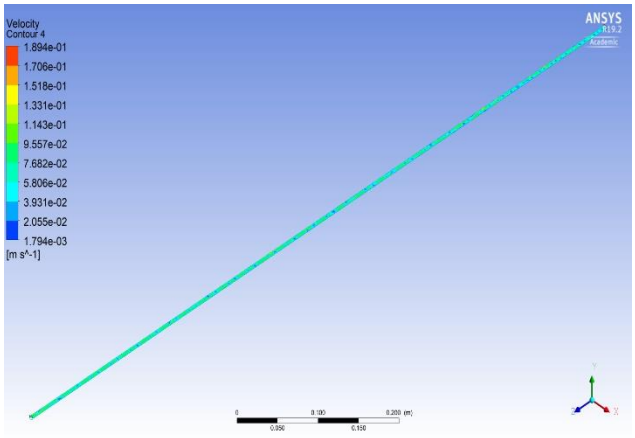

(b) At 6 RPM

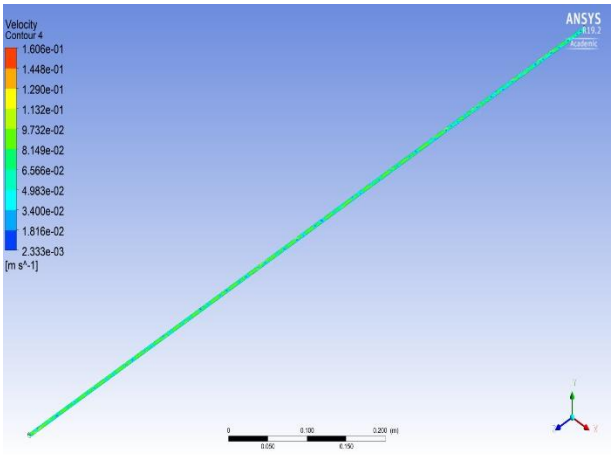

(c) At 8RPM

Figure 3.25 Velocity Contours at Different Rotation Rates for d = 0.006 m, L = 1.0 m (YZ plane)

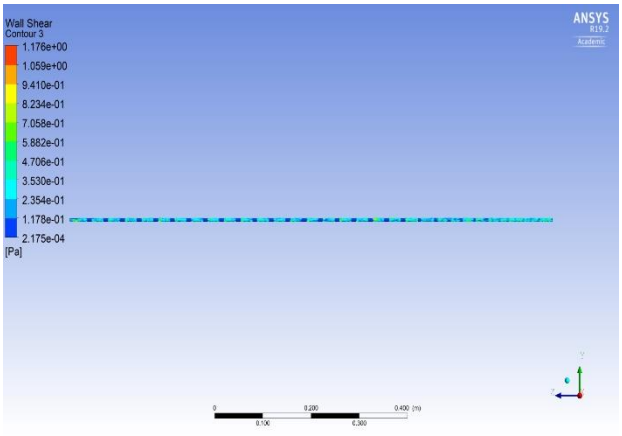

(d) Wall Shear at 4RPM

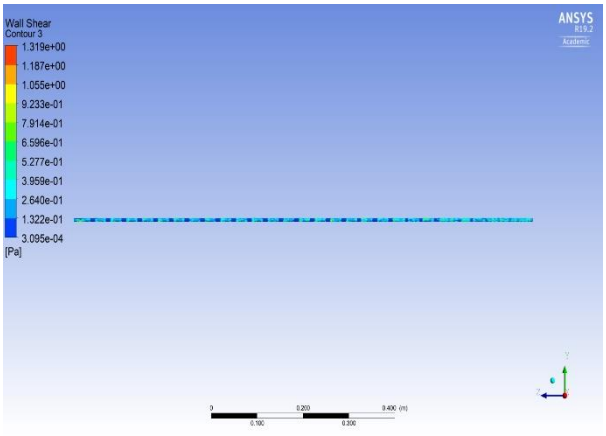

(b) Wall Shear at 6RPM

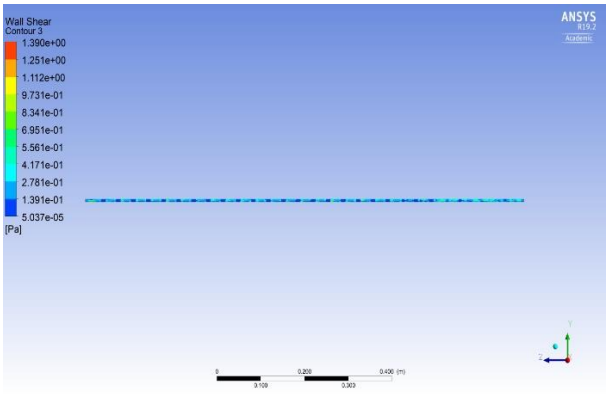

(c) Wall Shear at 8RPM

Figure 3.26 - Wall Shear Contours at Different Rotation Rates for d = 0.006 m, L = 1.0 m (YZ plane)

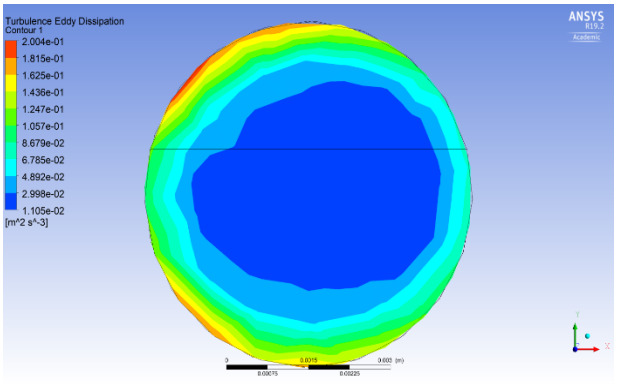

(c) At 4 RPM

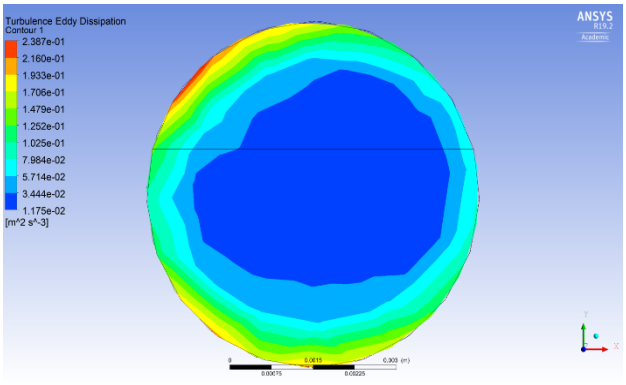

(b) At 6 RPM

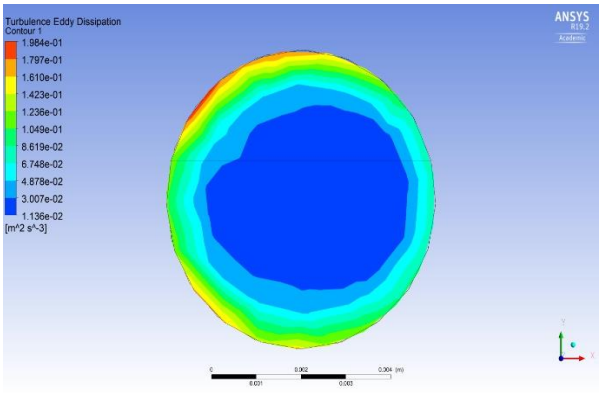

(c) At 8RPM

Figure 3.27 - Turbulent Eddy Dissipation Rate at Different Rotation Rates for d = 0.006 m, L = 1.0 m (XY plane)

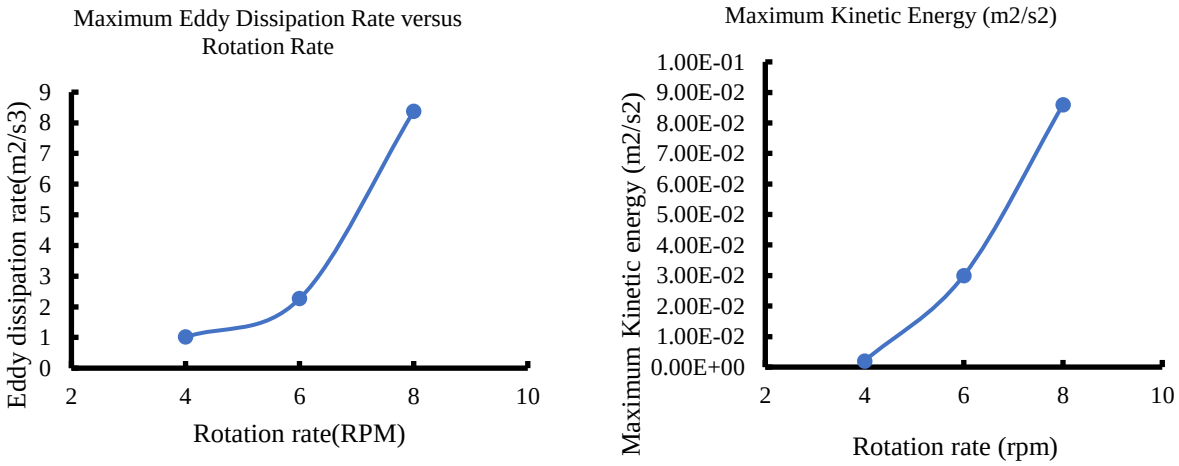

Figure 3.28 - Eddy Dissipation Rate and Maximum Kinetic Energy at Different Rotation Rates for d = 0.006 m, L = 1.0 m

Case 7: d = 0.004 m, L = 0.6, 0.7, 1.0 m

The simulations conducted at this case didn't converge and significant reverse flow was observed due to the smaller diameter of the tube.

3.5 Conclusions

CFD simulations were used to study the various hydrodynamic factors and flow variables in the spiroid. The spiroid didn't function at diameters lower than the 0.005 m. Due to low turbulence and low rotational rates, there was no major difference in velocity contours or wall shears. The maximum wall shear observed was in the order of 10^{-1} which enables this bioreactor to operate at a lower shear environment when compared to conventional bioreactors. Turbulence eddy dissipation rate is an important factor to determine bubble breakage. Smaller bubbles provide larger surface to volume ratios increasing available area for mass transfer. High eddy dissipation rates were noticed at 8 rpm. The spiroid was most effective in terms of mixing at 8 rpm. At 4 and 6 rpm, the interaction between gas and liquid was small resulting in low eddy dissipation rates. The rotation rate, diameter and length influence the hydrodynamic factors. These simulations can serve as auxiliary experiments for developing experimentation protocols on basis of rotation rates.

Abbreviations

μ	molecular dynamic viscosity (Pa-s)
μ_t	turbulent or eddy viscosity (Pa-s)
3D	Three Dimensional
CFD	Computational Fluid Dynamics
d	diameter (m)
DOE	Design of Experiments
G_b	generation term due to the buoyancy, (J s^{-1} m^{-3} or kg m^{-1} s^{-3});
G_k	generation term because of the mean velocity gradients (J s^{-1} m^{-3} or kg m^{-1} s^{-3})
k	turbulence kinetic energy per unit mass (J kg^{-1} or m^2 s^{-2})
ν	kinematic viscosity (m^2 s^{-1})
L	length (m)
MRF	Multiple Reference Frame
RANS	Reynolds-Averaged Navier-stokes
RPM	Rotations per minute
t	time (s)
VOF	volume of fluid
Y_M	effects from the fluctuating dilatation in the compressible turbulence on the overall dissipation rate (J s^{-1} m^{-3} or kg m^{-1} s^{-3})
ε	dissipation rate per unit mass (J kg^{-1} s^{-1} or m^2 s^{-3})

References

Ali, M., Yan, C., Sun, Z., Gu, H., Wang, J., & Mehboob, K. (2013). Iodine removal efficiency in non-submerged and submerged self-priming venturi scrubber. *Nuclear Engineering and Technology*, *45*(2), 203–210.

Amer, M., Feng, Y., & Ramsey, J. D. (2019). Using CFD simulations and statistical analysis to correlate oxygen mass transfer coefficient to both geometrical parameters and operating conditions in a stirred-tank bioreactor. *Biotechnology Progress*, *35*(3), 1–14.

ANSYS FLUENT 13 User's Guide. (2013). Ansys Fluent Theory Guide. *ANSYS Inc., USA*, *15317*(November), 724–746.

Argyropoulos, C. D., & Markatos, N. C. (2015). Recent advances on the numerical modelling of turbulent flows. *Applied Mathematical Modelling*, *39*(2), 693–732.

Ashfaq, T., Qureshi, K., Shah, A., Waheed, K., Siddique, W., Irfan, N., … Farooq, A. (2019). CFD investigation of iodine mass transfer in venturi scrubbing solution of Filtered Containment Venting System. *Progress in Nuclear Energy*, *111*(November 2018), 195–204.

Bezzo, F., Macchietto, S., & Pantelides, C. C. (2003). General hybrid multizonal/CFD approach for bioreactor modeling. *AIChE Journal*, *49*(8), 2133–2148.

Brannock, M., Wang, Y., & Leslie, G. (2010). Mixing characterisation of full-scale membrane bioreactors: CFD modelling with experimental validation. *Water Research*, *44*(10), 3181–3191.

Childs, P. R. N. (2011). Rotating Cylinders, Annuli, and Spheres. In *Rotating Flow*.

Dhanasekharan, K. M., Sanyal, J., Jain, A., & Haidari, A. (2005). A generalized approach to model oxygen transfer in bioreactors using population balances and computational fluid dynamics. *Chemical Engineering Science*, *60*(1), 213–218.

Hutmacher, D. W., & Singh, H. (2008). Computational fluid dynamics for improved bioreactor design and 3D culture. *Trends in Biotechnology*, *26*(4), 166–172.

Liow, K. Y. S., Tan, B. T., Thouas, G. A., & Thompson, M. C. (2009). CFD modeling of the steady-state momentum and oxygen transport in a bioreactor that is driven by an aerial

rotating disk. *Modern Physics Letters B*, *23*(2), 121–127.

Niño, L., Peñuela, M., & Gelves, G. R. (2018). Gas-Liquid Hydrodynamics Simulation using CFD in a Helical Ribbon Impeller Applied for Non-Newtonian Fluids. *International Journal of Applied Engineering Research*, *13*(11), 9353–9359. Retrieved from http://www.ripublication.com

Rathore, A. S., Kanwar Shekhawat, L., & Loomba, V. (2016). Computational Fluid Dynamics for Bioreactor Design. *Bioreactors*, 295–322.

Ravindram, M. (1987). Modeling of a venturi scrubber for the control of gaseous pollutants. "Reply to comments". *Industrial and Engineering Chemistry Research*, *26*(6), 1266.

Sergio S. de Jesus, Edgar Leonardo Martinez, Aulus R.R. Binelli, Aline Santana, R. M. F. (2013). CFD Simulation of Hydrodynamic Behaviors and gas liquid mass transfer in a stirred airlift bioreactor. *International Journal of Chemical Materials Science and Engineering*, *7*(12), 165–169.

Villiger, T. K., Neunstoecklin, B., Karst, D. J., Lucas, E., Stettler, M., Broly, H., … Soos, M. (2018). Experimental and CFD physical characterization of animal cell bioreactors: From micro- to production scale. *Biochemical Engineering Journal*, *131*, 84–94.

Werner, S., Kaiser, S. C., Kraume, M., & Eibl, D. (2014). Computational fluid dynamics as a modern tool for engineering characterization of bioreactors. *Pharmaceutical Bioprocessing*, *2*(1), 85–99.

Zhang, H., Williams-Dalson, W., Keshavarz-Moore, E., & Shamlou, P. A. (2005). Computational-fluid-dynamics (CFD) analysis of mixing and gas–liquid mass transfer in shake flasks. *Biotechnology and Applied Biochemistry*, *41*(1), 1.

Chapter 4 - Growth and Optimization of *Saccharomyces cerevisiae* in a Chemostat

Abstract

A 3D-printed novel continuous bioreactor with an internal spiroid was shown to increase gas-liquid contact areas which increases cell growth and mixing. Multiphase flow modeling using computational fluid dynamics showed that the bioreactor with spiroid works better at higher rotation rates of 6 RPM and 8 RPM. The bioreactor is fabricated by rapid prototyping and can be operated in either batch or continuous modes with inlet flows via rotary unions available to provide medium and oxygen and outlet flows for waste and in-line analysis. *Saccharomyces cerevisiae* was cultured in the reactor to validate the effect of the spiroid on cell growth. Cell growth was monitored at different operating conditions using a spectrophotometer. Results show that *Saccharomyces cerevisiae* could be cultured for more than 12 hours continuously at steady state. The reactor with spiroid produced higher biomass concentrations at high rotation rates and at low medium flow rates in both batch and continuous modes indicating the efficiency of the spiroid for enhanced production. Growth curves were generated for these cell lines, and the biomass production increased. Computational fluid dynamic simulation models were generated for the cell lines and were in good agreement with the experimental results. The use of bioreactor with spiroid showed a 21% increase in yeast cells in batch mode and the operating time reduced by 27% with the spiroid. These results indicate that the reactor with a spiroid has a greater potential in increasing cell production in upstream bioprocessing.

Keywords: continuous bioreactor, spiroid, *Saccharomyces cerevisiae*, cell growth

4.1 Introduction

With the implementation of good manufacturing standards for cell treatments, innovative suspension bioreactors may create a 25-fold growth of human embryonic cells in six days as compared to static culture flasks (Krawetz et al., 2010). Computational frameworks based on metabolic–hydrodynamic coupling can provide informative insights on cell lifelines and metabolic responses induced by environmental fluctuations in an industrial bioreactor (G. Wang et al., 2020). The integration of modeling and experiments can be used to determine the transfer of mammalian cell culture processes and the physical characterization of bioreactors. The findings of these analyses can be used to validate scale up and scale down procedures (Villiger et al., 2018). Guo et al. (2018) investigated the manufacturing and scaling up of docosahexaenoic acid (DHA) using computational fluid dynamics (CFD). Various impeller combinations were studied to generate a homogeneous flow field environment in the bioreactor, and the reactor was optimized to a productivity of 326.5 mg/ (L h). Teng et al., (2021) used a similar technique to analyze the behavior of BHK- 21 cells in three different sized scaled-up bioreactors using CFD. The results of itaconic acid optimization studies in a flask level stirred tank bioreactor utilizing the classical one factor approach and statistical experiment designs demonstrated the viability of high production on scale up (Bafana et al., 2019). He et al. (2019) created a mass transfer approach for calculating gassing requirements in the bioreactor cell culture environment. Predictive modeling may also help with carbon dioxide gassing by estimating the range of a gas flow meter. Das et al., (2019) demonstrated the use of microcarrier-based bioreactor systems for continued development and scale-up of flask-based mesenchymal stromal cells (MSC). Single-use bioreactors (SUB) may benefit shear-sensitive cell lines and may also be useful in continuous perfusion operations. SUBs enable scalable parallel cultivation on a tiny scale without cleaning, and numerous types of plates

and small reaction vessels are already available. When employed on a wider scale, continuous culture systems with cell retention are a better option to batch and fed-batch approaches (Junne et al., 2018). The addition of sensors to all bioreactor scales allows for robust and dependable online monitoring of cellular proliferation in all fed-batch cultures. This can result in rapid process development and risk minimization, and hence a more robust production process (Metze et al., 2020). The amount of nutrients, type of strain and cell culture medium effect the proliferation of yeast in exponential phase (R. N. Bento, M. A. Rendas, V. A. R. Semedo, C. E. S. Bernardes, M. E. Minas da Piedade, 2016). Yeast cell growth was best at pH=4 and largest cell sizes were also produced at this condition (Salari et al., 2017). Malairuang et al., 2020 showed that the right source of carbon and using a fed-batch operation can produce high cell densities of yeast and then could be cultured at large scale in industries.

This research investigated the growth of yeast at various operating conditions and medium flow rates. The reactor was operated at both batch and continuous modes allowing the feasibility of a chemostat operation. Desired cell concentrations and higher biomass values were studied under the influence of spiroid and rotation rates of 6 and 8 rpm.

4.2 Materials and Methods

The continuous bioreactor used for this study is a bench-scale bioreactor (Fang et al., 2017) which consists of an outer cylindrical shell with a spiroid. The spiroid is embedded onto the wall of this cylinder to increase gas-liquid contact areas which helps in enhancing oxygen transfer within the reactor. The bioreactor can be rotated horizontally with the help of a roller bed as shown in Figure 4.1. The two inlet and two outlet ports present at either end of the reactor help in providing medium and oxygen continuously to the reactor and facilitate in-line and off-line sampling. This bioreactor is prototyped using stereolithography (SLA) 3D printing techniques.

The end caps were prototyped using SLS technique and Nylon 66 material (Figure 4.2) for durability and for preventing cracks under pressure for longer periods of cell culture studies.

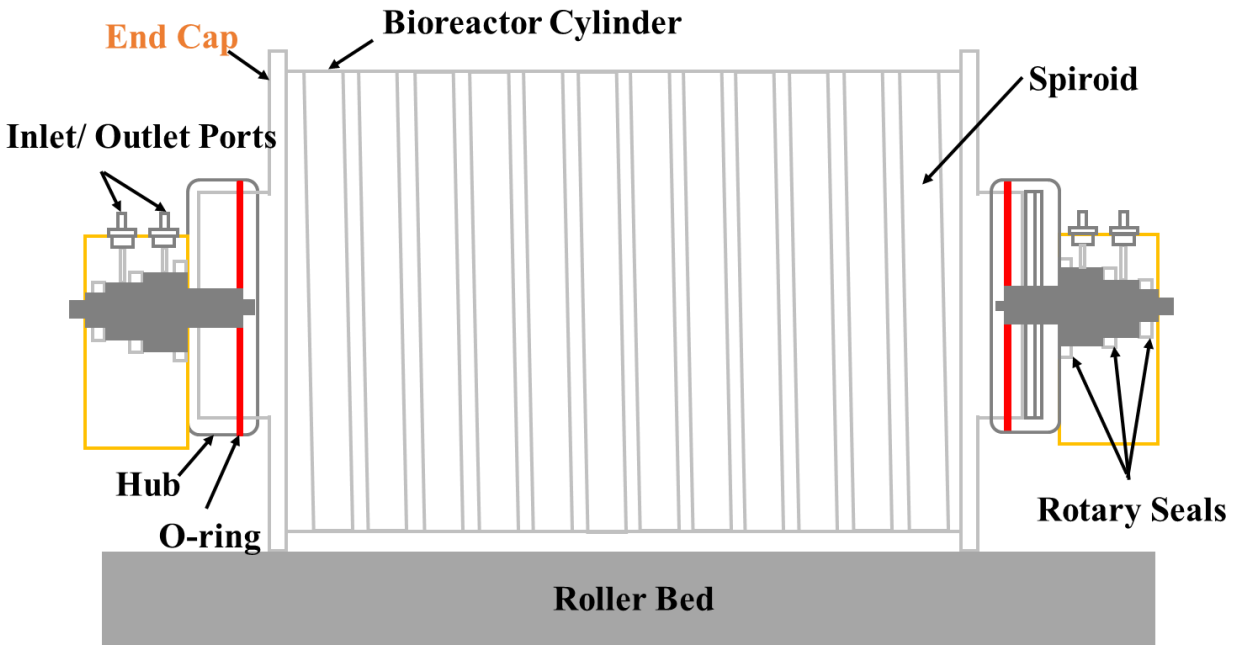

Figure 4.1 Bioreactor Schematic (Fang et al., 2018)

Figure 4.2 Image of Bioreactor and Endcaps

The dimensions of the scaled-up bioreactor are summarized in Table 4-1

Table 4-1 Bioreactor Dimensions

Parameter	Value
Chamber Length (m)	0.193
Chamber Inner Diameter (m)	0.0889
Spiroid Length (m)	3.12
Spiroid Inner Diameter (m)	0.00953
Spiroid Turns	12
Volume (10^{-4} m^3)	9.86

4.2.1 Computational Fluid Dynamics

The optimization of spiroid is a major factor which will enhance the oxygen transfer in the bioreactor. The length and diameter of the spiroid must be optimum to provide the highest amount of oxygen transfer in the reactor. ANSYS workbench 19.2 was used in this research to carry out the CFD simulations (Figure 4.3). The basic steps for performing any simulation in ANSYS workbench are as follows:

1. Create the geometry (Design Modeler was used in this research)
2. Mesh the geometry using ANSYS meshing tool.
3. Create 'Named selections' for the domain of study.
4. Setup the model needed to illustrate the flow phenomenon
5. Run the simulations
6. Analyze and predict the results using CFD-post processing.

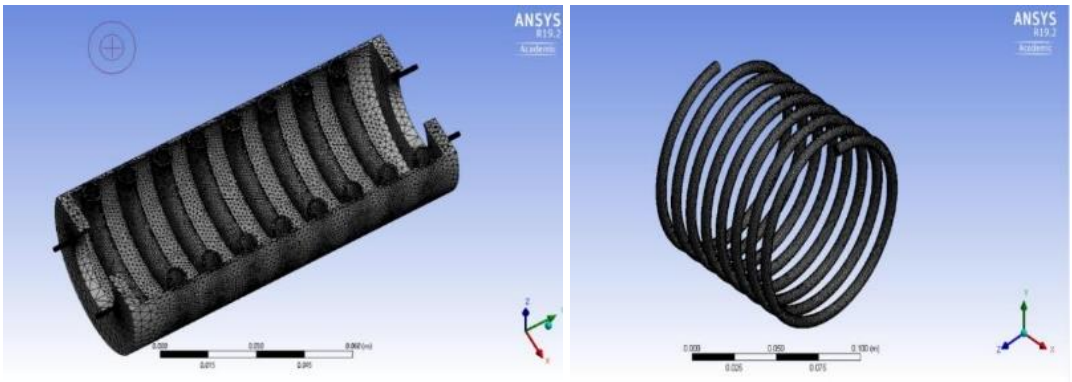

Figure 4.3 Bioreactor Cross-Section and Independent Spiroid Showing FEA Mesh Pattern. (ANSYS 19.2)

4.2.2 Cell culture

4.2.2.1 Strain and Medium

The culture used in this research was *Saccharomyces cerevisiae* (yeast) obtained from Ward's Science (VWR Life Sciences, USA). The growth medium used for yeast was YPD medium, which contained 20g peptone, 10g yeast extract, 20 glucose per L of distilled water (VWR life sciences, USA). The pH of the medium was 6.5 and it was autoclaved for 15 minutes or sterile filtered before use. The final concentration of glucose in the medium during experiments was 7 $g.L^{-1}$.

4.2.2.2 Operating Conditions

Saccharomyces cerevisiae was inoculated with a disposable inoculation loop from the petri dish and precultured in a shaker incubator with YPD medium at 200 rpm and 30°C for 12 hours. The optical density of the culture was then adjusted to 0.1 before transferring into the bioreactor under a hood. The reactor was operated in batch mode first for four hours, and then continuous

mode (chemostat) with different rotation rates (4 rpm, 6 rpm, 8 rpm) and fresh medium flowrates (0.6 ml/min, 1.5 ml/min and 3 ml/min). Oxygen was provided to the reactor periodically along with venting to maintain constant levels. After batch mode of 4 hours, fresh medium was pumped into the reactor and the same amount was removed to maintain constant volume. The feed was maintained sterile with the help of 0.22-micron filter, and the reactor was half filled in volume throughout the experiments.

The exponential growth in batch mode could be described as:

$$\frac{1}{X}\frac{dX}{dt} = \mu \tag{4-2}$$

where X is the biomass concentration (cell dry weight per unit volume, $g.L^{-1}$) at time t (hr); μ is the specific growth rate (hr^{-1}). The exponential equation was only applied when the substrates are in excess (Herbert et al., 1956).

In addition, if the feed media are sterile, the changes of bacterial concentration in a continuous system (or a chemostat) could be described as follows (Herbert et al., 1956):

$$\frac{dX}{dt} = \mu X - DX \tag{4-2}$$

where D is the dilution rate (hr^{-1}) defined as:

$$D = \frac{F}{V} = \frac{1}{\tau} \tag{4-3}$$

where F is the flowrate ($L.hr^{-1}$); V is the volume maintained in the reactor (L); $\boldsymbol{\tau}$ is the mean residence time (hr).

$$\mu = D \text{ (Steady state)}$$

$$\mu < D \text{ (wash out)}$$

When the specific growth rate is less than the dilution rate, the cells cannot maintain the concentration and this will lead to a condition called wash out; if the growth rate is equal to dilution

rate, the system reached steady state, i.e., cells maintain a constant concentration. Thus, through manipulating the dilution rate, the growth rate of the cells could be controlled and maintained.

4.2.2.3 Analytical Methods

The growth of yeast in the reactor was monitored by measuring OD_{600} of the samples using Flex Station 3 Micro plate reader (Molecular Devices) at different time intervals during the experiment. These optical density measurements were calibrated to cell concentrations (g/L) and reported. Samples for these readings were drawn periodically through the outlet and monitored. Metabolite concentration (glucose consumption) in the reactor was measured by using a glucose monitor (GM100, Bioreactor sciences, Inc., Lawrenceville, GA, USA). Duplicate readings were taken for every operating condition and fresh medium flowrate. Glucose samples were cooled to room temperature before taking the readings to ensure that they fall within the glucose monitor's measurement range.

4.3 Results and Discussion

4.3.1 CFD simulations

In this research, a pressure-based model was used. The simulations were carried out at steady-state and gravity was disabled. The VOF method is used in this research to simulate flow through the spiroid. The interface between the phases was applied using the sharp/dispersed option with implicit formulation. Water was set as primary phase (blue in Figure 4.4) and air as secondary phase (red in Figure 4.4). Phase interactions like surface tension were enabled at standard conditions. The boundary conditions were appropriately set for each phase and the pressure in the headspace of the spiroid was assumed to be 1.0 atmosphere.

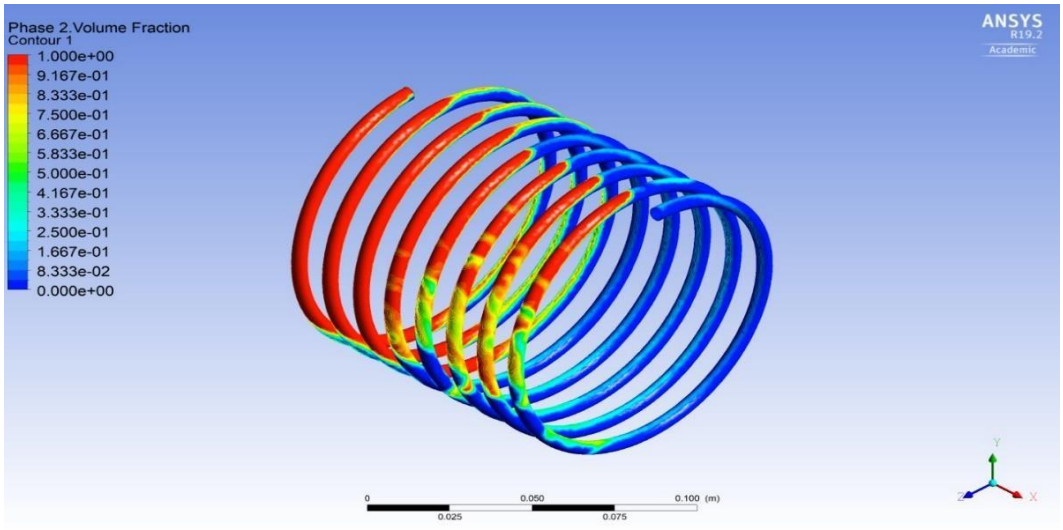

Figure 4.4 Multiphase Contours of Water and Air using the VOF method 8 RPM with Reactor Two-Thirds Full

The criterion for convergence was checked by using the residual profiles. In case the solution does not converge even after long iterations, convergence conclusions can be made if the residuals continue to remain almost the same or decrease at a very small rate. Mass conservation for each was also checked to validate the convergence. Figure 4.4 shows the formation of thin liquid film (areas of yellow to green) from which it can be interpreted that the interfacial area in the volumetric mass transfer coefficients consists of film area and gas-liquid contact area. The thin film area increased with increased rotation rate determining the increase in oxygen transfer and this film thickness or area was greatest at 8 RPM

4.3.2 Cell Culture Results

The growth of *Saccharomyces cerevisiae* in the bioreactor was relatively low at lower rotation rates which could be due to little to no aeration. For batch mode, the reactor was operated

for a period of 12 hours to analyze the growth of yeast at 4, 6 and 8 RPM with and without spiroid. Samples were collected every 2 hours in batch mode. Optical density measurements along with glucose consumption was monitored. Figure 4.5 shows the effect of spiroid on cell dry weight measurements at various rotation rates. The cell growth in the bioreactor with spiroid was 57% more than the reactor without spiroid (0.58 g/l over 0.37 g/l) over a period of 12 hours. The overall operating time for the reactor decreased by 27% using the spiroid in batch mode at 8 RPM as shown in Figure 4.6

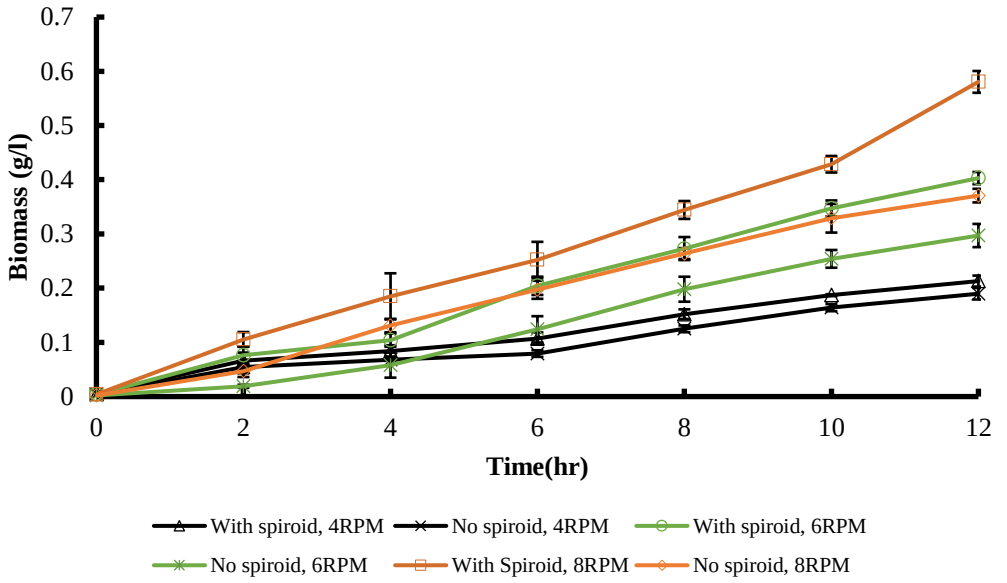

Figure 4.5 Batch Mode, Various Rotation Rates

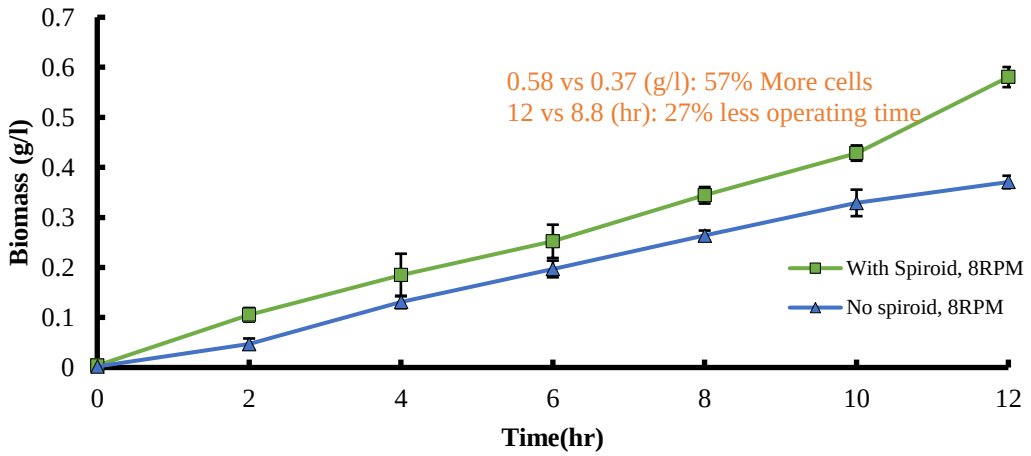

Figure 4.6 Batch Mode, 8 RPM

For continuous mode, experiments were conducted at two different rotation rates (6 RPM, 8 RPM) and three medium flowrates (0.6 ml/min, 1.5 ml/min and 3ml/min) to demonstrate different steady state level concentrations. Duplicate experiments were conducted at each condition and averaged. The reactor was operated in batch mode for four hours and then changed to chemostat setting. Cells grew in exponential phase in batch mode for four hours and eventually reached steady state concentration with continuous flow in both growth curve and glucose consumption profiles. Figure 4.7 (a-f) represents steady state concentrations controlled by different flow rates for the bioreactor with and without spiroid at 8 rpm. The growth curves were consistent in batch mode and the steady-state concentration decreased with increased flowrates due the increased rate of cell removal. Increase in cells at lower flowrates showed a decrease in metabolite concentration in the system as seen in glucose profile. Figure 4.7 indicates that in all the steady state levels used (0.6 ml/min, 1.5 ml/min and 3 ml/min), the bioreactor with spiroid produced greater steady state cell concentrations with a maximum of

0.2152 g/L for a 12-hour operation at 0.6 ml/min (for 8 rpm). These cell concentrations could be maintained in the reactor for a period of three days.

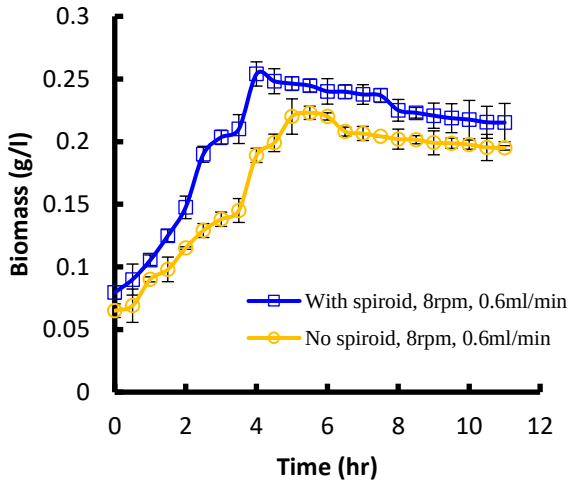

a) Growth Curve, 8rpm, 0.6 ml/min

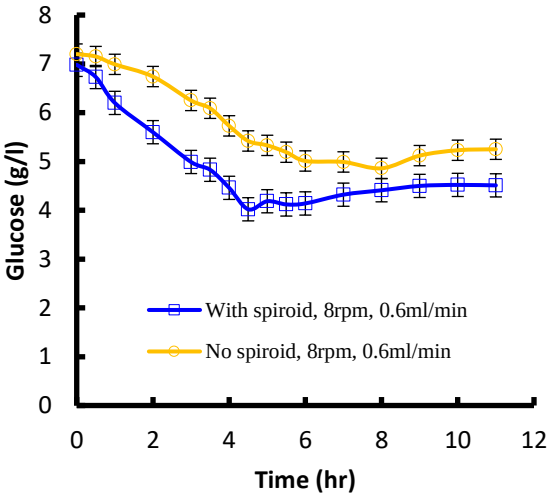

b) Glucose Profile, 8rpm, 0.6 ml/min

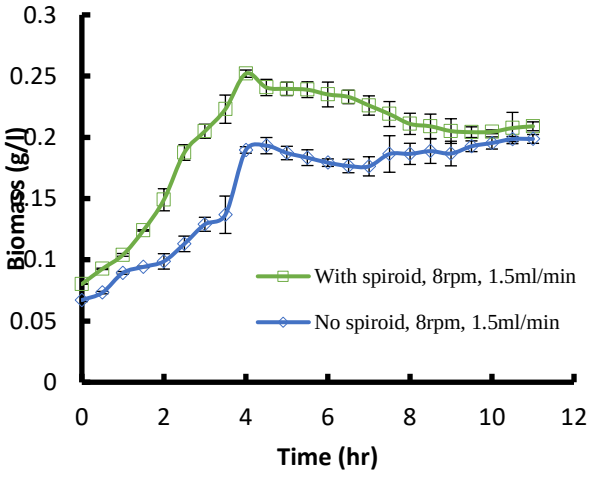

c) Growth Curve, 8 rpm, 1.5 ml/min

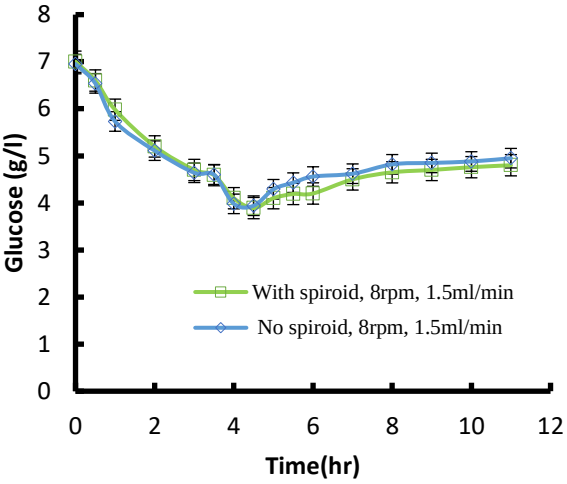

d) Glucose Profile, 8 rpm, 1.5 ml/min

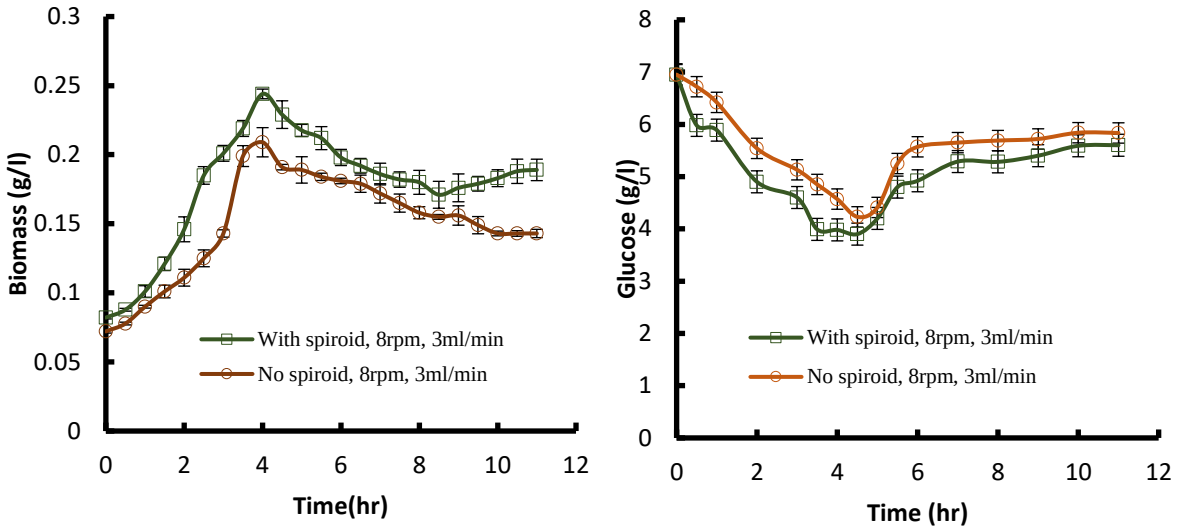

e) Growth Curve, 8 rpm 3 ml/min

f) Glucose Profile, 8 rpm, 3 ml/min

Figure 4.7 Comparison of Various Flowrates with and without Spiroid, 8 rpm

Figure 4.7 indicated that yeast cells grew faster in the system with spiroid at all three flowrates. In Figure 4.7 a), the biomass was increased by 34% with the use of spiroid in batch mode for the first 4 hours. In addition to increased biomass, a 4-hour process without the spiroid could be replaced by a 2.5-hour process with spiroid in batch, with a decreased operating time of 38%. In Figure 4.7e, when flow was established, the system with spiroid showed a 32% increased steady state level concentration in chemostat mode. This result could be attributed to the increased mixing and aeration with the use of spiroid at higher rotation rates and high flow rates (3 ml/min).

Figure 4.8(a-f) represents the growth curve and glucose profiles for rotation rate of 6 rpm at various flowrates in the bioreactor with and without spiroid. The highest biomass concentration (0.238 g/L) was seen at 0.6 ml/min with the use of spiroid. Additionally, Figure 4.8e showed that using the spiroid at 3 ml/min, cell concentrations could be obtained 1.2 hours faster in batch mode when compared to the system without spiroid with a reduction in operating time by nearly 43%. Figure 4.9 compared the system with spiroid for three different steady state levels. Though, batch

growth curves were nearly consistent, when the system was operated as a chemostat, a biomass concentration of 0.187 g/L was maintained at 0.6 ml/min which was 46% greater than that obtained using a 3ml/min flowrate (0.128 g/L) indicating the efficiency of spiroid at low flowrates which is due to cell washout at increased flowrates. Glucose profile also validated that the substrate level decreased with decreased flowrate indicating increased cell population.

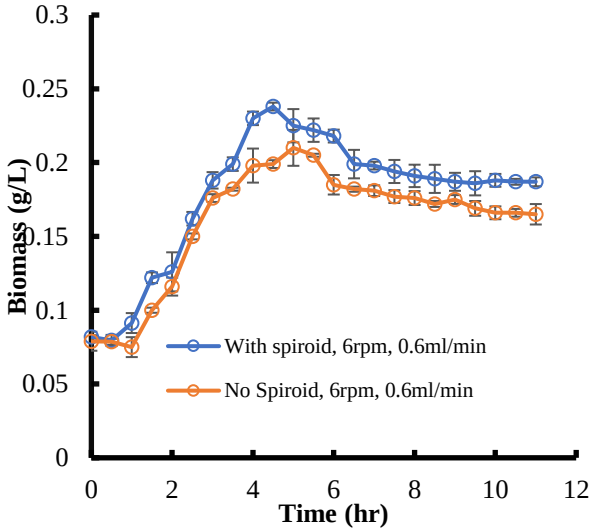

a) Growth Curve, 6 rpm, 0.6 ml/min

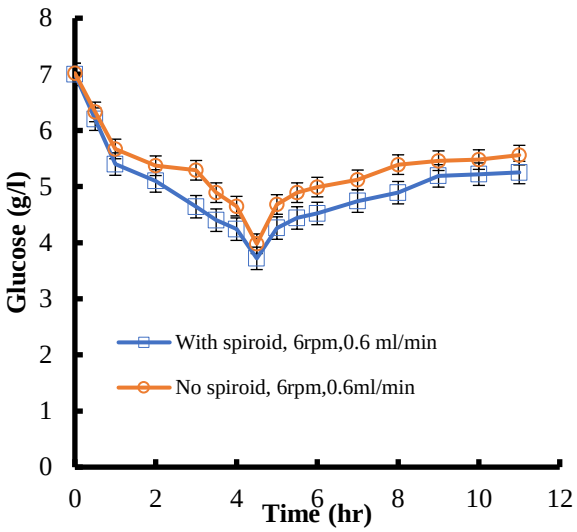

b) Glucose Profile, 6 rpm, 0.6 ml/min

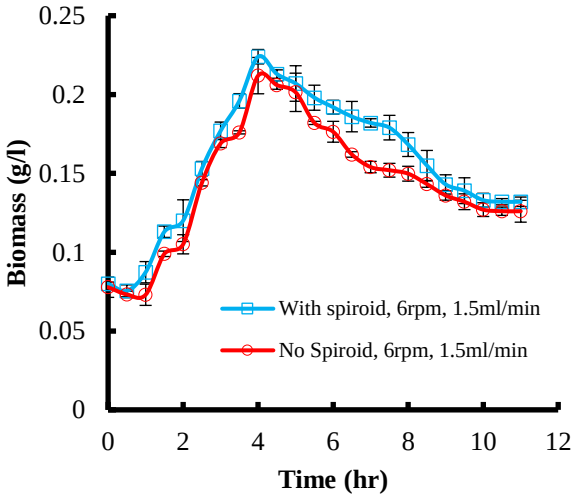

c) Growth Curve, 6 rpm, 1.5 ml/min

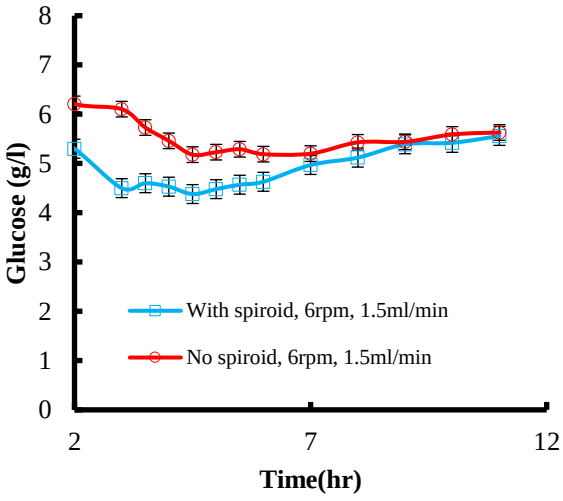

d) Glucose Profile, 6 rpm, 1.5 ml/min

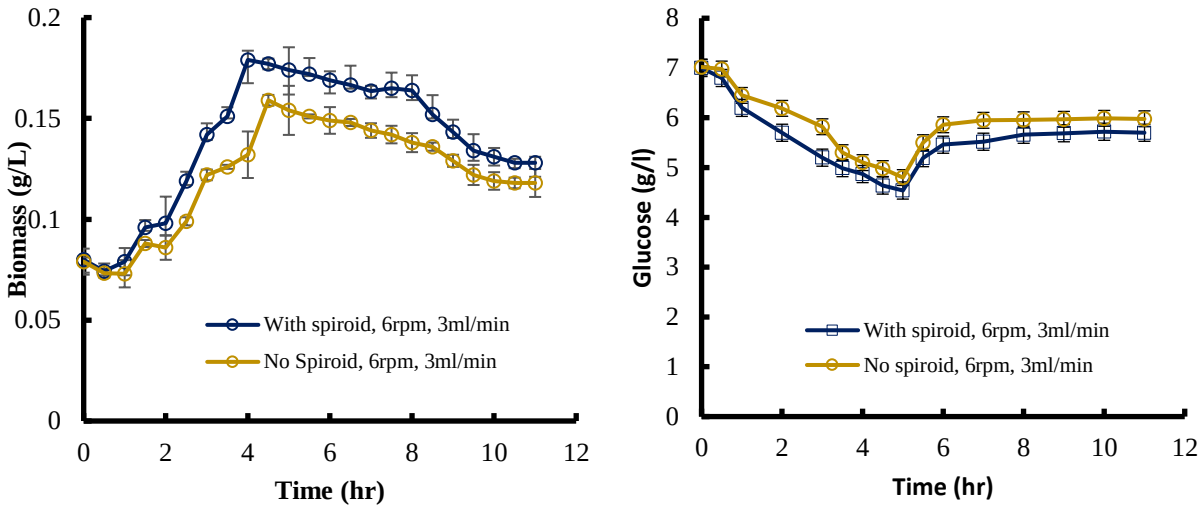

e) Growth Curve, 6 rpm, 3 ml/min

f) Glucose Profile, 6 rpm, 3 ml/min

Figure 4.8 Various Flowrates with and without Spiroid, 6 rpm

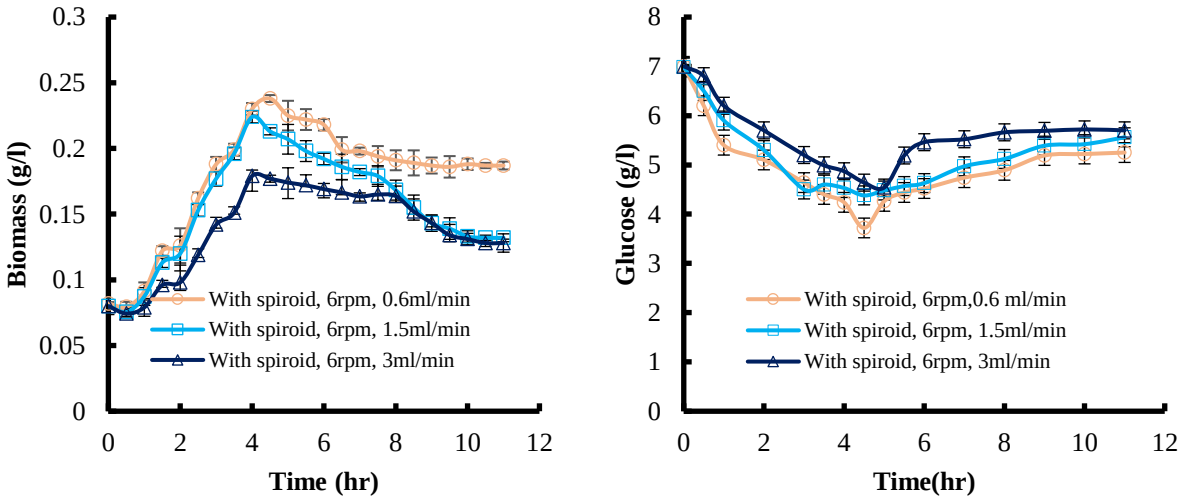

a) Growth Curve, 6rpm, Various flow rates

b) Glucose Profile, 6rpm, Various flowrates

Figure 4.9 Growth Curve and Metabolite Concentrations in Bioreactor, Various Flow Rates

Figure 4.10 compared the effect of rotations rates 6 and 8 rpm for the system with the spiroid. For 0.6 ml/min, the system showed a 15% increased biomass concentration in chemostat mode, and 58% increased biomass concentration was seen when the flowrate was changed to 1.5 ml/min keeping other parameters constant (Figure 4.10a-d). Though the obtained biomass concentration

at 8rpm with a flow rate of 1.5 ml/min was less than that obtained at 0.6 ml/min, these growth curves indicated that changing the dilution rate increased biomass concentrations significantly with spiroid.

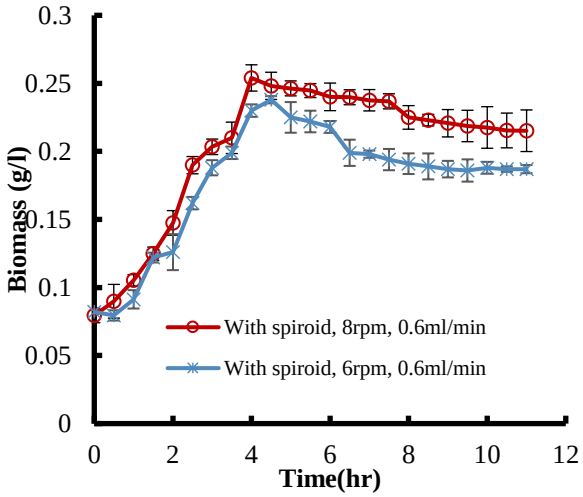

a) Growth Curve

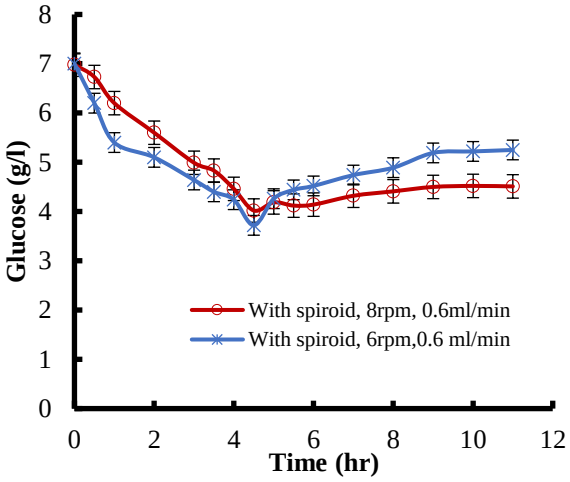

b) Glucose Profile

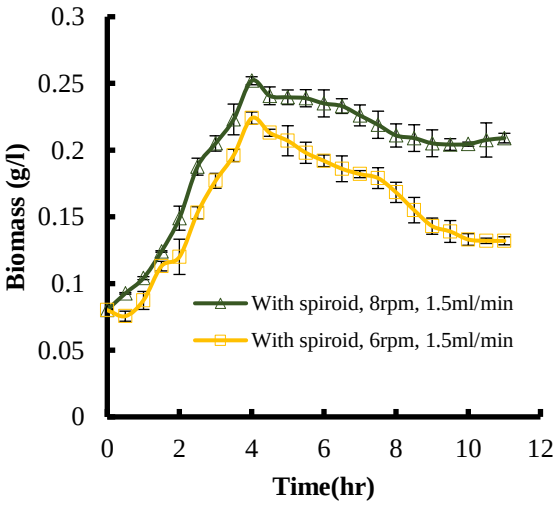

c) Growth Curve

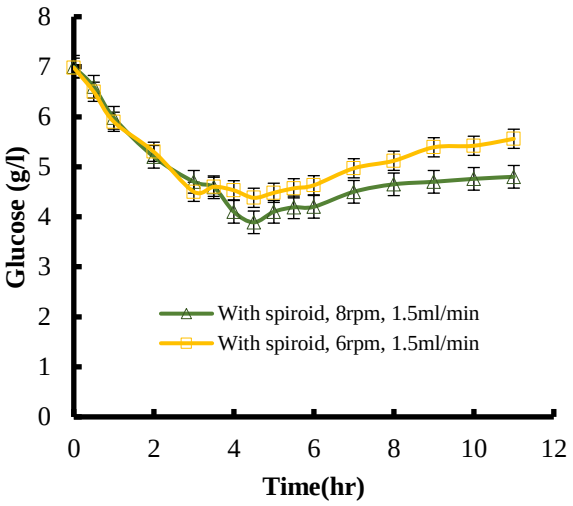

d) Glucose Profile

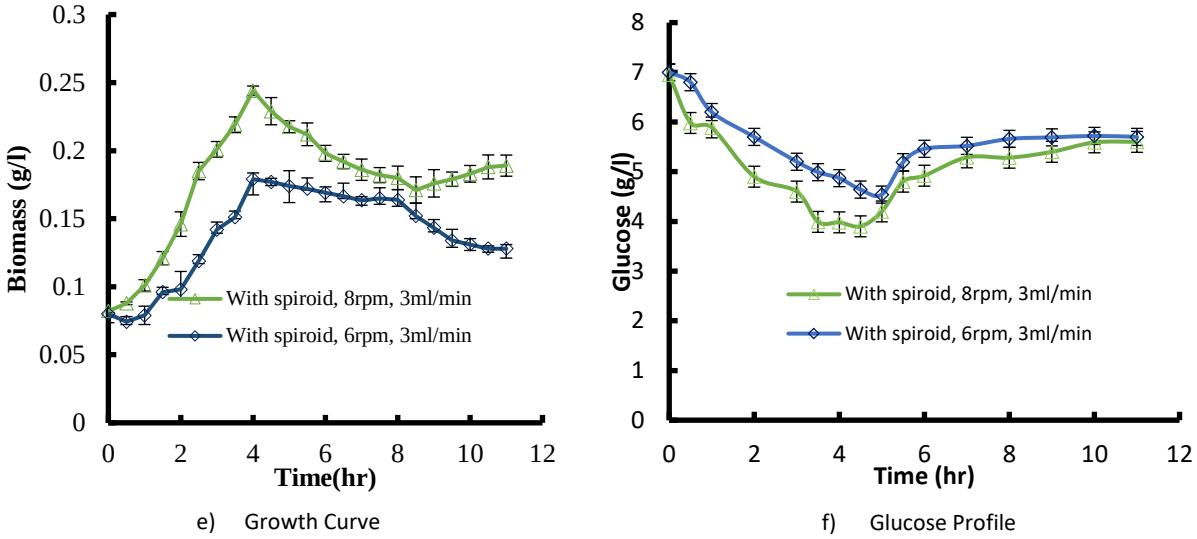

e) Growth Curve f) Glucose Profile

Figure 4.10 Growth Curve and Metabolite Concentration in Bioreactor with and without Spiroid, Various Rotation Rates

Figure 4.11 represented the growth rates and biomass concentrations obtained at both these rotation rates of 6 and 8 rpm. A growth rate of 0.2723 h^{-1} was obtained with spiroid at 8 rpm which was 35% greater than the growth rate at 6rpm (0.20134 h^{-1}). This indicated that yeast cells grew faster in the spiroid system at 8 rpm. Highest steady state concentrations were also obtained at 8 rpm with lower flow rates as summarized in Table 4-2.

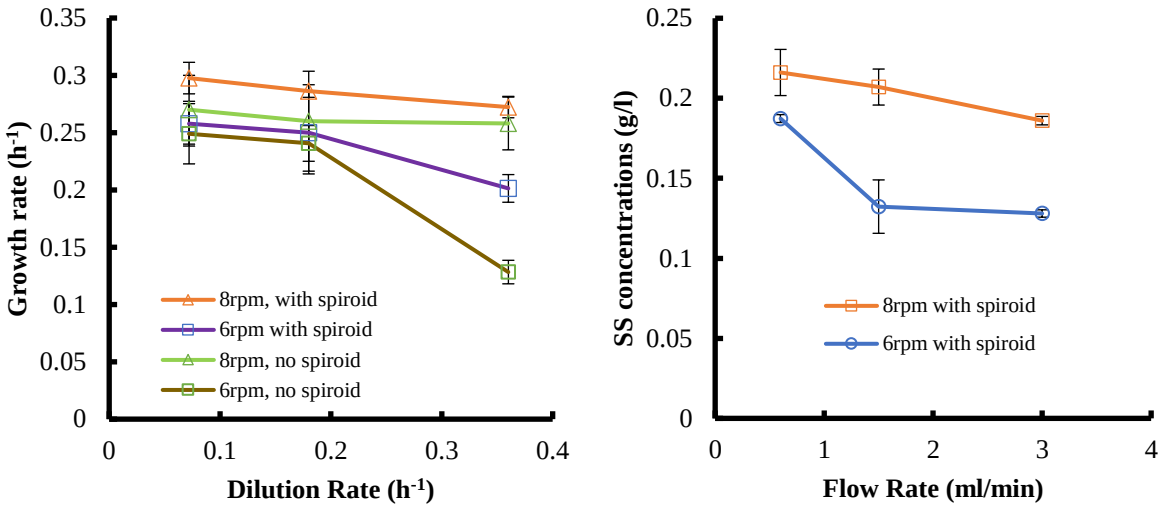

Figure 4.11 Growth Rates and Steady State Cell Concentrations, Various Rotation Rates

On comparison of all the flow rates for 8 rpm with spiroid, the bioreactor system was optimized for highest concentrations at low flow rates indicating that the system produces enhanced cell concentrations at higher rotation rates and low flow rates as shown in Figure 4.12. These results agreed with the computational fluid dynamic results obtained indicating the functioning of spiroid at 8 rpm.

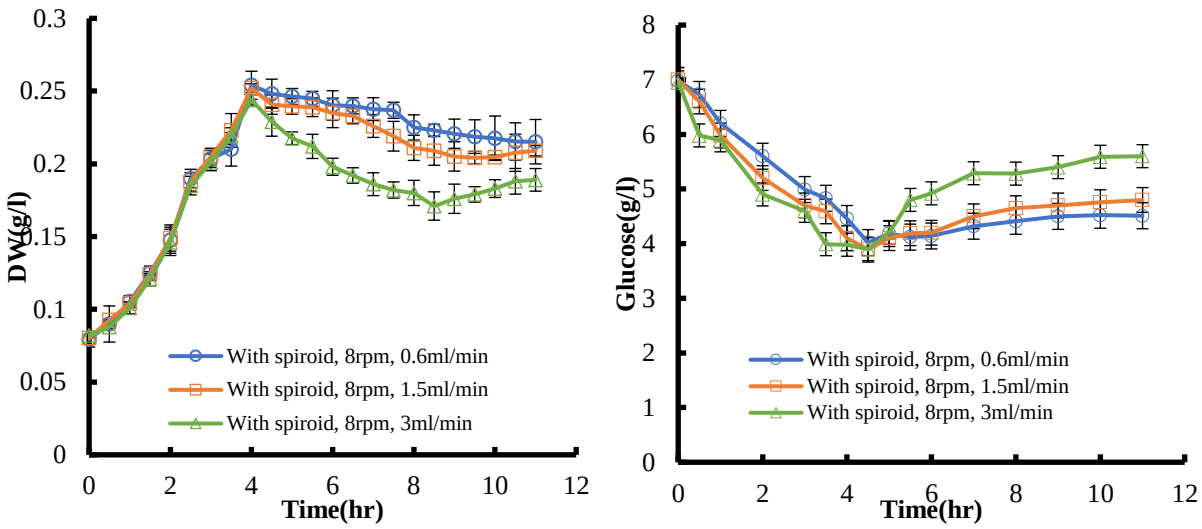

Figure 4.12 Spiroid Optimization, 8 RPM

Table 4-2 Summary of Cell Growth Parameters (Yeast)

RPM	μ, h^{-1}	F, ml/min	D, h^{-1}	SS concentration, g/L
8	0.2976	0.6	0.072	0.2161
	0.2863	1.5	0.18	0.20703
	0.2723	3	0.36	0.186
6	0.25784	0.6	0.072	0.1873
	0.25	1.5	0.18	0.1323
	0.2013	3	0.36	0.128

4.4 Conclusions

Oxygen and mixing enhance cell production. The use of the spiroid in the bioreactor increased oxygen transfer and mixing (Fang et al., 2017). This increase in oxygen transfer led to an increase in cell population. The bioreactor could be operated both in batch and continuous modes for improved durations. Various steady state concentrations for different medium flowrates were obtained. Increase in cell concentration and decrease in batch-mode operating time was observed for the bioreactor with spiroid. The comparison of results for the bioreactor

with and without spiroid supported the advantages of using the spiroid loop for increased cell growth. Maximum cell growth for yeast was observed in the bioreactor with spiroid at higher rotation rate (8 RPM) and low flow rate (0.6 ml/min). The rotation rate comparison was in good agreement with the computational fluid dynamic results. These results from yeast cell growth showed that this system can be used as a part of the bioreactor seed train at industrial scale for expressing proteins. Engineered cell lines can also be tested in this reactor for a required protein. Addition of cell retention devices can lead to increased densities of cells in this system for cell culture and antibody production using fermentation systems.

Abbreviations

BHK	Baby Hamster Kidney fibroblasts
CFD	Computational Fluid Dynamics
D	Dilution rate (hr-1)
DHA	docosahexaenoic acid
F	Flowrate (ml/min)
GM	Glucose monitor
MSC	mesenchymal stromal cells
OD_{600}	optical density at 600nm
rpm	Rotations per minute
SLA	stereolithography
SLS	Selective Laser Sintering
SS	Steady state
SUB	Single-use Bioreactors
t	time (s)
VOF	volume of fluid
YPD	yeast peptone dextrose
τ	mean residence time (hr)

References

Bafana, R., Sivanesan, S., & Pandey, R. A. (2019). Optimization and scale up of itaconic acid production from potato starch waste in stirred tank bioreactor. *Biotechnology Progress*, *35*(3), 1–9.

Das, R., Roosloot, R., van Pel, M., Schepers, K., Driessen, M., Fibbe, W. E., … Roelofs, H. (2019). Preparing for cell culture scale-out: establishing parity of bioreactor- and flask-expanded mesenchymal stromal cell cultures. *Journal of Translational Medicine*, *17*(1), 241.

Fang, S., Todd, P. W., & Hanley, T. R. (2017). Enhanced oxygen delivery to a multiphase continuous bioreactor. *Chemical Engineering Science*, *170*, 597–605.

Junne, S., & Neubauer, P. (2018). How scalable and suitable are single-use bioreactors? *Current Opinion in Biotechnology*, *53*, 240–247.

Krawetz, R., Taiani, J. T., Liu, S., Meng, G., Li, X., Kallos, M. S., & Rancourt, D. E. (2010). Large-scale expansion of pluripotent human embryonic stem cells in stirred-suspension bioreactors. *Tissue Engineering - Part C: Methods*, *16*(4), 573–582.

Malairuang, K., Krajang, M., Sukna, J., Rattanapradit, K., & Chamsart, S. (2020). High cell density cultivation of saccharomyces cerevisiae with intensive multiple sequential batches together with a novel technique of fed-batch at cell level (FBC). *Processes*, *8*(10), 1–26.

Metze, S., Ruhl, S., Greller, G., Grimm, C., & Scholz, J. (2020). Monitoring online biomass with a capacitance sensor during scale-up of industrially relevant CHO cell culture fed-batch processes in single-use bioreactors. *Bioprocess and Biosystems Engineering*, *43*(2), 193–205.

R. N. Bento, M. A. Rendas, V. A. R. Semedo, C. E. S. Bernardes, M. E. Minas da Piedade, F. A. (2016). The Metabolic Profile of Lag and Exponential Phases of Saccharomyces Cerevisiae Growth Changes Continuously. *BioRxiv Preprint*.

Salari, R., & Salari, R. (2017). Investigation of the Best Saccharomyces cerevisiae Growth Condition. *Electronic Physician*, *9*(1), 3592–3597.

Villiger, T. K., Neunstoecklin, B., Karst, D. J., Lucas, E., Stettler, M., Broly, H., … Soos, M. (2018). Experimental and CFD physical characterization of animal cell bioreactors: From micro- to production scale. *Biochemical Engineering Journal*, *131*, 84–94.

Wang, G., Haringa, C., Noorman, H., Chu, J., & Zhuang, Y. (2020). Developing a Computational Framework To Advance Bioprocess Scale-Up. *Trends in Biotechnology*, *38*(8), 846–856.

Chapter 5 - High Density CHO Cells using a Spiroid in a Novel Bioreactor

Abstract

A 3D printed novel continuous bioreactor comprising a one-liter rotating horizontal cylinder with an internal spiroid was shown to increase gas-liquid contact areas which increases cell growth and mixing. Multiphase flow modeling using computational fluid dynamics showed that the bioreactor with spiroid works better at higher rotation rates of 6 rpm and 8 rpm. The bioreactor is fabricated by rapid prototyping and can be operated in either batch or continuous modes with inlet flows via rotary unions available to provide medium and oxygen and outlet flows for waste and in-line analysis. Chinese Hamster Ovary (CHO) cells were cultured in the reactor to validate the effect of the spiroid on high cell densities and highly viscous cell lines. Viable cell density was monitored at different operating conditions using a hemocytometer and trypan blue assay. Results show that CHO cells could reach densities of 2.5×10^6 cells/ml using the bioreactor with spiroid which is possible only by combining multiple roller bottles. The reactor with spiroid produced higher viable cell densities at high rotation rates and at high medium flow rates in both batch and continuous modes indicating the efficiency of the spiroid for enhanced production. Growth curves were generated for this cell line, and the cell density increased. A viability of 90% could be maintained in the reactor with the spiroid at higher rotation rates of 10 rpm and higher flow rates of 4 ml/min. The reactor with spiroid could be operated for a maximum of 14 days for these highly viscous cell suspensions.

Keywords: continuous bioreactor, spiroid, CHO, cell growth

5.1 Introduction

Mammalian cells have been widely used in the biopharmaceutical industry to produce recombinant proteins. The production of monoclonal antibodies (mAbs) using these cells is rapidly developing sector in the industry. The lack of outer cell wall in these cells makes them highly sensitive to the environment stimuli such as osmotic changes, hydrodynamic forces, pH, and nutrients (Prokop et al., 1989). The effect of these variables was studied in CHO cells by Sieck et al. (2013) using a scaled down model. CHO cells are known for growing at a rapid rate under suitable culture conditions. The impact of hydrodynamic stress conditions on CHO cells showed that these cell lines were robust under shear. Although there was a slight decrease in the monoclonal antibody production with increasing hydrodynamic stress, cell lysis did not occur.

The implementation of cell culture processes for mAb production requires optimization of cell lines capable of synthesizing molecules at high productivities, culture media and bioreactor conditions, on-line and off-line sensors for process control and culture performance for easy scale-up. The use of stainless-steel bioreactors on large scale is costly and hard to maintain. To overcome these challenges, single use bioreactors (SUB) are being used. These disposable technologies are advantageous particularly at pilot scale (Li et al., 2010). Human carcinoma cells were cultured in a device with continuous perfusion of medium. The unit consist of a circular microfluidic chamber, multiple narrow perfusion channels and ports for fluidic access. An array of 10 x 10 was constructed of such single units. A resulting cell density of 5×10^7 cells/ml constituted a 10-fold increase compared to values reported for cultures in other bioreactors (Hung et al., 2005).

Encapsulated hybridoma cells in perfused fluidized-bed reactors produced monoclonal antibodies at a rate of 2.75 μg per $ml^{-}hr$. Continuous operation for 35 days represented a five-fold

increase over batch and fed-batch operations (Lecina et al., 2011). Increasing the cell seeding densities that are 25 to 40 times higher than the typical densities used in CHO cell production reduced the production time for N-1 bioreactor from 14 to 8 days (Padawer et al., 2013). While batch and fed-batch methods are the most used methods in mammalian cell manufacturing, the demand for perfusion systems is growing. The wave-induced bioreactor can generate a cell density of 2.14 x 10^8 cells/ml and remain in operation for two weeks. The employment of TFF and ATF methods results in cell cultures with a consistency of 20-35 x 10^6 cells/ml, however increasing viscosity creates limits (Clincke et al., 2013).

Shear rate increase with the use of cell retention devices such as TFF can be reduced with the use of low shear centrifugal pumps, which in turn maximizes the cell growth, particle concentration and product recovery to comparable levels of ATF (Wang et al., 2017). Coronel et al., 2019 grew suspension cells to a density of 50 x 106 cells/ml in perfusion mode using both ATF and TFF systems in an orbital shaken bioreactor. Cell retention is also affected by the material and pore size used in the ATF device. Changing the hollow fiber material in ATF from polyether sulfone to polysulfone increased the retention rate from 15 ± 8% to 43 ± 18% (Su et al., 2021).

Process intensification with the use of continuous operations has been successfully applied in the chemical industry but fed-batch is the primary mode for the production of mAbs rather than perfusion or continuous in biopharmaceutical industries. Increase in inoculation density in combination with non-perfusion strategies of the seed stage helped in achieving viable cell densities of 22to 34 x 10^6 cells/ml for a 14-day duration in the production of CHO cells. These results were scaled up from 5-L bioreactors to 500-L and 1000-L N stage bioreactors (Yongky et al., 2019). Tissot et al., 2012 studied the effects of k_La on CHO cell growth and determined that oxygen did not have a greater impact on cell growth in a shaken orbital bioreactor. The pH of the

cell culture medium appeared to be a limiting factor. Maintaining the k_La from 7 to 9 h^{-1} helped maintain cell viability without the use of pH or DO controllers.

This research investigated the growth of CHO cells at various operating conditions and medium flow rates. The reactor was operated at both batch and continuous modes allowing the feasibility of a chemostat operation. Viability and higher cell densities were studied under the influence of spiroid and rotation rates of 8 and 10 rpm. Due to the high viscosity of these cells, higher dilution rates were chosen. The reactor was also prototyped before the experiments with SLA technique to account for the cell debris generated from the previous yeast cell culture experiments. The effect of temperature, pH and working volumes was also reported.

5.2 Materials and Methods

5.2.1 Experimental Apparatus

Figure 5.1 illustrates the experimental setup of the bioreactor with spiroid. The continuous bioreactor used for this study is a bench-scale bioreactor (Fang et al., 2017) which consists of an outer cylindrical shell with a spiroid. The bioreactor can be rotated horizontally with the help of a roller bed (Model No: 88881003, Thermo Scientific, Waltham, MA, USA) as shown in Figure 5.1. The two inlet and two outlet ports present at either end of the reactor help in providing medium and oxygen continuously to the reactor during rotation. This bioreactor is prototyped using stereolithography (SLA) 3D printing techniques and PLA material previously. With continued use for various cell lines, the reactor had cell debris which could not be removed even with hypochlorite solution (Figure 5.2). The reactor was then prototyped using SLA technique and ClearVue material from Xometry LLC. This material is naturally-transparent polycarbonate material with excellent moisture resistance and high clarity (Figure 5.2). The end

caps were designed to be removable making the cleaning of both the reactor and spiroid easier. The required temperature was maintained with the help of an electric space heater. The flow in and out of the reactor was maintained with the help of peristaltic pumps on either side of the reactor. O-rings and rotary seals present between reactor body and endcaps helped to prevent leakages over long operating times.

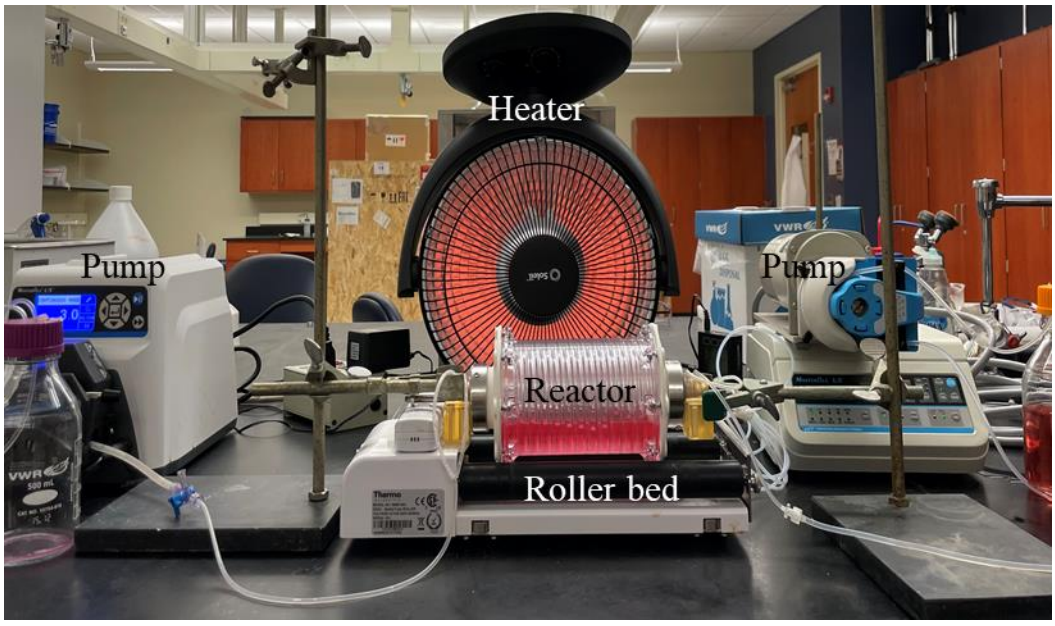

Figure 5.1 Experimental Setup

Figure 5.2 Cell Debris in the Reactor and Newly Prototyped SLA-Printed Bioreactor

5.2.2 Cell culture

5.2.2.1 Strain and Medium

The cell line used in this research was CHO-K1 obtained from Dr. Allan David's laboratory (Department of Chemical Engineering, Auburn University, AL, USA). The cell culture medium used for CHO cells contained 89% (v/v) F-12k medium (Kaighn's Modification of Ham's F-12 Medium, ATCC 30-2004, VA, USA), 10% (v/v) Fetal Bovine serum (Life Technologies Corporation, CA, USA) and 1% (v/v) Antibiotics (Dr. Allan David's laboratory, Department of Chemical Engineering, Auburn University, AL, USA). The media was prepared in sterile conditions under BSL2 cabinet and stored at 2 to 8 ℃ before use.

5.2.2.2 Operating Conditions

Batch Culture

The CHO cells vial was thawed, and cells were passaged into a 75 cm^2 flask with cell culture media. These cells were maintained in a five% CO2/air mixture, humidified at 37℃. Exponentially growing cells were inoculated at 1 x 10^5 cells/ml into the bioreactor with a working volume of 200 ml in batch mode. The reactor was operated for rotation rates of 6 rpm, 8 rpm and 10 rpm. The temperature was controlled at 33 to 37℃ with the help of an electric space heater. The dissolved oxygen in the bioreactor was maintained at 30% with the help of a flow through dissolved oxygen electrode system (DO-166MT-1SXS, Lazar research laboratories, LA, CA). The culture pH was controlled at various pH values (6.8, 7.0, 7.2) by addition of 1M $NaHCO_3$ and monitoring it with the help of a micro pH electrode (PHR-146S, Lazar research laboratories, LA, CA).

Chemostat Culture

Based on the results obtained from batch mode experiments, the optimum temperature was maintained at 37℃ and pH was maintained at 7.2. Exponentially growing cells were inoculated at 2 x 10^5 cells/ml into the bioreactor with a working volume of 300 ml in chemostat mode. The reactor was operated in batch mode for 3 days, and then changed to continuous mode (chemostat) with different rotation rates (8 rpm, 10 rpm) and fresh medium flowrates (1 ml/min, 3 ml/min and 4 ml/min). After batch mode of 3 days, fresh medium was pumped into the reactor and the same amount was removed to maintain constant volume. The feed was maintained sterile with the help of 0.22-micron filter. All the experiments were done with and without spiroid for comparison.

The exponential growth in batch mode could be described as:

$$\frac{1}{X}\frac{dX}{dt} = \mu \tag{5-3}$$

where X is the biomass concentration (cell density, cells/ml) at time t (hr); μ is the specific growth rate (hr^{-1}). The exponential equation was only applied when the substrates are in excess (Herbert et al., 1956).

In addition, if the feed media are sterile, the changes of cell concentration in a continuous system (or a chemostat) could be described as follows (Herbert et al., 1956):

$$\frac{dX}{dt} = \mu X - DX \tag{5-2}$$

where D is the dilution rate (hr^{-1}) defined as:

$$D = \frac{F}{V} = \frac{1}{\tau} \tag{5-3}$$

where F is the flowrate ($L.hr^{-1}$); V is the volume maintained in the reactor (L); **τ** is the mean residence time (hr).

$$\mu = D \text{ (Steady state)}$$

$$\mu < D \text{ (wash out)}$$

When the specific growth rate is less than the dilution rate, the cells cannot maintain the concentration and this will lead to a condition called wash out; if the growth rate is equal to dilution rate, the system reached steady state, i.e., cells maintain a constant concentration. Thus, through manipulating the dilution rate, the growth rate of the cells could be controlled and maintained.

5.2.2.3 Analytical Methods

The total cell concentration or the total number of cells was determined by cell counting using a hemocytometer at different time intervals during the experiment. Viable cell density was calculated with the help of a trypan blue test. Aliquots were diluted as required for each test and the total and viable cell count was then noted. Duplicate readings were taken for every operating condition and fresh medium flowrate.

5.3 Results and Discussion

5.3.1 Cell Culture Results

The growth of CHO cells in the bioreactor with spiroid was slow at the lower rotation rate of 6 rpm which could be due to lack of aeration and an increase in viscosity. The cell densities reached a maximum of 6.8 x10^5cells/ml in the bioreactor with spiroid on day four and then cell growth started to decline. The reactor could be operated only for 7 days in batch mode at 6RPM as shown in Figure 5.3. Cell densities of 5 x 10^5 cells/ml were obtained in the reactor without spiroid on day five of the test which is approximately 36% less than that was obtained for the bioreactor system with spiroid. Figure 5.3 depicts the effect of spiroid on cell densities at various

rotation rates. CHO cells grew faster with the spiroid at higher rotation rates of 8 rpm and 10 rpm in the bioreactor with spiroid. Cell densities obtained at 8 rpm with spiroid were 2.1 x 10^6 cells/ml after running the reactor for 9 days whereas the same cell densities could be attained at 10 rpm within 6 days. This result indicates that reactor operating time could be reduced by 3 days with the use of spiroid at a higher rotation rate of 10 rpm. Though higher cell density was obtained at 8 rpm when compared to 6 rpm, the reactor could be operated for 12 days in the case of 8 rpm. After day ten, cell death was observed.

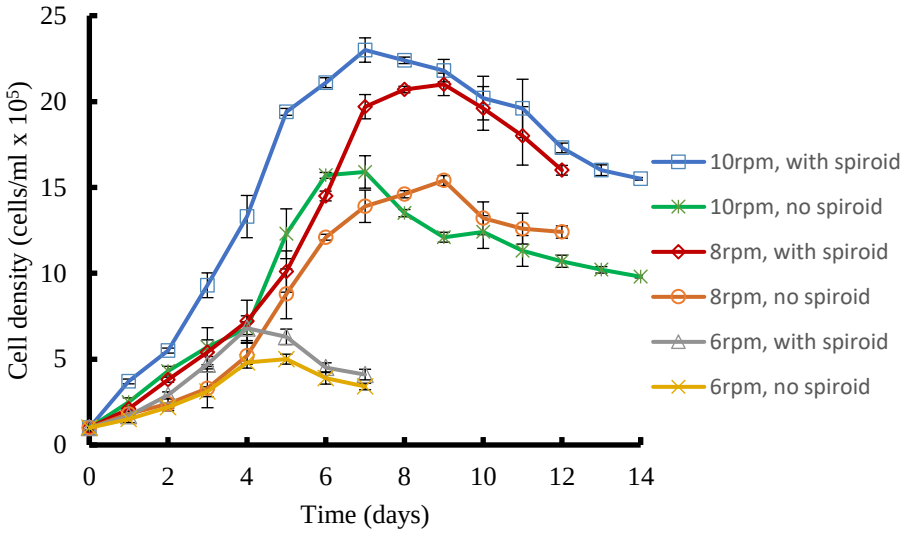

Figure 5.3 Batch Mode, Various Rotation Rates

Highest cell densities of 2.3 x 10^6 cells/ml were obtained at 10 rpm in the bioreactor with spiroid which could be attributed to increase in aeration which was provided with the recirculation of contents and nutrients with the help of the spiroid as shown in Figure 5.4. The cell densities in the bioreactor with spiroid was 45% more than the reactor without spiroid when tested over a period of 7 days. The overall operating time for the reactor decreased by 31% using the spiroid in batch mode at 10 rpm as shown in Figure 5.4

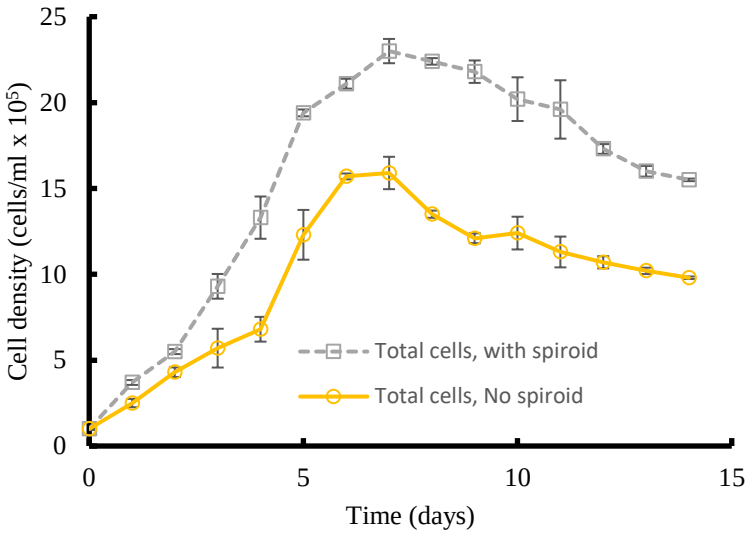

Figure 5.4 Batch Mode, 10 rpm

To study the effect of temperature, three different temperatures were selected for the reactor with spiroid at 10 rpm. In Figure 5.5, data indicated that for T=33°C, there was a long lag phase and decreased cell densities, extending the duration of exponential phase by 4 days. Maximum cell densities obtained at this temperature were 7.2 x 10^5 cells/ml after 10 days of operation. When the temperature was changed to T=35°C, the cells grew exponentially from day 2, and a maximum cell density of 1.64 x 10^6 cells/ml were achieved after nine days. The cell densities were promising at 10 rpm and could be achieved faster in batch mode as seen in Figure 5.5. Based on these results, a temperature of T=37°C was maintained for the next set of experiments.

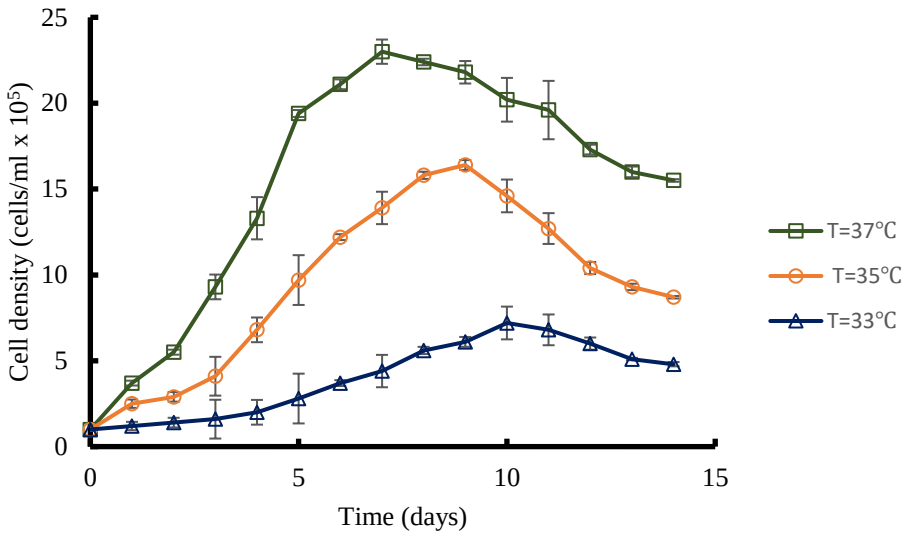

Figure 5.5 Temperature Comparison, 10 rpm

Figure 5.6 indicates the effect of pH on cell densities in batch mode. At a pH of 6.8, cells did not grow and simply entered a slow decline phase. A pH of 7.0 generated cell densities of 10.1 x 10^5 cells/ml, and a pH=7.2 generated cell densities of 2.3 x 10^6 cells/ml. This result determined that the optimum conditions of pH=7.2 and T=37°C were best suited for CHO cell growth in the reactor with spiroid.

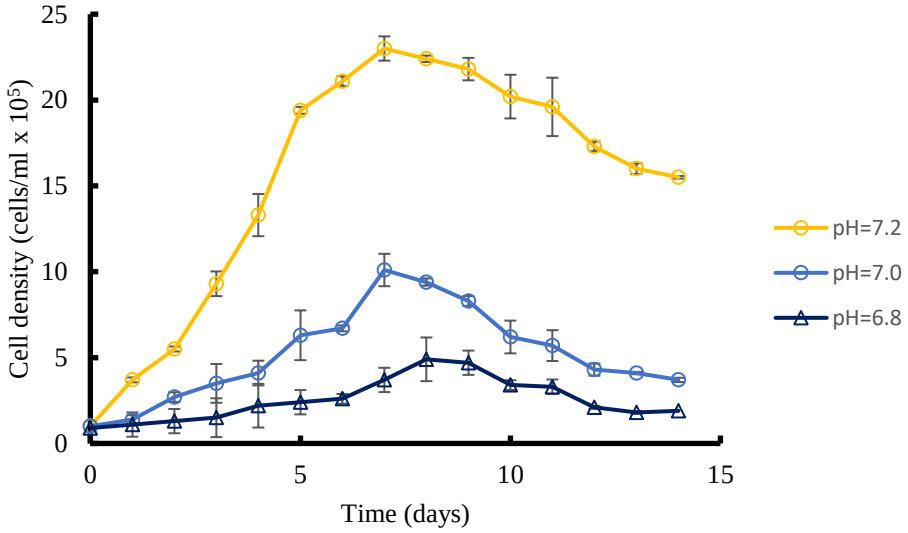

Figure 5.6 pH Comparison, 10 rpm

Based on the findings from batch mode, all the experiments in continuous mode were conducted at standard conditions of pH=7.2 and T= 37°C. For chemostat mode, experiments were conducted at two different rotation rates (8 rpm, 10 rpm) and three medium flowrates (1 ml/min, 3 ml/min and 4 ml/min) to demonstrate different steady state level cell densities. Higher medium flowrates were considered as with the growth of CHO cells in the reactor, the viscosity also increased. In trial experiments, low flow rates of 0.5 to 1 ml/min could not pump the cells through the reactor. Duplicate experiments were conducted at each condition and averaged.

The reactor was operated in batch mode for three days and then changed to chemostat setting. Cells grew in exponential phase in batch mode for three days and eventually reached steady state concentration with continuous flow. For each of these dilution rates of 0.2, 0.6 and 0.8 h^{-1}, the working volume was maintained at 300 ml. The inoculation density in chemostat mode was 2 x 10^5 cells/ml. The total and viable cell densities were noted. Percentage viability was then calculated and reported for the reactor with the spiroid and without the spiroid.

Figure 5.7(a-f) represents cell densities obtained controlled by different dilution rates for the bioreactor with and without spiroid at 8 rpm. The growth curves were consistent in batch mode and the cell densities decreased with decreased flowrates due the increased product accumulation resulting from growing CHO cells. Increase in cells at higher flowrates or dilution rates showed a decrease in metabolite concentration in the system. Figure 5.7 indicated that in all the different dilution rates used, the bioreactor with spiroid produced greater cell densities with a maximum of 2.42 x 10^6 cells/ml for a 11-day operation of the reactor at 4 ml/min (for 8 rpm).

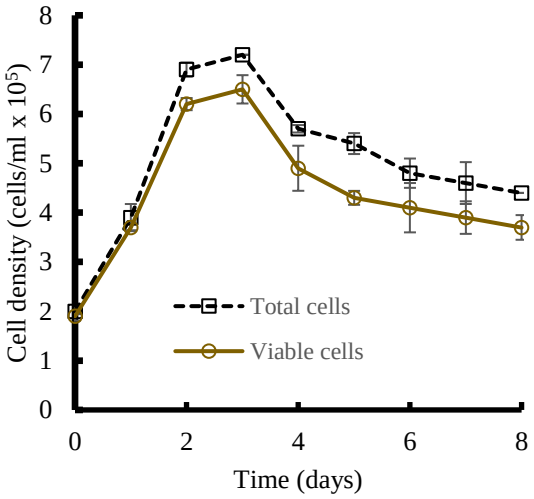

b) 8 rpm, 1ml/min – with spiroid

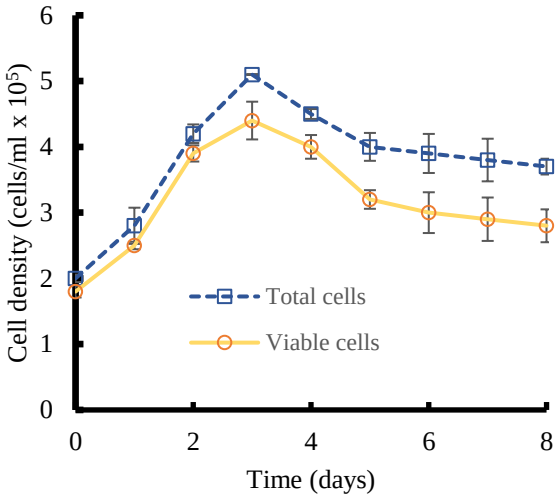

b) 8 rpm, 1 ml/min – no spiroid

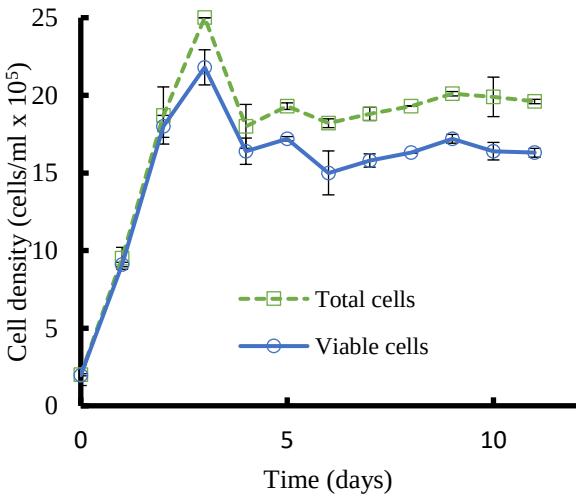

c) 8 rpm, 3ml/min – with spiroid

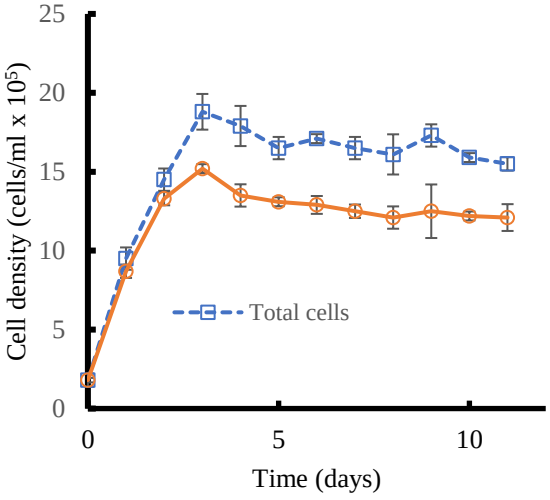

d) 8 rpm, 3ml/min – no spiroid

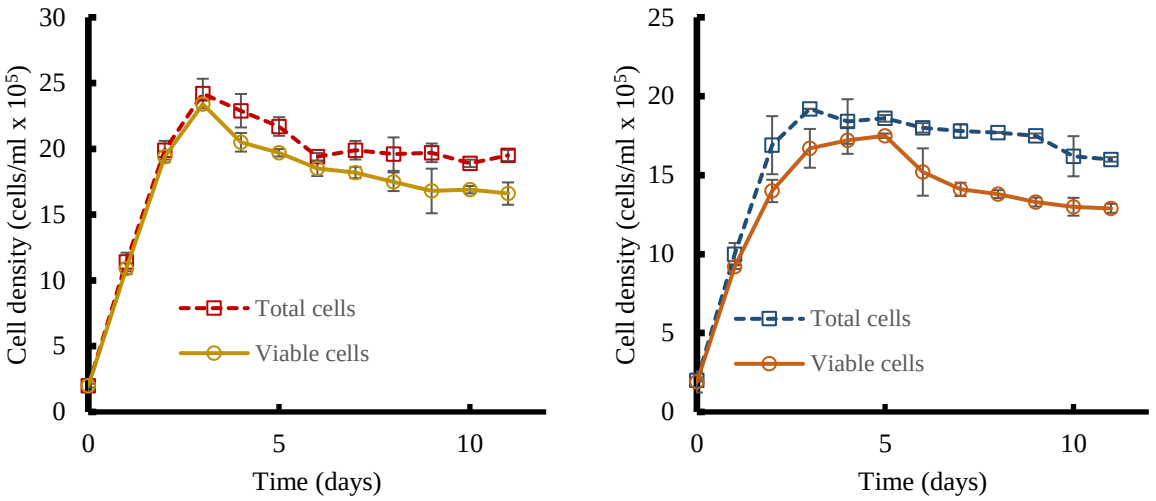

e) 8rpm, 4ml/min – with spiroid

f) 8rpm, 4ml/min – no spiroid

Figure 5.7 Cell density at Various Flowrates with and without Spiroid, 8 rpm

Figure 5.7 indicated that CHO cells grew rapidly and at higher densities in the bioreactor with spiroid at all three flowrates. In Figure 5.7 (a-b), the maximum viable cell densities obtained in the reactor with spiroid was 6.5 x 10^5 cells/ml and the cell densities obtained in the reactor without spiroid were reported as 4.4 x 10^5 cells/ml which is 47% less when compared to the bioreactor with spiroid. In addition, viable steady state densities of 4.4 x 10^5 cells/ml could be maintained in the reactor with spiroid for a period of 11 days. In Figure 5.7 (c-d), at 3 ml/min, the reactor with spiroid showed a 63% increase in viable cell densities for three-day batch mode (2.48 x 10^6 cells/ml vs 1.52 x 10^6 cells/ml). This increase results as the spiroid increases gas-liquid contact areas for oxygen transfer as all other conditions remained constant. Figure 5.7 Cell density at Various Flowrates with and without Spiroid, 8 rpm

(e-f) depicted that highest cell densities were obtained in batch mode for reactor with spiroid. Additionally, steady state cell densities increased by 29% when compared to the results for operation without the spiroid.

Percentage cell viability for these three flow rates were reported in Figure 5.8 (a-c). In all the three cases, the bioreactor with spiroid could maintain up to 85% viability which cannot be achieved in conventional roller bottles. The reactor without spiroid in the case of 4 ml/min achieved viability percentage of nearly 80% during steady state which could be due to the incoming fresh nutrients supplied to the cells growing in the reactor. Based on these observations, the flow rate of 4 ml/min was selected for conducting experiments at 10 rpm as steady state densities could be maintained for longer durations.

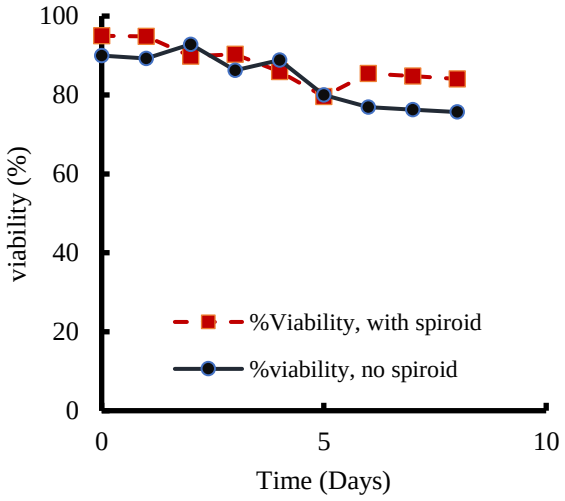

b) %Viability, 8 rpm, 1 ml/min

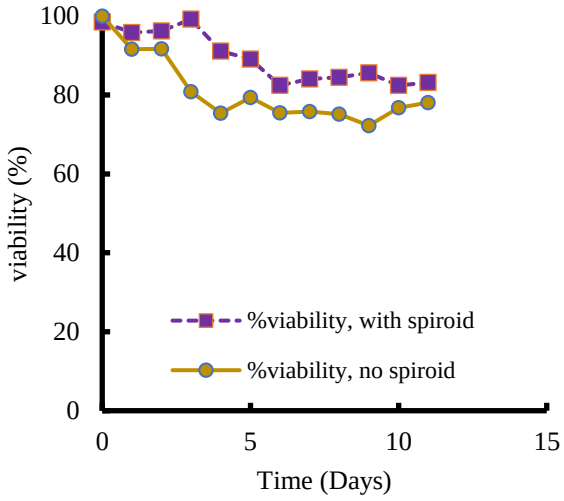

c) %Viability, 8 rpm, 3 ml/min

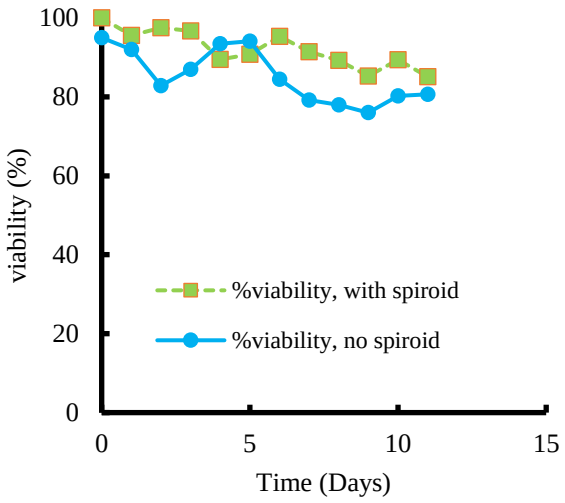

c) %Viability, 8 rpm, 4 ml/min

Figure 5.8 %Viability – comparison at 8rpm

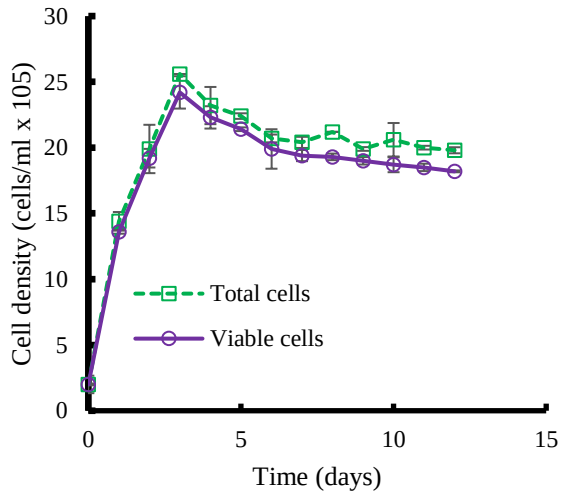

a) 10 rpm, 4 ml/min – with spiroid

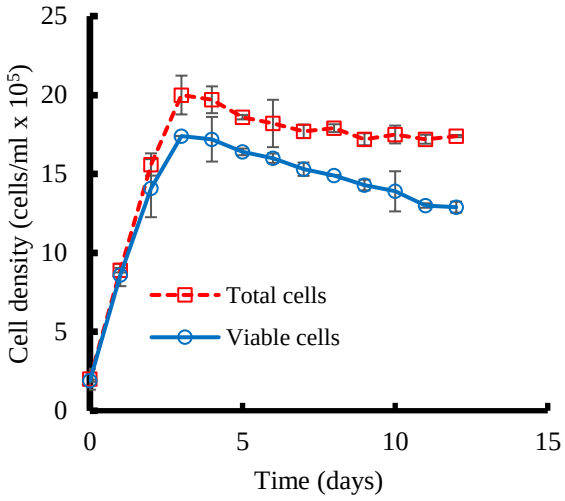

b) 10 rpm, 4 ml/min – no spiroid

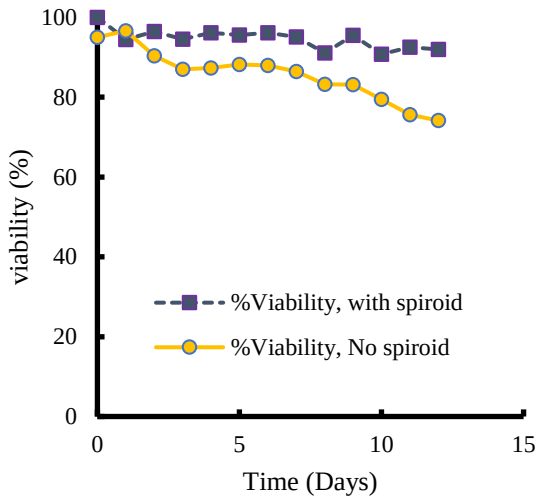

c) %Viability, 10 rpm, 4 ml/min

Figure 5.9 Cell density & Viability – 10 rpm, 4 ml/min

Figure 5.9 (a-b) compared the effect of rotations rate 10 rpm for the reactor with and without the spiroid. For 4 ml/min, the bioreactor showed a 28% increase in cell density in batch mode of three days, and a 14% increase in steady state cell densities when the spiroid was used. In comparison of percentage viability between 8 and 10 rpm for 4 ml/min, the cells at 10 rpm with spiroid could be maintained nearly 92% viable for 12 days which could not be achieved with 8 rpm for CHO cells. The highest steady state cell density of 18.2 x 10^5 cells/ml was obtained at 10 rpm, 4 ml/min for the bioreactor with spiroid as shown in Table 5-1. The table below shows the maximum viable cell count was also the greatest in this case indicating the efficiency increase due to the spiroid.

Table 5-1 Summary of Cell Growth Parameters (CHO)

RPM	F, ml/min	D, h^{-1}	Maximum Viable cell count, 10^5 cells/ml	SS cell densities, 10^5 cells/ml	Cell Viability at 8 days (With spiroid)	Cell Viability at 8 days (No spiroid)
8	1	0.2	6.5	3.7	84%	75.7%
	3	0.6	21.8	16.3	84.4%	75%
	4	0.8	23.4	16.6	89%	77.9%
10	4	0.8	24.2	18.2	91%	83.2%

5.4 Conclusions

CHO cell growth is directly affected by the oxygen concentration, temperature and pH maintained in the bioreactor. The effect of temperature on the CHO cell growth determined that cells grow at higher densities at 37°C; pH studies showed that a pH of 7.2 is suitable for maintaining these cell densities for longer durations. CHO cells do not have a cell wall and the cell growth is impacted by the amount of shear. Higher impeller rotation rates in conventional bioreactors lead to cell death. Cell growth results from higher rotation rates of 8 and 10 rpm show that the reactor with spiroid is feasible for a low shear environment by maintaining cell viabilities ranging from 80 to 90% in both the cases. Maximum cell densities of 25.6 x 10^5 cells/ml were obtained in the bioreactor with spiroid when the reactor was operated in batch mode for three days. The reactor could be operated continuously for a maximum of 14 days duration without any leakages while maintaining steady state cell densities. The spiroid is effective in pumping high viscosity cells like CHO cells and is capable of producing cell densities which are not possible with a single roller bottle. Various steady state concentrations for different medium flowrates showed improved performance at higher rotation rates of 10 rpm and higher flow rates of four ml/min for highly viscous cell lines. With the use of traditional

impellers, shear sensitive cell lines like CHO cannot be cultured for longer durations in the reactor and maintained at higher densities but, this can be achieved with the help of a rotating bioreactor with spiroid.

Abbreviations

ATF	Alternating tangential flow filtration
CFD	Computational Fluid Dynamics
CHO	Chinese Hamster Ovary
D	Dilution rate (hr-1)
DO	Dissolved oxygen
F	Flowrate (ml/min)
FBS	Fetal Bovine serum
rpm	Rotations per minute
SLA	stereolithography
SLS	Selective Laser Sintering
SS	Steady state
SUB	Single-use Bioreactors
t	time (s)
TFF	Tangential flow filtration
τ	mean residence time (hr)

References

Clincke, M. F., Mölleryd, C., Zhang, Y., Lindskog, E., Walsh, K., & Chotteau, V. (2013). Very high density of CHO cells in perfusion by ATF or TFF in WAVE bioreactorTM: Part I: Effect of the cell density on the process. Biotechnology Progress, 29(3), 754–767.

Coronel, J., Behrendt, I., Bürgin, T., Anderlei, T., Sandig, V., Reichl, U., & Genzel, Y. (2019). Influenza A virus production in a single-use orbital shaken bioreactor with ATF or TFF perfusion systems. Vaccine, 37(47), 7011–7018.

Fang, S., Todd, P. W., & Hanley, T. R. (2017). Enhanced oxygen delivery to a multiphase continuous bioreactor. Chemical Engineering Science, 170, 597–605.

Hung, P. J., Lee, P. J., Sabounchi, P., Lin, R., & Lee, L. P. (2005). Continuous perfusion microfluidic cell culture array for high-throughput cell-based assays. Biotechnology and Bioengineering, 89(1), 1–8.

Lecina, M., Tintó, A., Gálvez, J., Gòdia, F., & Cairó, J. J. (2011). Continuous perfusion culture of encapsulated hybridoma cells. Journal of Chemical Technology and Biotechnology, 86(12), 1555–1564.

Li, F., Vijayasankaran, N., Shen, A., Kiss, R., & Amanullah, A. (2010). Cell culture processes for monoclonal antibody production. MAbs, 2(5), 466–479.

Padawer, I., Ling, W. L. W., & Bai, Y. (2013). Case study: An accelerated 8-day monoclonal antibody production process based on high seeding densities. Biotechnology Progress, 29(3), 829–832.

Prokop, A., & Rosenberg, M. Z. (1989). Bioreactor for mammalian cell culture. Advances in Biochemical Engineering/Biotechnology, 39, 29–71.

Sieck, J. B., Cordes, T., Budach, W. E., Rhiel, M. H., Suemeghy, Z., Leist, C., … Soos, M. (2013). Development of a Scale-Down Model of hydrodynamic stress to study the performance of an industrial CHO cell line under simulated production scale bioreactor conditions. Journal of Biotechnology, 164(1), 41–49.

Su, Y., Wei, Z., Miao, Y., Sun, L., Shen, Y., Tang, Z., … Tian, J. (2021). Optimized process operations reduce product retention and column clogging in ATF-based perfusion cell

cultures. Applied Microbiology and Biotechnology, 105(24), 9125–9136.

Tissot, S., Michel, P. O., Hacker, D. L., Baldi, L., Jesus, M. De, & Wurm, F. M. (2012). KLa as a predictor for successful probe-independent mammalian cell bioprocesses in orbitally shaken bioreactors. New Biotechnology, 29(3), 387–394.

Wang, S., Godfrey, S., Ravikrishnan, J., Lin, H., Vogel, J., & Coffman, J. (2017). Shear contributions to cell culture performance and product recovery in ATF and TFF perfusion systems. Journal of Biotechnology, 246, 52–60.

Yongky, A., Xu, J., Tian, J., Oliveira, C., Zhao, J., McFarland, K., … Li, Z. J. (2019). Process intensification in fed-batch production bioreactors using non-perfusion seed cultures. MAbs, 11(8), 1502–1514.

Chapter 6 - Summary and Recommendations

A novel continuous bioreactor with enhanced cell production was successfully operated in a multiphase environment. The addition of a spiroid facilitated the growth of cells by increasing the gas-liquid contact areas and providing nutrient recirculation. The complex flow in spiroid was predicted using computational fluid dynamics (CFD) simulations to calculate the hydrodynamic parameters for the fluid flow in the bioreactor with spiroid. The results from these simulations showed that the spiroid has a design space and rotation rate where it works to its full potential in the one liter bioreactor. Simulating the spiroid as a straight tube showed the formation of gas-liquid segments in the reactor which assist in oxygen transfer area.

Saccharomyces cerevisiae experiments validated the CFD results by showing enhanced growth at 8 rpm and was optimized at low flow rates and higher rotation rates for this cell line. The harvesting of these cells could be carried out for almost two days without leakage. Different steady state levels were achieved by varying the flowrate. The feasibility of the reactor for a shear-sensitive Chinese hamster ovary (CHO) mammalian cell line was also tested. The cultures could be grown to higher cell densities of 2.42×10^6 cells/ml which is usually not possible by using a single roller bottle. The bioreactor with spiroid showed potential for cell production for highly viscous cell lines. The reactor with spiroid could be operated continuously for a maximum of 14 days in both batch and chemostat modes. Cell viabilities could be maintained up to 90% at a rotation rate of 10 rpm and medium flow rate of 4 ml/min. Without the use of traditional impellers, adequate mixing was provided with the use of spiroid as no clumping of CHO cells was seen when cultured in suspension. The bioreactor with spiroid offers potential for both mammalian and fermentation cell culture systems in biopharmaceutical industries and can be used as part of the inoculum seed train for high cell densities before a production bioreactor.

As part of future work, the shear sensitivity of the reactor could be tested by using insect cell lines. The effect of spiroid on the production of higher titer antibodies can be tested with the use of an antibody producing cell line. The capability of the bioreactor with current industry perfusion can be validated by modifying the bioreactor with feedback control loop for temperature, pH, pressure, and dissolved oxygen concentrations. Once the reactor is modified with automated controls, it can further be tested for greater cell densities by using cell retention devices such as tangential flow filters (TFF), alternating tangential flow filters (ATF), or a flow-through filter in the existing outlet hub of the bioreactor to include perfusion systems within bioreactors. Perfusion system setup can be followed to culture cells for antibody or vaccine production.